ตัวรับรู้วัสดุระดับนาโนเมตรสำหรับการตรวจวัดแบบเลือกจำเพาะของสารประกอบไบโอไทออล

นางสาวจิราภรณ์ ไชยแจ่ม

วิทยานิพนธ์นี้เป็นส่วนหนึ่งของการศึกษาตามหลักสูตรปริญญาวิทยาศาสตรดุษฎีบัณฑิต
สาขาวิชาเคมี ภาควิชาเคมี
คณะวิทยาศาสตร์ จุฬาลงกรณ์มหาวิทยาลัย
ปีการศึกษา 2560

NANOMATERIAL SENSORS FOR SELECTIVE DETECTION OF BIOTHIOL COM POUNDS

Miss Chiraporn Chaicham

A Dissertation Submitted in Partial Fulfillment of the Requirements
for the Degree of Doctor of Philosophy Program in Chemistry
Department of Chemistry
Faculty of Science
Chulalongkorn University
Academic Year 2017

Thesis Title	NANOMATERIAL SENSORS FOR SELECTIVE DETECTION OF BIOTHIOL COMPOUNDS
By	Miss Chiraporn Chaicham
Field of Study	Chemistry
Thesis Advisor	Assistant ProfessorBoosayarat Tomapatanaget, Ph.D.

Accepted by the Faculty of Science, Chulalongkorn University in Partial Fulfillment of the Requirements for the Doctoral Degree

.....Dean of the Faculty of Science
(ProfessorPolkit Sangvanich, Ph.D.)

THESIS COMMITTEE

.....Chairman
(Associate ProfessorVudhichai Parasuk, Ph.D.)

.....Thesis Advisor
(Assistant ProfessorBoosayarat Tomapatanaget, Ph.D.)

.....Examiner
(ProfessorSupason Wanichwecharungruang, Ph.D.)

.....Examiner
(Assistant ProfessorFuangfa Unob, Ph.D.)

.....External Examiner
(Gamolwan Tumcharern, Ph.D.)

จิราภรณ์ ไชยแจ่ม : ตัวรับรู้วัสดุระดับนาโนเมตรสำหรับการตรวจวัดแบบเลือกจำเพาะของสารประกอบไบโอไทออล (NANOMATERIAL SENSORS FOR SELECTIVE DETECTION OF BIOTHIOL COMPOUNDS) อ.ที่ปรึกษาวิทยานิพนธ์หลัก: ผศ. ดร.บุษยรัตน์ ธรรมพัฒนกิจ, 96 หน้า.

วัสดุนาโนเซ็นเซอร์ชนิดใหม่ได้รับการออกแบบในสองหลักการที่แตกต่างกันของวิธีการตรวจวัด ระบบการตรวจวัดแบบแรก การรวมตัวของนาโนไมเซลล์ (TSC และ TSD) ถูกสังเคราะห์ขึ้นเพื่อใช้ตรวจวัด GSH บนพื้นฐานของการแตกของพันธะซัลไฟด์ในไมเซลล์ จากผลการทดลองพบว่า ความเข้มของแสงฟลูออเรสเซนซ์ที่ความยาวคลื่น 587 nm และ 528 nm เป็นของ TSC และ TSD ตามลำดับ จะลดลงอย่างมากเมื่อเติม GSH ลงใน 2.5% DMSO/PBS ที่ pH 6 นอกจากนี้ข้อดีของ TSD ยังนำไปใช้ประโยชน์สำหรับการตรวจวัดค่าการเรืองแสงตามระยะทางของอุปกรณ์วิเคราะห์กระดาษแบบสามมิติ(3D-μPAD) สำหรับการตรวจวัด GSH

ในส่วนของเซ็นเซอร์ GQDs ผู้วิจัยแสดงให้เห็นถึงประโยชน์และการนำไปประยุกต์ใช้อย่างกว้างขวางของไฮบริดนาโน GQDs/AuNPs โดยนำมาตรวจวัดซีสเทอีน (Cys) และไลซีน (Lys) โดยใช้ยูวีวิสิเบิลและฟลูออเรสเซนต์สเปกโทสโกปีตามลำดับ สำหรับวิธีการตรวจวัด Cys สามารถเหนี่ยวนำให้เกิดการรวมตัวของ GQD/AuNPs ทำให้เกิดการเปลี่ยนสีของสารละลายจากสีแดงเป็นสีน้ำเงินและค่าการดูดกลืนแสงเลื่อนจาก 525 nm เป็น 645 นาโนเมตร ส่วน Lys จะคายแสงกลับคืนมาที่ 450 นาโนเมตร ซึ่งเป็นการคายแสงของ GQDs จากผลการทดลองนี้เป็นการบ่งชี้ถึงการแทนที่ของ Lys บนพื้นผิวของ AuNPs และปลดปล่อย GQDs อิสระออกมาในสารละลาย เซ็นเซอร์ GQD/AuNPs มีการเลือกจำเพาะอย่างสูงต่อ Cys และ Lys โดยให้ค่าขีดจำกัดของการตรวจวัดเท่ากับ 5.88 μM และ 16.14 μM ตามลำดับ นอกจากนี้ GQDs/AuNPs ยังสามารถวิเคราะห์ Cys ในตัวอย่างปัสสาวะและ Lys ในตัวอย่างนม ในเชิงปริมาณได้อย่างมีประสิทธิภาพ ในด้านเวลาวิเคราะห์และความเลือกจำเพาะอย่างดี

ภาควิชา เคมี ลายมือชื่อนิสิต .....

สาขาวิชา เคมี ลายมือชื่อ อ.ที่ปรึกษาหลัก .....

ปีการศึกษา 2560

5572860023 : MAJOR CHEMISTRY
KEYWORDS: NANOMATERIAL SENSORS, BIOTHIOL, MICELLE, 3D MICROFLUICDIC DEVICE, GRAPHENE QUANTUM DOTS

CHIRAPORN CHAICHAM: NANOMATERIAL SENSORS FOR SELECTIVE DETECTION OF BIOTHIOL COMPOUNDS. ADVISOR: ASST. PROF.BOOSAYARAT TOMAPATANAGET, Ph.D., 96 pp.

Novel nanomaterial sensors have been designed two different strategies of sensing approach. The first sensing system, the aggregation nanomicelles (TSC and TSD) were synthesized for GSH sensing based on disulfide-cleavaged trigger in the micelle. The result showed a large quenching fluorescent intensity around 587 nm and 528 nm corresponding to TSC and TSD, respectively, upon the addition of GSH in 2.5% DMSO/PBS at pH 6. Additionally, the benefit of TSD is utility for the distance-based fluorescence detection of 3D paper analytical device (3D-µPAD) for the detection of GSH.

Apart from GQDs sensors base, we demonstrated the utility and board applicability of GQDs/AuNPs nanohybrid with measurements of Cysteine (Cys) and Lysine (Lys) using UV-Visible and fluorescent spectroscopy, respectively. For Cys sensing approach, the Cys enable to induce the self-aggregation of GQDs/AuNPs resulting in the color change from red to blue and red shift from 525 nm to 645 nm. On the other hand, Lys exhibited the fluorescence recovery at 450 nm belonging to emission band of GQDs. This is indicative of the displacement of Lys on AuNPs and releasing free GQDs in the solution. This sensor provided a high selectivity toward Cys and Lys with LOD of 5.88 µM and 16.14 µM, respectively. Furthermore, GQDs/AuNPs offered an efficient quantitative determination of Cys in urine samples and Lys in milk samples with real time analysis and highly specific detection.

Department:	Chemistry	Student's Signature	.....
Field of Study:	Chemistry	Advisor's Signature	.....
Academic Year:	2017		

ACKNOWLEDGEMENTS

I wish to express deepest appreciation to my thesis advisor, Assist. Prof. Dr. Boosayarat Tomapatanaget for kindness, constant encouragement, suggestions and assistance, involving supports throughout my Ph. D career. In addition, I would like to thank Assoc. Prof. Dr. Vudhichai Parasuk, Prof. Dr. Supason Wanichwecharungruang, Asst. Prof. Dr. Fuangfa Unob and Dr. Gamolwan Tumcharern for their interest, value suggestions, comments as committee members and thesis examiners.

This thesis would not be successful without kindness, encouragement, and helps of the members of the Supramolecular Chemistry Research Unit. Particularly, Mr. Anusak Chaicham provides for consultation and assistance about my research. Moreover, I would like to thanks Miss. Piyanan Pranee for supporting blood sample and characterization nanomaterials.

I would like to thanks the Human Resource Development in Science Project (Science Achievement Scholarship of Thailand, SAST) to support covering full tuition and stipend in academic program. Moreover, I wish to thanks many supporting for the 90th Anniversary of Chulalongkorn University and Center of Excellence on Petrochemical and Materials Technology, Thailand.

Finally, I would like to express my deepest gratitude to my family for their love, care, kindness, encouragement and other assistance throughout my life.

CONTENTS

Page

Page

LIST OF FIGURES

CHAPTER I: Introduction and literature reviews

CHAPTER II: Glutathione sensing

APPENDIX

LIST OF SCHEMES

LIST OF TABLES

CHAPTER II: Glutathione sensing

CHAPTER III: Cysteine sensing

LIST OF ABBREVIATIONS

°C	Degree Celsius
^{13}C-NMR	Carbon nuclear magnetic resonance
^{1}H-NMR	Proton nuclear magnetic resonance
equiv.	Equivalent
g	Gram
Hz	Hertz
J	Coupling constant
mmol	Millimole
mL	Milliliter
nm	Nanometer
M	Molar
M^{-1}	Per molar
δ	Chemicalshift
ppm	Part per million
s, d, t, m	Splitting patterns of ^{1}H-NMR (singlet, doublet, triplet, multiplet)

Chapter I
Introduction and Literature reviews

Biothiols are biological molecules that are commonly found in the biological environment. There are three biothiol molecules including cysteine (Cys), homocysteine (Hcy), and glutathione (GSH) as shown in the Figure 1.1. These compounds consist of mercaptan (-SH) as a main functional group in their structures. Generally, biothiols demonstrated a pivotal role in maintaining proper body function, including protein and DNA synthesis, enzyme activity, metabolism and cell protection [1]. Moreover, all thiols also play important antioxidants to prevent oxidative damage. Abnormal biothiol levels can indicate a malfunction of the body. For instance, Cys is also one of major amino acid to healthy immune system. The deficiency of Cys caused many diseases such as liver damage, skin lesions, slow growth in the children and lethargy [2]. Hcy is normally generated in the part of methylation process of human body. The high level of Hcy in plasma could take a part of increased risk of cardiovascular disease, Alzheimer's disease, inflammatory bowel disease, and osteoporosis [3]. Interestingly, GSH is a powerful antioxidant that can prevent the DNA and RNA destructions. The abnormal level of GSH directly links to various diseases such as cancer, ageing and heart problem [4]. Therefore, the intracellular biothiol levels sensing has been applied for diagnostic tool. There are few reports of chemosensor for detection of small bio-thiol molecule [5, 6]. The identical reaction of thiol moiety causes a strong interference. Thus, the design of the molecular sensor with high selectivity and classify type of bio-thiol have been challenged.

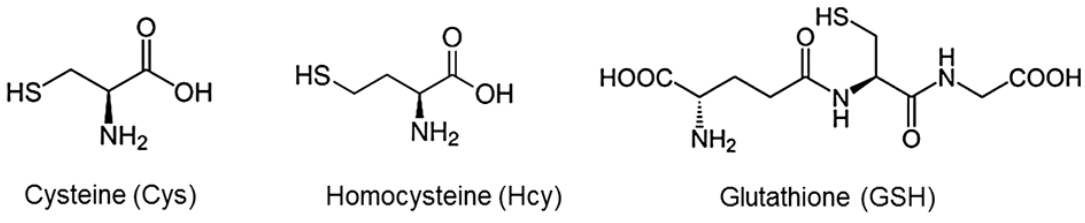

Figure 1.1. The chemical structures of biothiol molecules

Zhang and co-workers [7] designed the fluorescence probe based on GSH-responsive disulfide-cleavaged bond. The naphthalimide derivative containing disulfide moiety was synthesized. Upon adding the GSH, the emission band shifted from 485 nm to 533 nm and the color solution changed from colorless to yellow. The amount of GSH was related to the ratio of the metrical fluorescence change as shown in Figure 1.2.

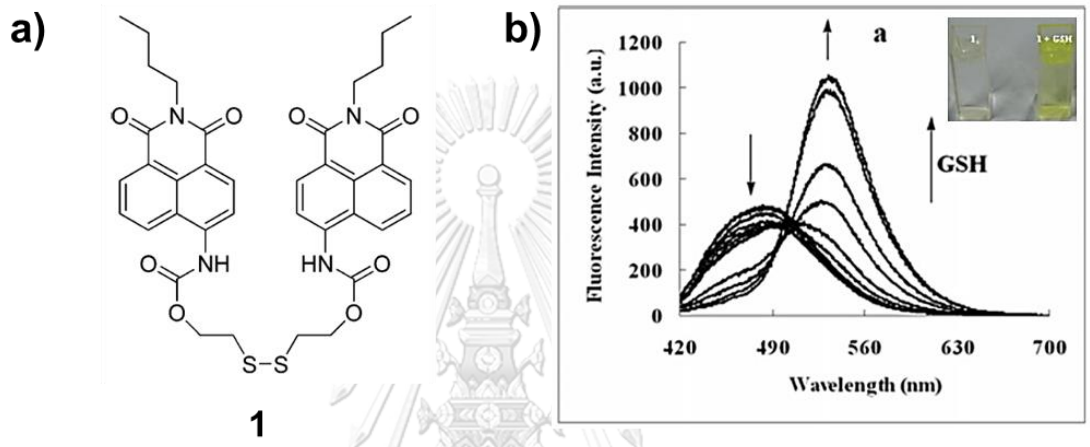

Figure 1.2. The molecular structure of compound **1** (a); and the emission spectra of compound **1** in the presence of GSH and inset showed the visual color solution (b**)** [7]

In order to increase the effective selectivity and sensitivity of biothiol molecules, the molecular nanosensor has been developed to determine the biological compounds. The interesting properties of nanomolecular materials are good biocompatibility, low toxicity, highly dispersability and stability in water [8]. Cui and coworkers [9] synthesized nanocarrier of PEG modified on surface of mesoporous silica nanoparticles (MSNs). The MSNs-SS-mPEG nanohybrid system composes of disulfide bond as a linker between MSNs and PEG acting as a storage and gatekeeper, respectively. The labeling fluorescein dye was employed as a biomarker to follow the change of fluorescence signal after adding GSH. The control-released aspect of fluorescein molecules depends on the concentration of GSH which induced redox reaction process of the cleavage of disulfide bond as shown in Figure 1.3.

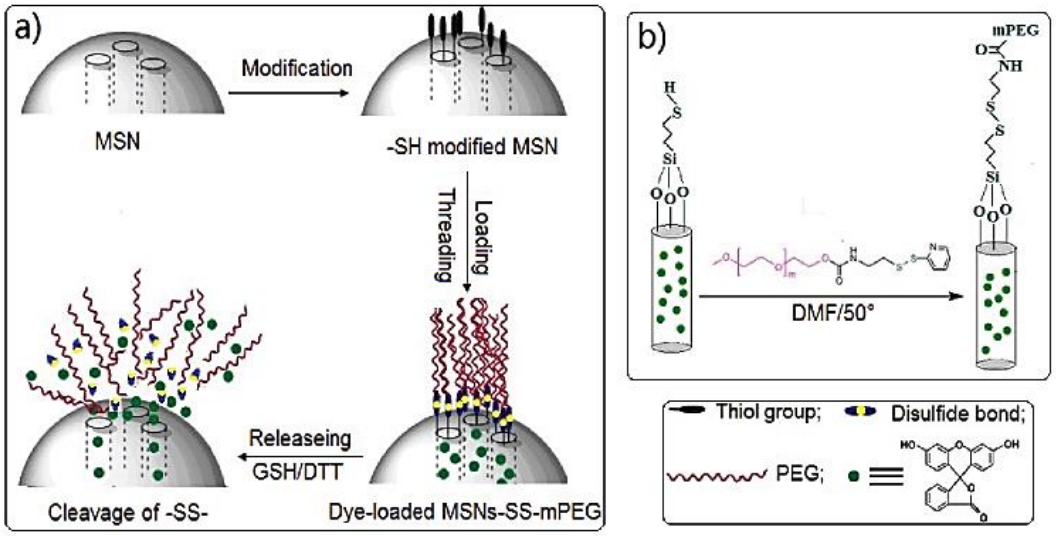

Figure 1.3. Synthetic pathway of MSNs-ss-mPEG nanoparticle and disulfide cleavage model after adding GSH/DTT under redox reaction process (a); and the modification disulfide bound on MSNs (b) [9]

Self-assembly micellar nanocarrier is the one of popular method for monitoring analytes of intracellular. The micellar assemblies are relatively soluble in aqueous solution and provide hydrophobic nanocontainers to encapsulate the fluorescent molecular sensors. Micelle formation consists of surfactant molecules which contain a polar head group and a hydrophobic chain. There are 3 types of surfactant including SDS, CTAB and Triton-X 100 as a anionic, cationic and neutral molecule as shown in the Figure 1.4. Surfactants are mostly used to form heterogeneous organized assemblies such as micelles, bilayers, and vesicles [10] depending on the concentration [11], temperature [12] and pH [13].

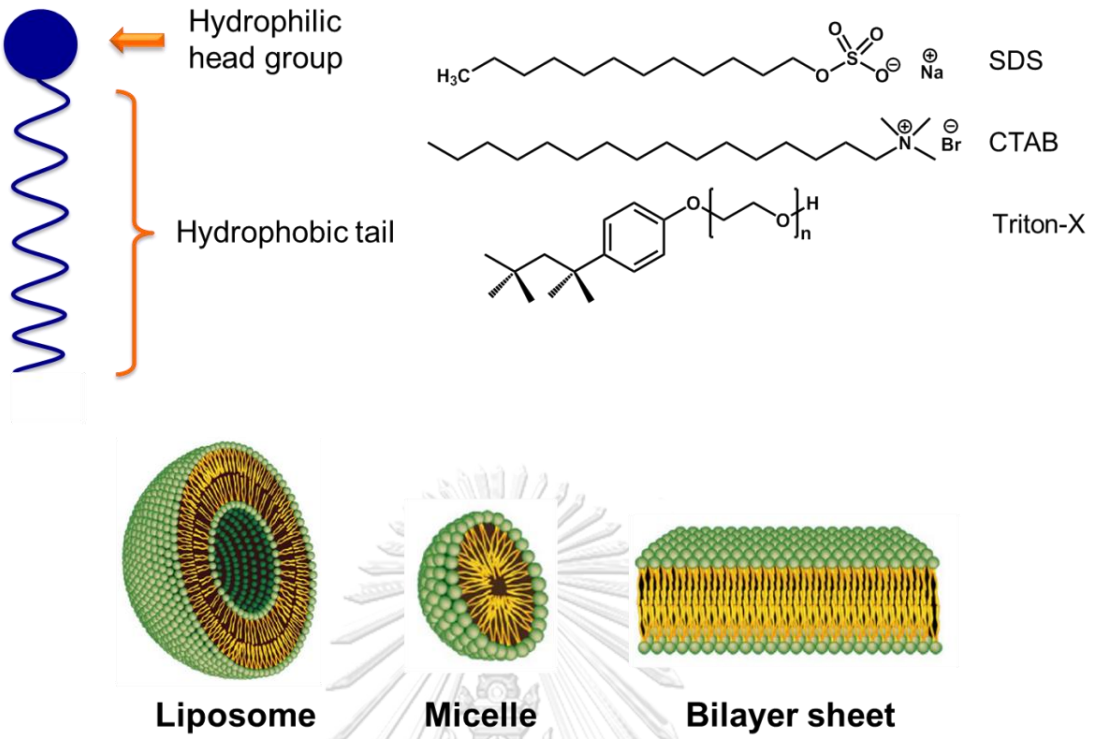

Figure 1.4. Conformation of surfactant and self-aggregation of surfactant

Xu and coworkers [14] reported a responsive polymeric micellar system to GSH. The polymeric nanosphere contained disulfide bond located in the center of two hydrophilic PEG chains to encapsulate DOX drug (Figure 1.5). Upon the addition of GSH, the anticancer drug in micelle was released by deconstruction of self-assembled PEG via the cleavage of disulfide linkages in polymeric micelle. The degradation rate of micelle depending on the concentration of GSH is higher than 5 mM.

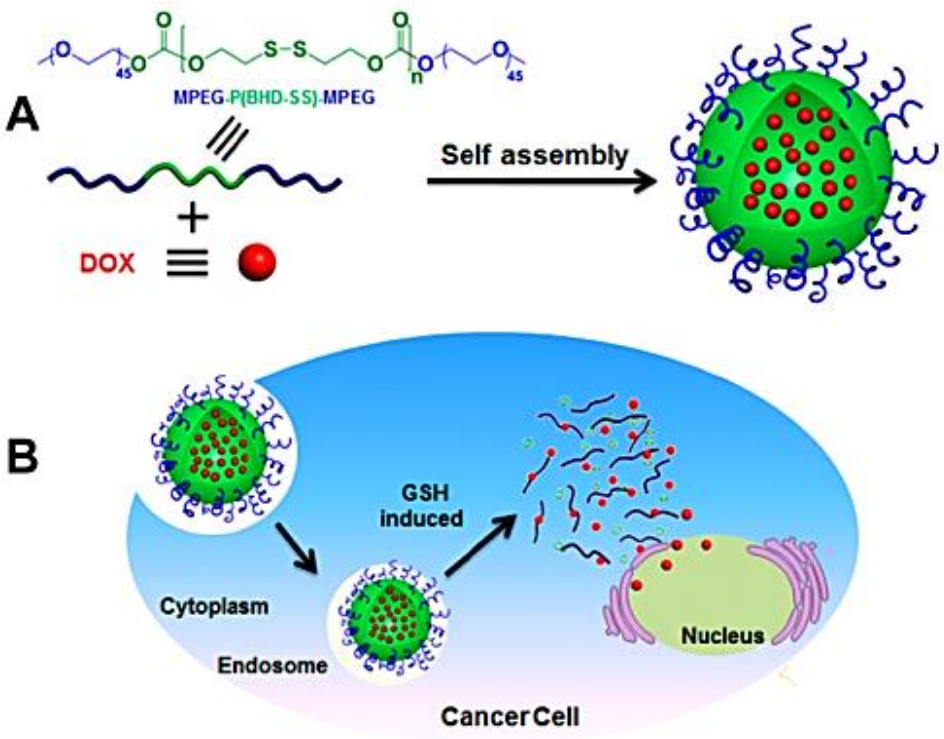

Figure 1.5. Self-assembly of polymeric micelle structure of MPEG-P(BHD-SS)-MPEG (A) and the degradation of polymeric micelles under GSH control release (B) [14]

Na Re Ko and Jung Kwon Oh [15] have successfully developed the aliphatic polyesters of polylactide (PLA)-based copolymer for GSH responsive. The PLA block copolymer consists of disulfide as a middle block to link two hydrophobic block (DL-ssABP). The self-assembled nanomicelle of DL-ssABP copolymer showed a great encapsulation of doxorubicin drug as a cancer drug therapy. The degradation of disulfide bond in DL-ssABP micelle was chemically cleavaged to thiol moiety at the high GSH concentrations (Figure 1.6) from the confocal laser scanning microscopy confirmed the demicellization of nanocarrier in the HeLa cancer cell.

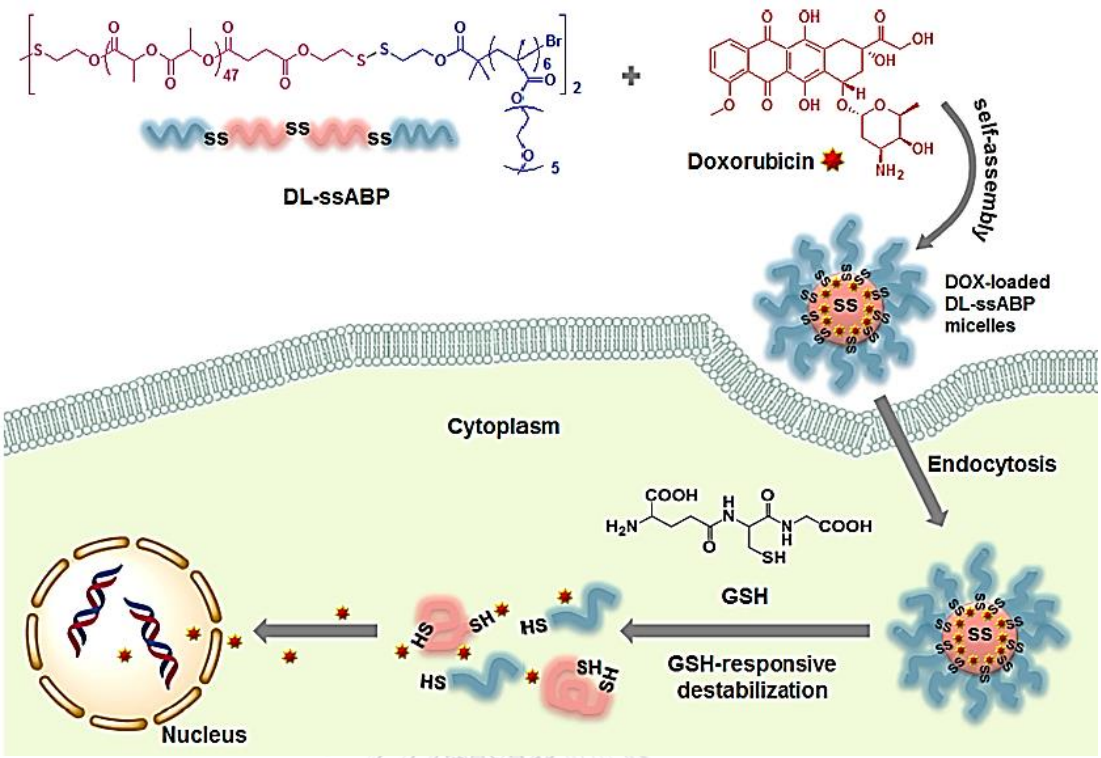

Figure 1.6. Drug delivery nanocarriers of DL-ssABP triblock copolymer responded to GSH in intracellular [15]

In the case of cysteine sensing, metal nanoparticles (Ag and Au) have been reported in a range of biological environment especially biothiol molecules. The self-aggregation of particles induced to simply visualize by the naked eye [16, 17]. It is well-known that, the sulfhydryl (thiol) and amine side chain of amino acids are highly sensitive bound to AuNPs. Moreover, self-aggregation of AuNPs can be easily induced undergone an electrostatic interaction of zwitterion species. The mechanism of functionalized-AuNPs aggregation toward biothiol species (cysteine, cysteine, and glutathione) was reported by Acres [18]. The results showed that both of Cys and GSH were chemically adsorbed on AuNPs through thiol species of cysteine residue. The color of solution changed immediately to dark blue (Figure 1.7).

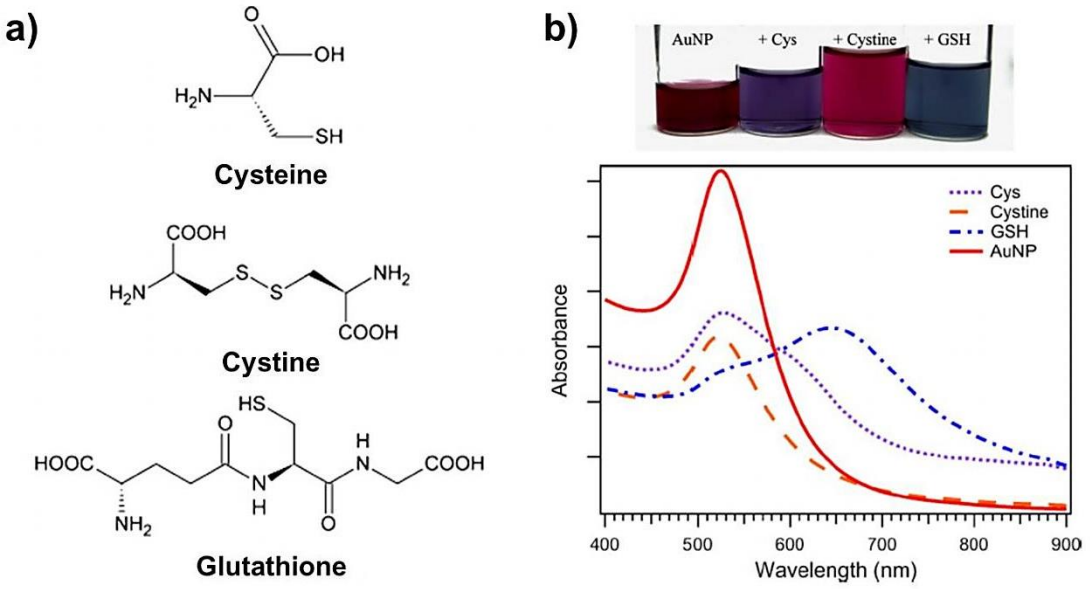

Figure 1.7. The chemical structures (a) and absorpsion spectra and photograph (b) of molecular sensor AuNPs, Cys/AuNPs, cysteine/AuNPs, and GSH/AuNPs solution [18]

Moreover, a luminescent quantum dots (QDs) is one of a nanoparticles of semiconducting material with an average diameter size in the range of 2-10 nm. The electronic characteristics of quantum dots were determined by size of the particles. The quantization energy level of QDs consists of the electron in the conduction band and the hole in the valence band [19, 20]. The difference of energy level depended on particles size (Figure 1.8). Due to the small particles, the difference of energy level between conducting band and valence band increased. It required more energy to excite the dot in the hole of valence band and returned to its ground state, resulting in a color shift from blue to red in the emitted light. This phenomenon of QDs produced luminescence light by changing the size of particle dots [21].

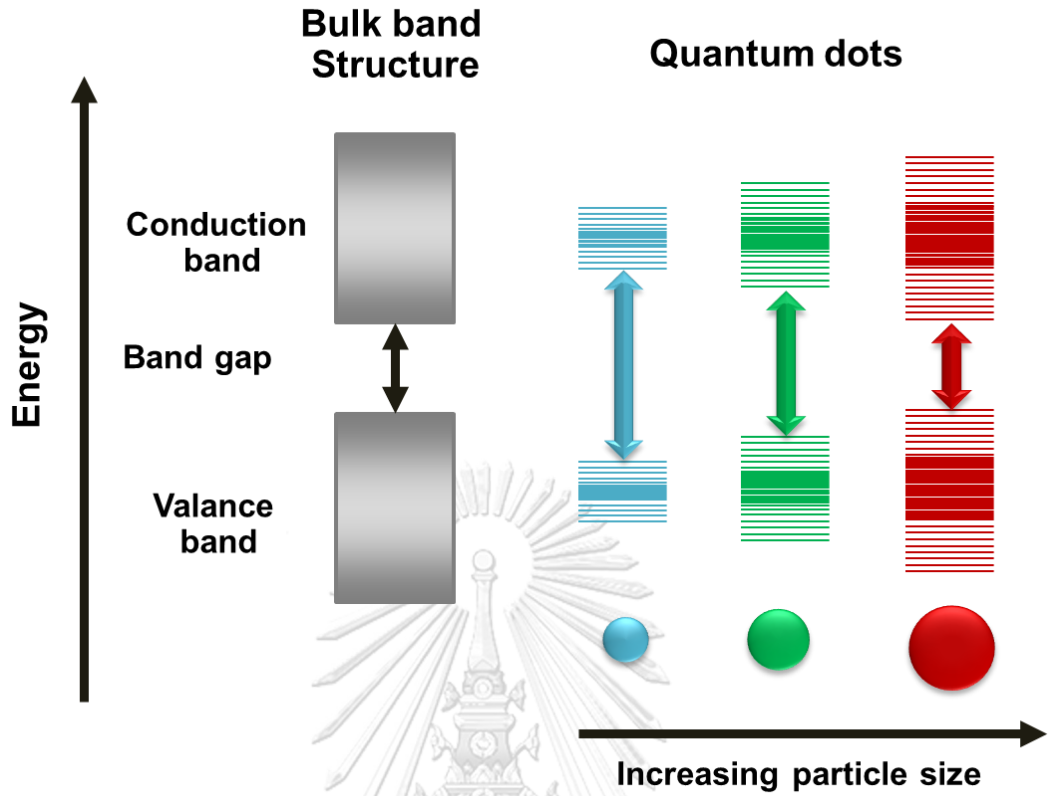

Figure 1.8. The quantization energy levels of quantum dots related in size and chemical composition

Graphene quantum dots (**GQDs**) are the one type of QDs that are carbon based nanomaterial and showed unique optical properties and great potential application in many fields [22-24]. The functionalization on the surface of GQDs was reported by doping other atoms to make a great selectivity of target molecule [25, 26]. Moreover, AuNPs incorporated with graphene quantum dots (**GQDs**) to form nanohybrid material as a model target analyst have generated a great deal of attention and more activity in the past decades [27-29]. This interest has been motivated by the potential that these materials offer in sensor development both *in vitro* and *in vivo* [30, 31]. For example, the hydrazide-modified graphene quantum dots (HM-GQDs-AuNPs) was reported by Dong's research [32]. The nano-hybrid was synthesized between HM-GQDs and AuNPs. The $HAuCl_4$ was reduced by HM-GQDs to produce AuNPs which lead to form HM-GQDs-AuNPs as a model target analyst in bio-sensing (Figure 1.9).

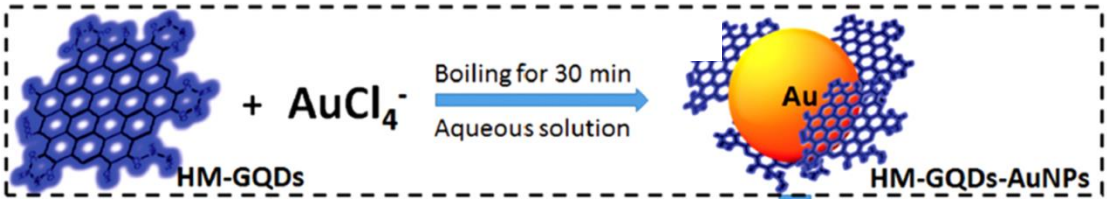

Figure 1.9. The preparation of HM-GQDs-AuNPs as a model target analyst in bio-sensing [32]

Zhang and co-workers [31] developed the multi-signals of nanosensor composite for discrimination of biothiol compounds. The nanosensors composed of AuNPs supported on nitrogen-doped C-dots (NC-dots) using electrochemical carbonization method. Upon adding Cys incubated with NaOH (pH 12) for 12 h, the absorbance band of NC-dots/AuNPs hybrids shifted from 680 nm to 525 nm. The color solution of nanohybrids changed from purple to red and the recovered fluorescence of NC-dots under these optimum conditions as shown in Figure 1.10.

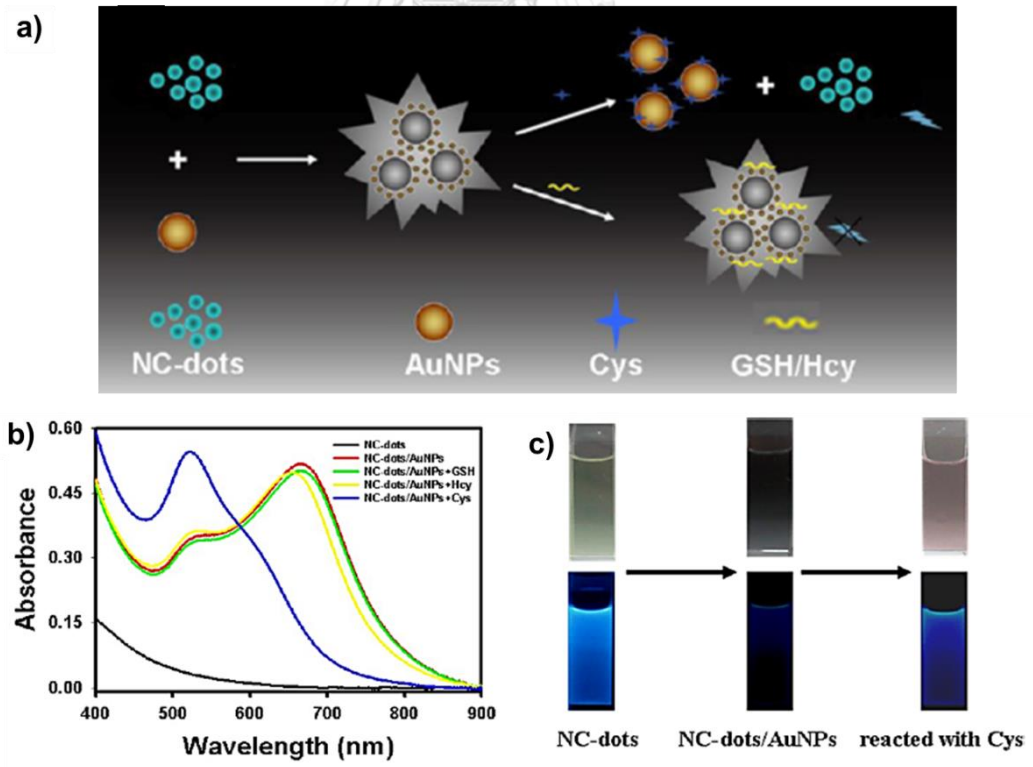

Figure 1.10. The multi-signals of NC-dots hybrid AuNPs for discrimination of biothiol compounds (a), the absorption spectra (b) and digital pictures (c) in the presence of Cys under visible light (top) and fluorescence light (bottom) [31]

Moreover, the fluorescent nanoprobe was designed by Tang 's research [30]. The nanoprobe was synthesized by amino N-dots combine with AuNPs (aN-dots/AuNPs) acting as a model target probe which induced the fluorescence quenching through energy transfer process. The enhancement of fluorescence feature of aN-dots/AuNPs was recovered in the presence of Cys because of thiol species of Cys bound on AuNPs surface (Figure 1.11). Moreover, these nanoprobes can be utilized to detect Cys in biological samples.

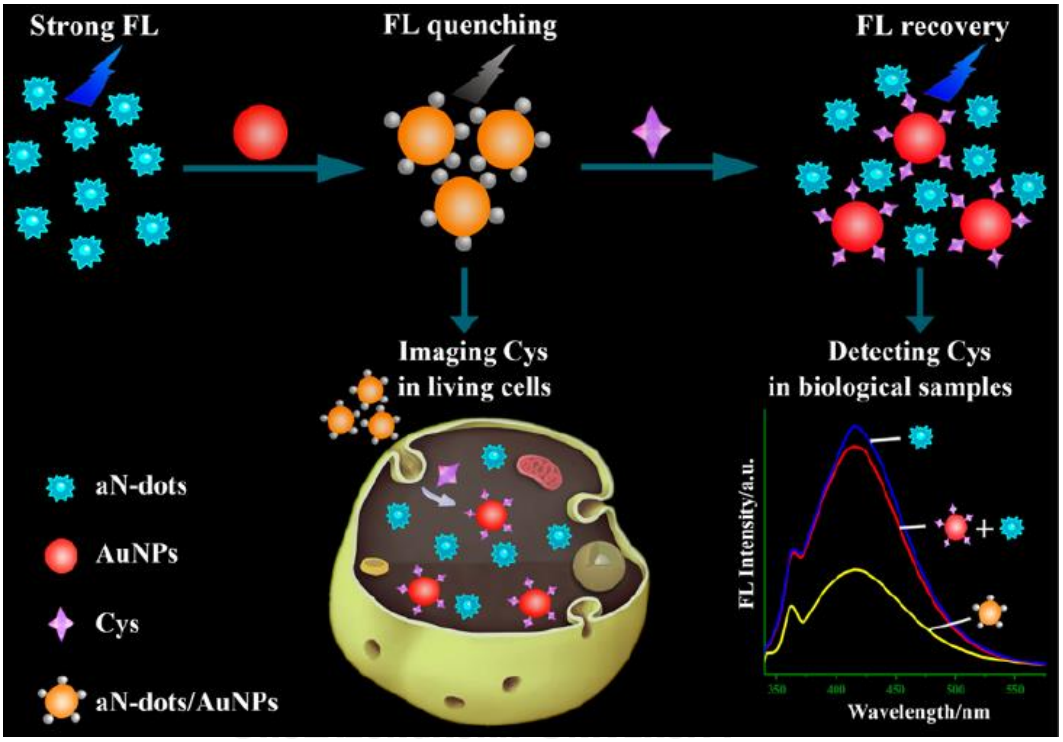

Figure 1.11. The principle of fluorescent nanoprobe hybride of aN-dots with AuNPs for Cys sensing approach [30].

Taking on broad for the efficient applicability of sensor in paper based device, Gregory G. Lewis and co-workers [33] synthesized compound **1** to detect the H_2O_2 on 3D-μPAD by counting the number of colored bars. This device was designed into 8 layers and 16 bars. All bars were deposited in the same reagent in each layer but the hydrophobic molecule was deposited in layer 3 and layer 5 at different concentration in each bar (Figure 1.12). After adding the H_2O_2, the hydrophobic molecule of compound **1** changed to hydrophilic molecule. Consequently, the green bae on the top

of the layer was observed. The number of green bar depended on concentration of analyte. Thus, this device could be used to determine the concentration of analyte.

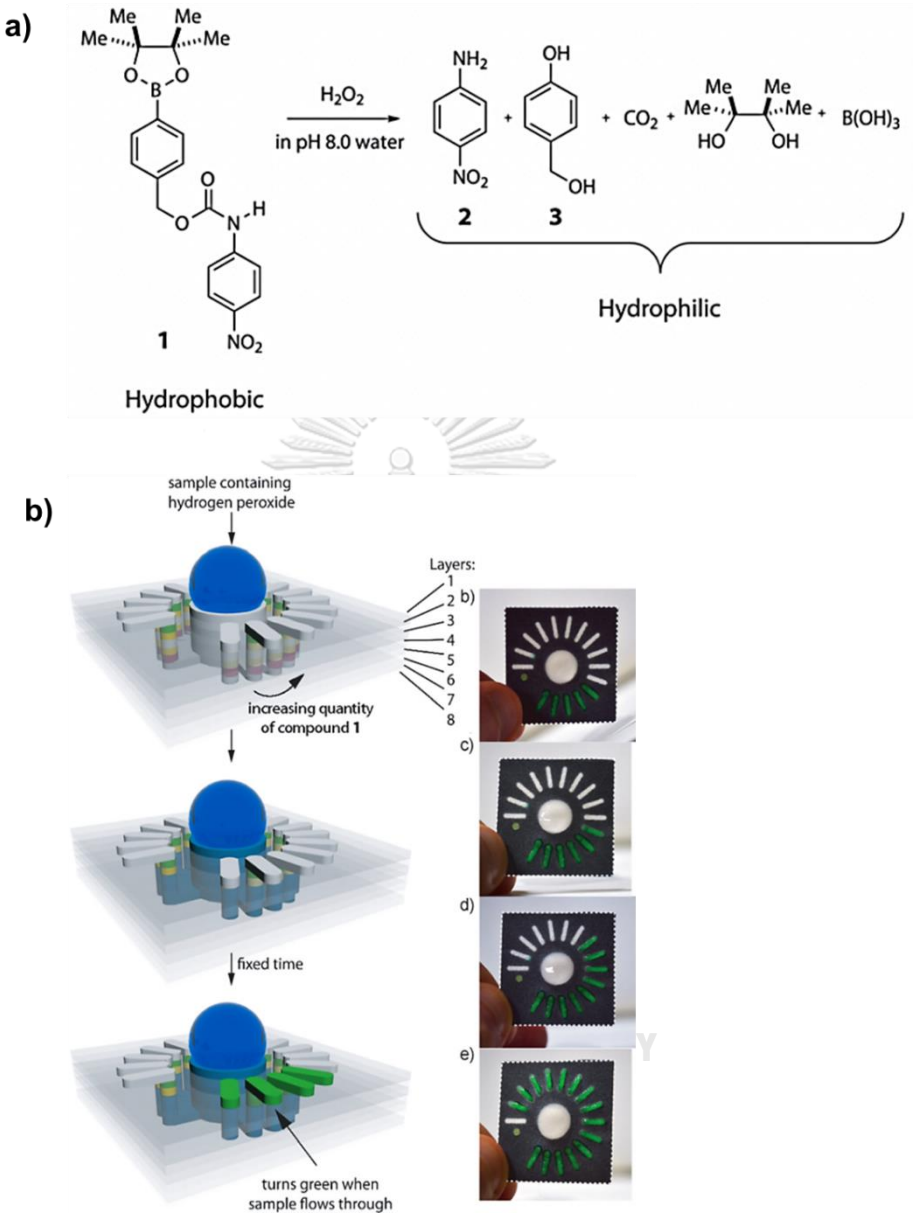

Figure 1.12. The detection of hydrophobic of compound **1** toward H_2O_2 sensing approach (a); and photograph of 3D-μPAD in the different concentration of H_2O_2 (b) [33]

Due to the biothiol substances in intracellular, the required sensor molecule should be low toxicity and biocompatibility. However, the discrimination of amino acids is also quite difficult due to these amino acids comprising thiol and amine group

as a consequence of inferences for monitoring in biological samples. Consequently, the molecular nanosensor is a popular alternative material that can be functionalized on the surface of nanomaterial and is highly selective toward biomolecules. From the mentioned above, we have paid attention to design and synthesize the new nanomaterial for bio-thiol detection. In our work, this research aims to fabricate the nanomaterial for discrimination of biological thiols under different approaches including:

(I) Self-assembly micellar nanosensor for GSH sensing approach and applied into 3D-μPAD for quantitative analysis,

(II) *In situ* preparation of **GQDs/AuNPs** hybrid materials effectively used for Cys and Lys sensing approach by UV-Visible and fluorescence technique, respectively.

Chapter II
Glutathione sensing

2.1. Introduction

Glutathione (g-L-glutamyl-L-cysteinglycine, GSH) is an essential endogenous antioxidant that plays an important role in maintaining proper biological functions, including protein and DNA synthesis, enzyme activity, metabolism and cell protection, inside an organism [1]. GSH is the most abundant intracellular biothiol which has multiple cellular functions such as xenobiotic metabolism, gene regulation, intracellular signal transduction and also cellular protection from the destruction of reactive oxygen species (ROS) [34]. Abnormal levels of GSH lead to cancer, aging, heart problems, and other [4, 35, 36]. Thus, the detection and quantification of GSH in biological samples is crucial. There are several techniques for the detection of GSH such as electrochemistry [17, 37], HPLC [6], mass spectroscopy [38], etc. All of techniques that mentioned above have the high sensitivity. However, many disadvantages of them are high costs and long time-response sample treatment.

Recently, great efforts to develop bio-molecule sensors based on the organic/inorganic hybrid materials have been reported to employ versatile nanomaterials as platforms. Among various nanomaterials, excellent solubility, stable fluorescence and good biocompatibility of self-assembled colloidal carriers has been suggested as well-defined fluorescent probe since it can be easily prepared to endow the excellent encapsulation of dyes for enhancement of high optical properties in aqueous. Nevertheless, the ease and cost-effectiveness of the surfactant based micelle or vesicle systems have made them widely used until today. Furthermore, self-assembly micellar nanocarrier is one of the popular methods for monitoring intracellular analytes. Such supramolecular assemblies are relatively soluble in aqueous solution and provide hydrophobic nanocontainers to house the fluorescent molecular sensors. In this structural motif, the fluorescent sensors entrapped in nanocontainer play an important role in detection of required targets in aqueous environments. A fascinating disulfide-cleavage-triggered behaviour is inspired for drug delivery and sensing aspects. Of particular effective chemical properties of

disulfide bond is stable under physiological conditions in blood circulation and extracellular cells. However, this bond can be quickly broken in a highly reductive environment within cells promoting the relative intracellular release. This holds out a tremendous promise to create the biothiol sensing platform based on disulfide-cleavage-triggered mechanism.

Furthermore, self-assembly micellar nanocarrier is the one of popular method for monitoring analytes of intracellular. Micelle formation consists of surfactant molecules which contain a polar head group and a hydrophobic chain. Surfactants are mostly used to form heterogeneous organized assemblies such as micelles, bilayers, and vesicles [10], depending on the concentration [11], temperature [12] and pH [13]. Such supramolecular assemblies are relatively soluble in aqueous solution and provide hydrophobic nanocontainers to house the fluorescent molecular sensors. In this structural motif, the fluorescent sensors entrapped in nanocontainer are important role for detection of targets in aqueous environments.

Herein, we attempt to construct the self-aggregation inverse micelles for hydrophobic surface to allow only glutathione to perform the disulfide-cleavage-triggered mechanism with an expectation of fluorescent change. This study has been designed based on cost reduction, time saving for operation, easy preparation and environment friendly. We choose the commercial surfactant of Triton-X 100 and a co-surfactant of a simple disulfide compound which enables to be prepared only one step. The fluorescent dyes in this study are Dansyl boronic acid (**DA**) and Curcumin derivatives (**Cur-BF_2**) obtained from Turmeric plant which is spread grown in Thailand. As a challenging task for optimization of the ratio between Triton-X 100 and **S2**, it was found that the higher concentration of **S2** in forming the nanomicelle would effectively control the disulfide-cleavage-trigger reaction regarding to the significant fluorescent change in a proportional to the amount of GSH in the system. Interestingly, this nanomicelle would be applied to the distance-based 3D μPAD for a real time detection and a convenient portable device.

2.2. Conceptual design

In this research we attempt to design the fluorescent probe to measure the concentration of GSH. Based on the information mentioned above, GSH could be used as a reducing agent to cleave the disulfide bond and consequently produce the thiol groups. In this concept, we have designed inverse nanomicelle based on the mix surfactant of Triton-X 100 and a long chain disulfide compound to encapsulate the fluorescent dye. Upon addition of GSH, we expected that the disulfide bond of **S2** in micelles would be chemically cleaved resulting in deconstruction of micelle and the encapsulated fluorescence dye would be released. This phenomenon induces the change of fluorescent signal of the dye as shown in Scheme 2.1. Curcumine-BF_2 (**Cur-BF_2**) and dansyl boronic acid (**DA**) were chosen as a fluorescent dye which is encapsulated in inverse micelle. Since both of fluorescent dyes normally provide a strong fluorescent signal in the organic solvent but they exhibit a weak fluorescent signal in an aqueous media.

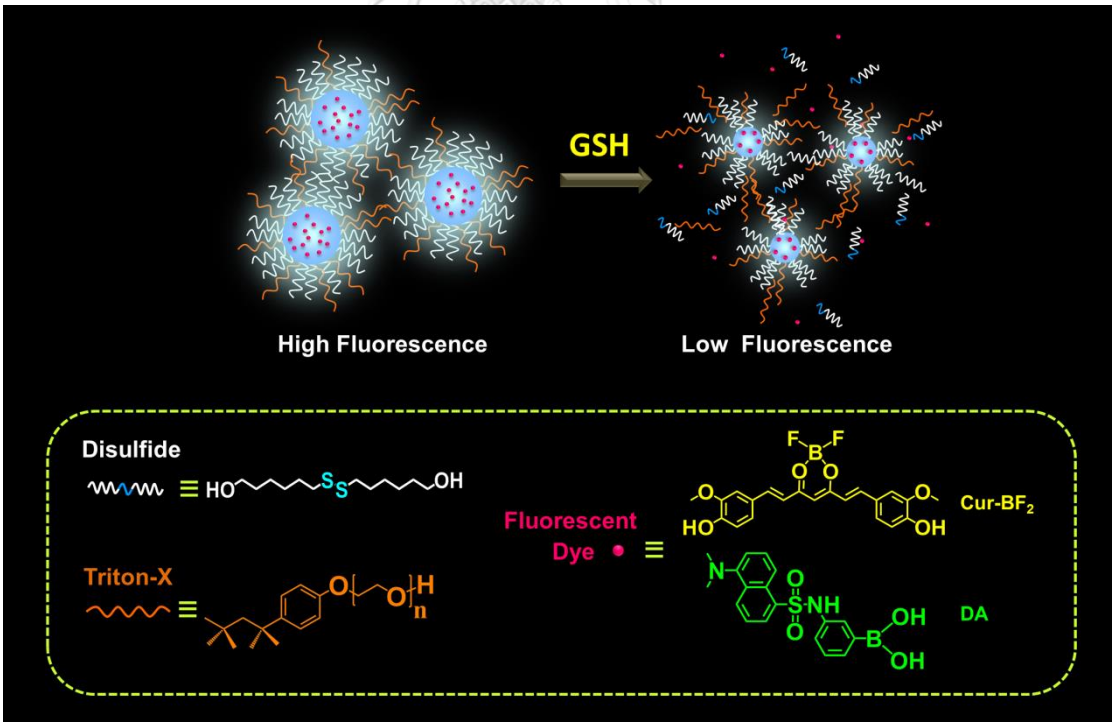

Scheme 2.1. The conceptual design of glutathione detection based on disulfide-cleavage

2.3. Experiments

2.3.1. General procedure

2.3.1.1. Reagents and Materials.

The 6-mercapto-1-hexanol was purchased from TCI. Iodine crystal was received from Alpha Chemika. Sodium thiosulfate pentahydrate ($Na_2S_2O_3 \cdot 5H_2O$) was purchased from Merck. Triton-X 100 surfactant was purchased from OmniPur. L-glutathione (GSH, reduced > 98%) was bought from Calbiochem. Amino acids (Leu, Met, Thr, Phe, Lys, Ala, Gly, Hcy and Cys) were purchased from Sigma Aldrich. All solvents and reagents are analytical grade and used without further purification. Milli-Q ultrapure water was used for experimental analysis.

2.3.1.2. Analytical instrument.

All nuclear magnetic resonance (^1H and ^{13}C) spectra were recorded on a Varian 200, 400 and Bruker DRX 400 MHz. In all cases, samples were dissolved in deuterated chloroform ($CDCl_3$). Absorption spectra were measured on a Varian Cary 50 UV-Vis spectrophotometer. Fluorescence spectra were performed on a Varian spectrofluorometer by personal computer data processing unit. The mass spectra were recorded by MALDI-TOF on Bruker Daltonic using doubly recrystallized 2-cyano-4-hydroxy cinnamic acid (CCA) as matrix. All nanomicelle were separated by using Eppendorf centrifuge 5804R and were characterized by High Resolution Transmission Electron Microscopy (HR-TEM) with an accelerating voltage of 80 kV. Size distributions of nanomaterials were reported by Dynamic Light Scattering (DLS). UV light was used on paper based device under wavelength 254 nm.

2.3.2. Synthesis of bis(6-hydroxyhexyl disulfide), S2

The 6-mercapto-1-hexanol (1.304 g, 5.564 mmol) and iodine (0.758 mL, 5.564 mmol) were completely dissolved in 15 mL methanolic solution and stirred until the solution turned from colorless to a persistent yellow under ambient temperature for 24 h. After the reaction complete, the solvent was removed under reduced pressure and

the saturated aqueous solution of sodium thiosulfate pentahydrate was added for quenching reaction. The crude product was extracted with dichloromethane and the organic phase was collected. Anhydrous sodium sulfate was used to dry the organic phase and the organic solvent was removed in vacuum. A residue was purified by column chromatography using 100% dichloromethane to afford the white solid of **S2** (1.289 g, 87%).

Characterization data for bis(6-hydroxyhexyl) disulfide (S2)

^{1}H-NMR spectrum (400MHz, $CDCl_3$): δ (in ppm) = 3.66 (t, 4H, *J* = 2.8 Hz), 2.68 (t, 4H, *J* = 7.2 Hz), 1.73-1.66 (m, 4H), 1.62-1.55 (m, 4H), 1.47-1.35 (m, 8H).

^{13}C-NMR spectrum (100 MHz, $CDCl_3$): δ (in ppm) = 62.8, 39.0, 32.6, 29.1, 28.2, 25.3.

MS(ESI): m/z for **S2** = 265.27 $[M+H]^+$.

2.3.3. The preparation of micelle

*2.3.3.1. The micelle formation of Triton-X 100@S2⊂**Cur-BF_2 (TSC)**micelle, Triton-X 100 ⊂**Cur-BF_2 (TC)**micelle and S2⊂**Cur-BF_2 (SC)** micelle*

Typically, the stock solution of **S2** (0.1 M) and **Cur-BF_2** (0.001 M) in DMSO was prepared in 5 mL volumetric flask. The stock solution (0.1 M) of Triton-X 100 in phosphate buffer (0.5 mM) pH 6 was also prepared in 5 mL volumetric flask as shown in Table 2.1. The prepared stock solutions were used in all experiments.

Table 2.1. The amount of reagents were used to prepared a stock solution

Reagent	Molecular weight	Weight (mg)
Triton-X 100	646.86	323.43
S2	266.14	133.07
Cur-BF_2	416.18	2.08

The 10 µL of 0.1 M Triton-X 100 in PBS and 38 µL of 0.10 M **S2** in DMSO were mixed together and then the solution was adjusted to 3 mL by 2.5% DMSO/PBS solution. The mixture solution was sonicated for 10 min. After that, 15 µL of 1 mM

Cur-BF_2 in DMSO was added into the mixture solution and stirred for 5 min. The nanomicelle was purified by centrifuge under 5000 rpm for 5 min to obtain **TSC** nanomicelles.

The synthesis of **TC** was performed as the following procedure. 10 µL of 0.1 M Triton-X 100 and 15 µL of 1 mM **Cur-BF_2** in DMSO was mixed and stirred for 5 min. After forming micelle, the **TC** was purified by centrifuge under 5000 rpm for 5 min.

The **SC** micelle was formed by using 38 µL of 0.1 M **S2** in DMSO and 15 µL of 1 mM **Cur-BF_2** in DMSO was mixed and stirred for 5 min. The nanomicelle product was purified by centrifuge under 5000 rpm for 5 min to obtain **SC** nanomicelles.

All synthesized micelles were preliminary characterized by fluorescence spectroscopy technique under the excitation wavelength at 517 nm.

*2.3.3.2. Study on critical micelle concentration (CMC) of **TC** and **SC** by using fluorescence spectroscopy*

The CMC value of **TC** was evaluated as the following procedure: the concentration of Triton-X 100 (0.0333-1.1667 mM) was prepared as shown in Table 2.2. Then, 15 µL of 0.001 M **Cur-BF_2** was added directly into the mixture solution and adjusted to 3 mL. The fluorescence spectra were recorded under the excitation wavelength at 517 nm. Similarly, the preparation of **SC** was carried out by various concentration of S2 from 0.0083 to 0.0200 mM (Table 2.3).

Table 2.2. The amount of Triton-X 100 were used for study on CMC of **TC**

Entry	V of Triton-X 100 (mL)	[Triton-X 100] (mM)
1	0.001	0.0333
2	0.002	0.0667
3	0.005	0.167
4	0.010	0.3333
5	0.015	0.5000
6	0.020	0.6667
7	0.025	0.8333
8	0.030	1.0000
9	0.035	1.1667

Table 2.3. The amount of **S2** were used for study on CMC of **SC**

Entry	V of S2 (mL)	[S2] (mM)
1	0.025	0.8333
2	0.030	1.0000
3	0.035	1.1667
4	0.040	1.3333
5	0.041	1.3667
6	0.042	1.4000
7	0.045	1.5000
8	0.050	1.6667
9	0.060	2.0000

*2.3.3.3. The micelle formation studies of Triton-X 100 @S2⊂**DA (TSD)**micelle, Triton-X 100⊂**DA (TD)** micelle and S2⊂**DA** micelle (**SD***

Typically, the stock solution of **S2** (0.1 M) and **DA** (0.001 M) in DMSO was prepared in 5 mL volumetric flask. The stock solution (0.1 M) of Triton-X 100 in phosphate buffer (0.5 mM) pH 6 was also prepared in 5 mL volumetric flask as shown in Table 2.4. The prepared stock solutions were used in all experiments.

Table 2.4. The amount of reagents was used in micellar system studies

Reagent	Molecular weight	Weight (mg)
Triton-X 100	646.86	323.43
S2	266.14	133.07
DA	371.24	1.86

The micellar system of **TSD** was similarly prepared in the same manner as **TSC** in the topic of 2.3.3.1. Firstly, the 10 µL of 0.1 M Triton-X 100 of PBS and 38 µL of 0.10 M **S2** in DMSO were mixed together and then the solution was adjusted to 3 mL by 2.5% DMSO/PBS solution under sonication for 10 min. After that, 15 µL of 1 mM **DA** in DMSO was added into the mixture solution and stirred for 5 min. The nanomicelle was purified by centrifuge under 5000 rpm for 5 min to obtain **TSD** nanomicelles.

The synthesis of **TD** was performed as the following procedure. 10 µL of 0.1 M Triton-X 100 and 15 µL of 1 mM **DA** in DMSO was mixed and stirred for 5 min. After the forming of micelle, the **SD** was purified by centrifuge under 5000 rpm for 5 min.

For **SD** preparation, 38 µL of 0.1 M S2 and 15 µL of 1 mM **DA** were mixed and stirred for 5 min. The nanomicelle product was purified by centrifuge under 5000 rpm for 5 min to obtain **SD** nanomicelles.

All synthesized micelle were preliminary characterized by fluorescence spectroscopy technique under the excitation wavelength at 327 nm.

*2.3.3.4. Study on critical micelle concentration (CMC) of **TD** and **SD** by using fluorescence spectroscopy*

Similarly, the CMC value of Triton-X 100 was evaluated as the following method in the topic of 2.3.3.2. The concentration of Triton-X 100 (0.0667-1.0000 mM) was prepared as shown in Table 2.5. Then, 15 µL of 0.001 M **DA** was added directly into the mixture solution and adjusted to 3 mL. The fluorescence spectra were recorded under the excitation wavelength at 327 nm. The case of CMC of **SC** was

similarly prepared by various concentration of **S2** from 0.6667 to 2.0000 mM as shown in Table 2.6.

Table 2. 5. The amount of Triton-X 100 were used for study on CMC of **TD**

Entry	V of Triton-X 100 (mL)	[Triton-X 100] (mM)
1	0.002	0.0667
2	0.005	0.1000
3	0.007	0.2333
4	0.010	0.3333
5	0.013	0.4333
6	0.015	0.5000
7	0.020	0.6667
8	0.025	0.8333
9	0.030	1.0000

Table 2.6. The amount of **S2** were used for study on CMC of **SD**

Entry	V of S2 (mL)	[S2] (mM)
1	0.020	0.6667
2	0.030	1.0000
3	0.033	1.1111
4	0.035	1.1667
5	0.038	1.2667
6	0.040	1.3333
7	0.050	1.6667
8	0.060	2.0000

*2.3.3.5. Study on critical micelle concentration (CMC) of **TSC** and **TSD** by using fluorescence spectroscopy*

The CMC value of **TSC** was evaluated as the following procedure: 10 µL of 0.1 M Triton-X 100 was mixed with a various portions of **S2** in the range of 1.06-1.40 mM and then the mixture solution was continuously sonicated for 10 min. A constant amount of **Cur** dye 15 µL (from stock solution) was added into the solution and stirred for 5 min as shown in Table 2.7. After the **TSC** micelle forming, 20 µL of 1 mM GSH was added into the mixture solution and stirred for 20 min. Then fluorescent spectra were measured under excitation wavelength of 517 nm. The %quenching was calculated by using equation 1 to evaluate the CMC value. For **TSD** nanomicelle, the CMC of **TSD** was similarly preformed but **DA** was used as fluorescent dye as shown in Table 2.8 and the fluorescent spectra were recorded under excitation wavelength of 327 nm.

$$\% \text{ Quenching} = \frac{\text{Difference of sensor intensity before and after adding GSH}}{\text{intensity of sensor before adding GSH}} \times 100 \qquad (1)$$

Table 2.7. The amount of **S2** was used for study on CMC value of **TSC**

Entry	V of S2 (mL)	[S2] mM
1	0.032	1.0667
2	0.034	1.1333
3	0.036	1.2000
4	0.038	1.2667
5	0.040	1.3333
6	0.041	1.3667
7	0.042	1.4000

Table 2.8. The amount of **S2** was used for study on CMC value of **TSD**

Entry	V. of S2 (mL)	[S2] mM
1	0.032	1.0667
2	0.034	1.1333
3	0.036	1.2000
4	0.038	1.2667
5	0.040	1.3333
6	0.042	1.4000

2.3.4. Studies on selectivity toward amino acids

Typically, a stock solution (1 mM) of amino acids (Leu, Met, Thr, Phe, Lys, Ala, Gly, GSH, Hcy and Cys) was prepared in 5 mL volumetric flask with pH 6 PBS buffer solutions (shown in Table 2.9).

Table 2.9. The amount of amino acids were used for study on selectivity

Amino acids	Mw	Weight (mg)
Leucine, Leu	131.18	0.66
Methionine, Met	149.21	0.75
Threonine, Thr	119.12	0.60
Phenylalanine, Phe	165.19	0.83
Lysine, Lys	146.19	0.73
Alanine, Ala	89.09	0.45
Glycine, Gly	75.07	0.38
Glutathione, GSH	307.32	1.54
Homocysteine, Hcy	135.18	0.68
Cysteine, Cys	121.15	0.61

The selectivity of the prepared micelles was evaluated as the following procedure. From stock solution, 10 µL of 0.1 M Triton-X 100 was pipetted and added into a mixture of 38 µL of 0.1 M **S2** and 15 µL of 1 mM fluorescent dye (**Cur-BF_2** or **DA**). The total solution was adjusted to 3 mL by 2.5% DMSO/PBS solution (pH 6).

The mixture solutions were sonicated for 10 min to form micelle. Then 10 equiv of each amino acid (Leu, Met, Thr, Phe, Lys, Ala and Gly, GSH, Hcy and Cys) was added into the micelle solution which was stirred for 20 min before measurement of fluorescent spectrum under an excitation wavelength at 517 nm and 327 nm for **TSC** and **TSD**, respectively.

2.3.5. Studies on the quantitative analysis of TSC and TSD nanomicelle toward GSH by using fluorescent titration

A stock solution of GSH (1 mM) in PBS buffer solutions (pH 6) was prepared in 5 mL volumetric flask. The nanomicelle (**TSC** and **TSD**) was similarly preformed to the previous method as shown in the topic of 2.3.3.1 and 2.3.3.3. For quantitative analysis of **TSC** toward GSH, the **TSC** was titrated with various concentration of GSH from 0 to 0.33 mM and then the reaction was stirred for 20 min (as shown in Table 2.10). The fluorescent spectra of **TSC** with increment of GSH were recorded under an excitation wavelength at 517 nm. Upon the addition of GSH in the range of 0 – 0.5 mM into TSD solution, the solution was stirred for 20 min prior to the measurement of the fluorescent spectra under an excitation wavelength at 327 nm as shown in Table 2.11.

Table 2.10. The various concentration of GSH for fluorescent titration of **TSC** nanomicelles

Entry	V of GSH (mL)	[GSH] mM
1	0.00	0.00
2	0.05	0.02
3	0.10	0.03
4	0.15	0.05
5	0.25	0.08
6	0.40	0.13
7	0.60	0.20
8	0.80	0.27
9	1.00	0.33

Table 2.11. The various concentration of GSH for fluorescent titration of **TSD** nanomicelles

Entry	V of GSH (mL)	[GSH] mM
1	0.00	0.00
2	0.05	0.02
3	0.10	0.03
4	0.25	0.08
5	0.50	0.17
6	0.65	0.22
7	0.75	0.25
8	1.00	0.33
9	1.30	0.43
10	1.50	0.50

2.3.6. Construction of three-dimensional (3D) paper based microfluidic devices

The 3D paper-based microfluidic device (50 mm wide × 15 mm long × 1.5 mm high) was designed for quantitative analysis of GSH under length-based assays. This device consisted of 2 layers of papers and 2 layers of tapes. Watman Chromatography Paper No. 1 was used to be a patterned paper which was designed to hydrophilic and hydrophobic zone by Adobe Illustrator CS6 program. The hydrophobic zone was fabricated by a wax printer and double adhesive tape was assembled layer by layer to conduct 3D microfluidic devices as shown in Figure 2.1.

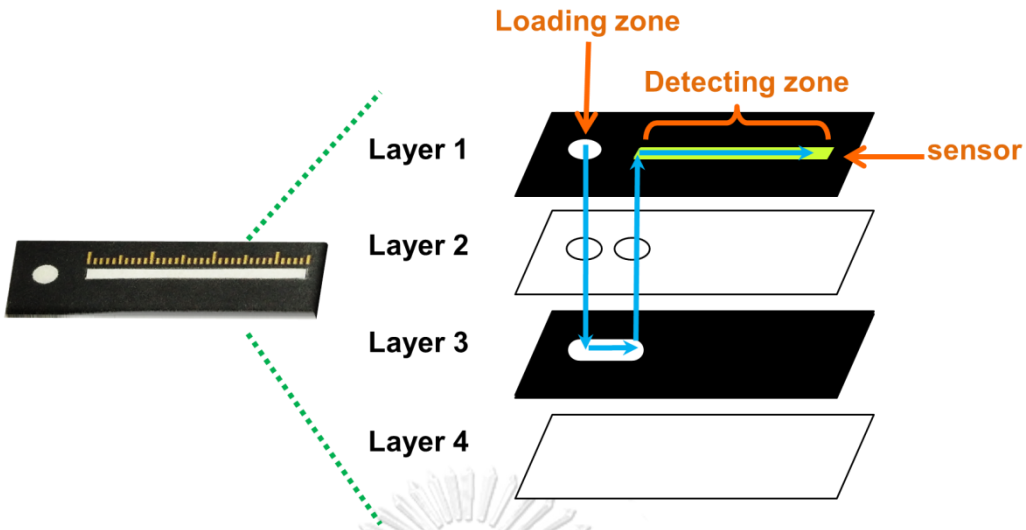

Figure 2.1. Design paper-based microfluicdic devices for determination of GSH concentration by the photo of prepared 3D paper base under light

The first layer of 3D-μPAD device was designed for measuring the fluorescent darkness. This layer composed of loading zone and detecting zone. The loading zone was designed to be a cycle with 0.5 cm of diameter. The detection zone was designed to be a rectangle with 0.3 cm x 3.5 cm as shown in Figure 2.2. The detection zone of layer 1 was deposited by the fluorescent probe, **TSD**. The filter paper in a rectangle shape with 3.5 cm wide and 0.3 cm wide of the detection zone was cut and then put in the solution of **TSD** (5 μM) for 2 min under continuous sonication. After that the deposited paper was left to dry at the room temperature. The **TSD**-deposited paper was reassembled in the rectangle hole of layer 1 (green area of Figure 2.2).

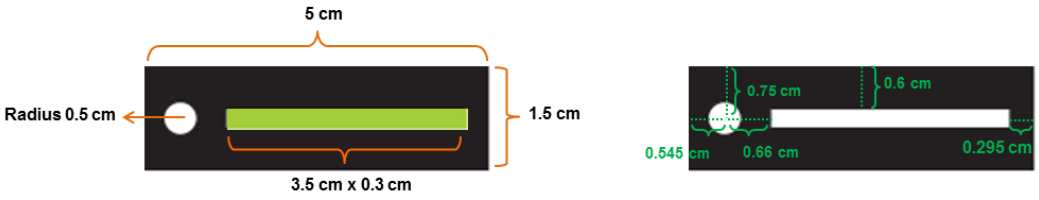

Figure 2.2. The pattern-designed layer 1 of 3D-μPAD

A double adhesive tape of layer 2 was design as shown in Figure 2.3. The layer composed of 2 cycles of hole which a dimension of 0.5 cm to be connecting conduct between layer 1 and 3.

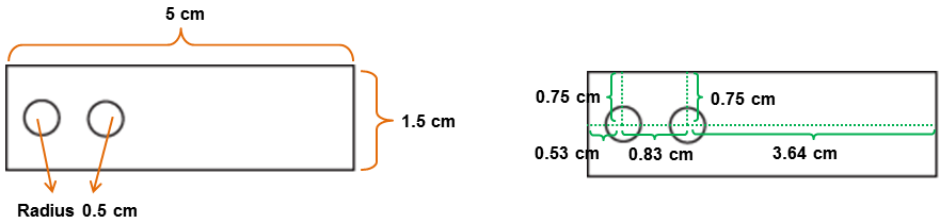

Figure 2.3. The pattern-designed layer 2 of 3D-μPAD

The hydrophilic zone of layer 3 was designed to be a cylinder shape with 0.5 cm of diameter and 1.33 cm of length as shown in Figure 2.4. This layer was fabricated to connect loading zone and detection zone. The layer 4 was rectangle tape with 5 cm x 1.5 cm as shown in Figure 2.5.

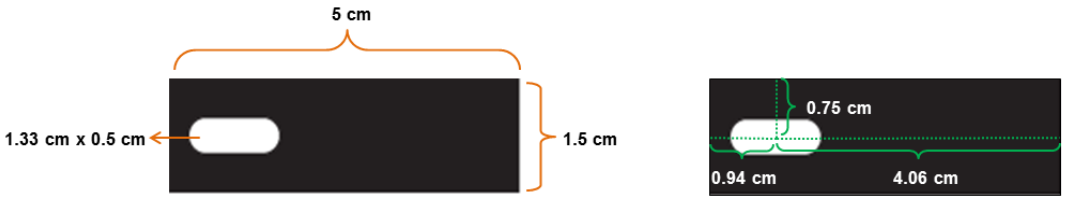

Figure 2.4. The pattern-designed layer 3 of 3D-μPAD

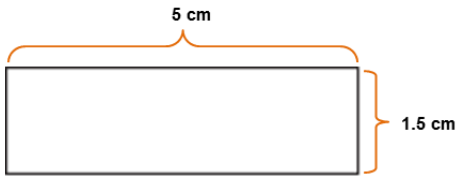

Figure 2.5. The pattern-designed layer 4 of 3D-μPAD

The cycle hole in layers 2 was filled with a 180 μm thick disk of Watman Chromatography Paper No. 1. For the quantitative analysis, the various concentration of GSH in the range of 0 - 6 mg/mL was dropped to the central disk in layer 1. The readout signal was measured under UV light at λ = 254 nm. The 50 μL of the GSH was loaded into the central disk on layer 1 of μPAD and left to dry prior to

measurement of the distance of darkness on detecting zone of layer 1. To validate the precision and accuracy of this device, the experiment was repeated for 20 times.

2.4. Results and discussion

2.4.1. Synthesis and characterization of bis(6-hydroxyhexyl) disulfide (S2)

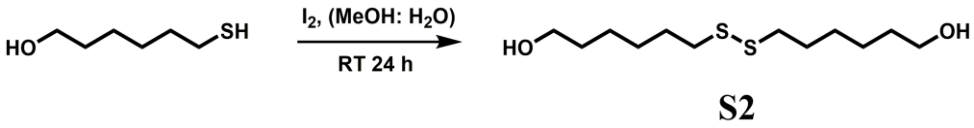

S2

Figure 2.6. Synthesis pathway of bis(6-hydroxyhexyl) disulfide, **S2**

The synthesis of **S2** co-surfactant was illustrated in Figure 2.6. The aliphatic chains bearing disulfide moieties was synthesized via subsequent oxidation of the free thiols with catalytic reaction by using iodine as a catalyst under highly dilute conditions. The formation of disulfide bond was completely monitored by the observation of colorless reaction [39]. The residue was purified by column chromatography using 100% dichloromethane to afford the white solid in 87 %yield.

From ^{1}H-NMR spectrum of **S2**, the characteristic peaks of methyl proton adjacent to thiol group (-SC*H*$_2$) slightly showed the downfield shift at 2.68 ppm due to the influence of the electron acceptor group by sulfur atom (Figure 2.7). The disappearance of the thiol proton (-S*H*) at 2.33 ppm was showed in the Figure A1. Furthermore, the observation of characteristic peak of carbon (^{13}C-NMR) in –SSCH$_2$ at 39.0 ppm confirmed the structure of disulfide compound (Figure A2) [39].

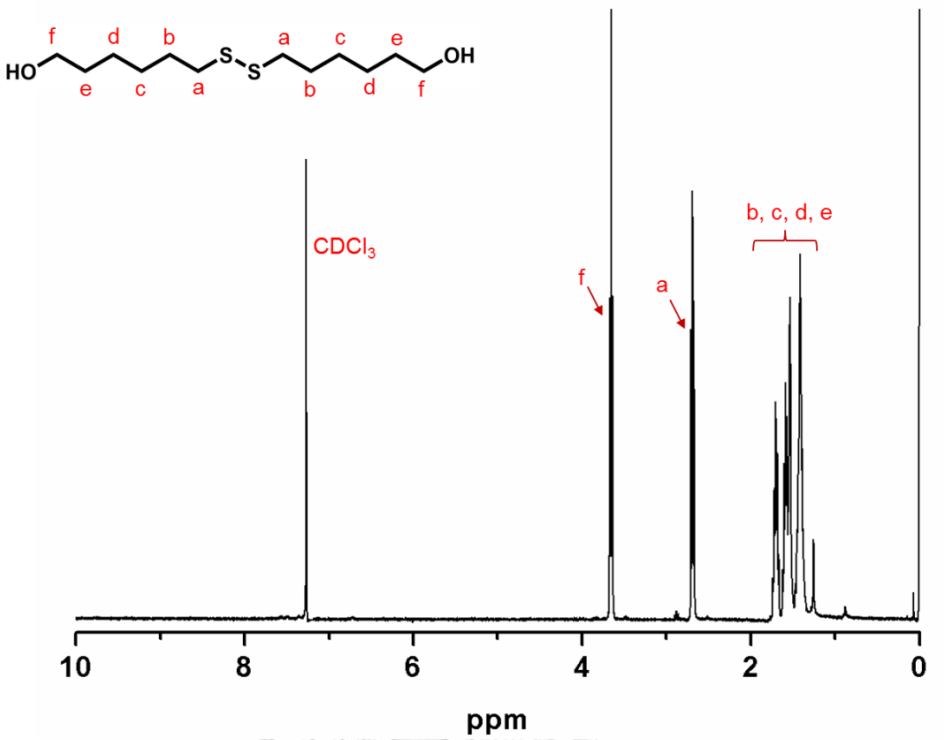

Figure 2.7. The ^{1}H-NMR spectrum of **S2**

2.4.2. Optimization of micelle forming

In this system, self-assembled microemulsion was prepared by using Triton-X 100 and **S2** as a surfactant and co-surfactant, respectively, to encapsulate the fluorescent dyes (**Cur-BF$_2$** and **DA**).

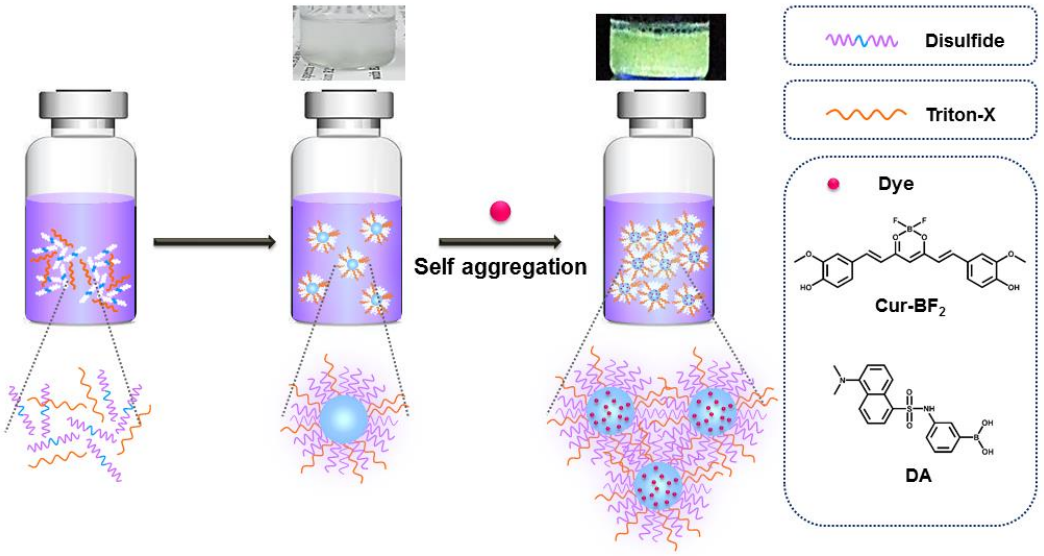

Scheme 2.2. Schematic representation of the preparation of micelle for GSH sensing

Firstly, micelle was prepared by stirring the mixture of Triton-X 100 and **S2** in the bottle to produce the small emulsion droplet. Then, self-aggregation of nanomicelle was addressed after adding fluorescent dye in the solution (Scheme 2.2). The emulsion droplets were centrifuged under 5000 rpm for 5 min to remove the organic residue. In this work, the fluorescence dyes of **DA** and **Cur-BF**$_2$ were used to be the dye-doped nanomicelle called **TSD** and **TSC**, respectively. The Figure 2.8 and 2.9 exhibited the fluorescence spectrum of **TSD** and **TSC** which demonstrated a strong emission bands at 525 nm and 587 nm, respectively. Moreover, the visual observation of the solution showed the green brightness and red brightness for **TSD** and **TSC**, respectively. These results revealed that the nanomicelle enables to increase the fluorescence response due to protection of dye to react with water and rigidity of dye in micelle.

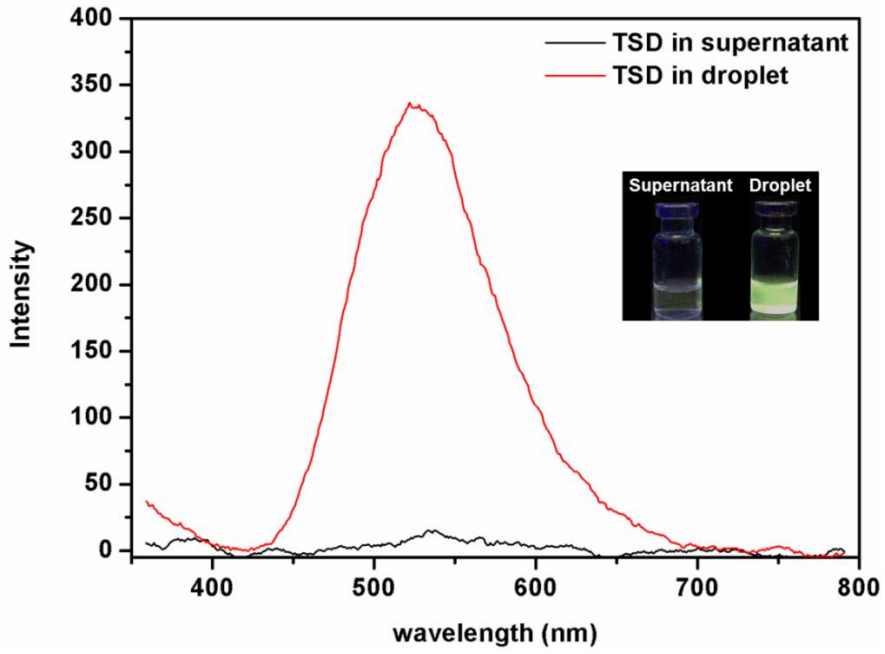

Figure 2.8. The fluorescence spectra of **TSD** nanomicelle (red) and supernatant (black) in 2.5%DMSO/PBS upon an excitation wavelength at 327 nm and inset: the brightness of supernatant and **TSD** solution upon the UV light at 254 nm.

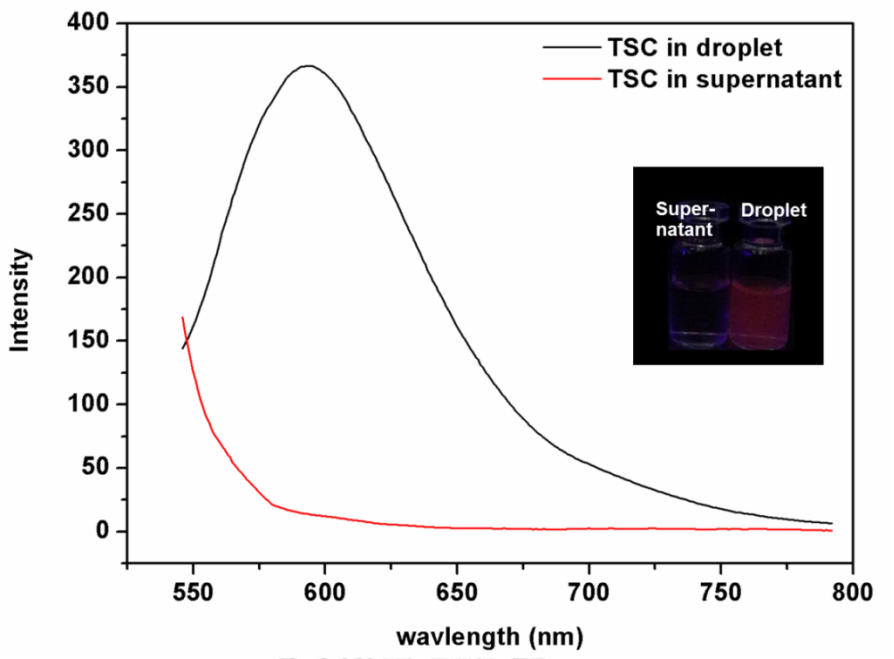

Figure 2.9. The fluorescence spectra of **TSC** nanomicelle (black) and supernatant (red) in 2.5%DMSO/PBS upon an excitation wavelength at 517 nm and inset: the brightness of supernatant and **TSC** solution upon the UV light at 254 nm.

Based on the well-known knowledge, GSH normally reduces the disulfide bond to produce the thiol group. As anticipated, **S2** was used to cooperate with surfactant to form micelle in order to protect dye molecule from water. In the presence of GSH, the disulfide bond in **S2** molecule would be reduced and cleavage. Consequently, the fluorescent dye in micelle was released resulting in the change of fluorescent signal of dye. According to the conceptual design, **S2** in micelles is the important role for efficient detection of biothiol compounds. Hence, the proper amount of **S2** for forming micelles was particularly investigated. Apart of well-constructed micelles by combining two surfactants of Triton- X 100 and **S2**, the CMC of Triton-X 100 and **S2** in formation of micelles was firstly investigated with both dyes. Figure 2.10 showed the CMC of Triton-X 100 and **S2** at 0.5 mM and 0.43 mM as well as 1.367 mM and 1.267 mM for **Cur-BF$_3$** and **DA**, respectively.

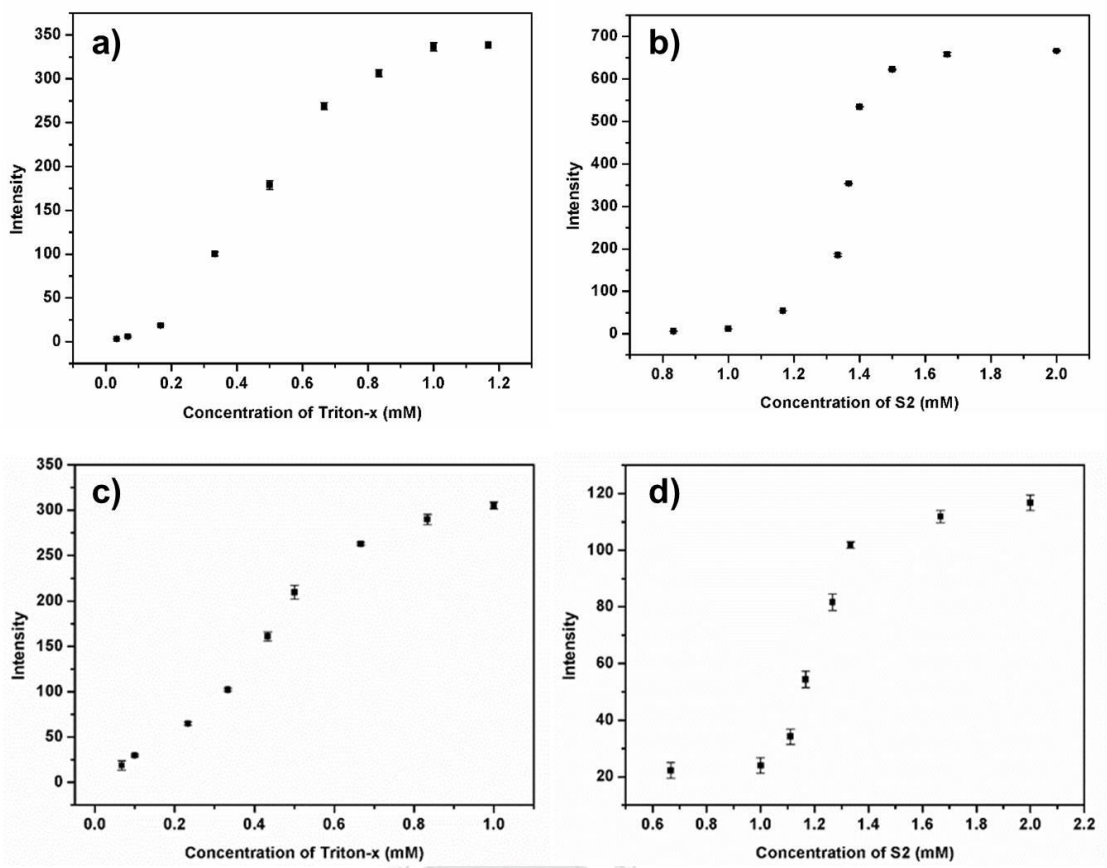

Figure 2.10. Critical micelle concentration (CMC) of (a) **TC** (b) **SC** (c) **TD** and (d) **SD**

To verify the proper amount of **S2** in micellar formation, the various amount of **S2** was carried out by using the amount of Triton-X 100 at 0.33 mM in both dyes. The Figure 2.11 displayed the highest FL response suggesting the proper amount of **S2** for **Cur-BF3** and **DA** at approximately 1.198 mM and 1.176 nm, respectively. In comparison of the self-assembled micelle of **Cur-BF2** system by one surfactant, it was found that the Triton-X 100⊂**Cur-BF2** (**TC**) (0.33 mM) displayed a weak emission band around 587 nm while this emission band was completely disappeared in the case of S2⊂**Cur-BF2** (**SC**) (Figure 2.10). The different fluorescence feature indicated that this concentration at 1.23 mM of **S2** cannot induce micelle formation of **Cur-BF2**. On the other hand, the strong emission band of **TSC** was explicitly observed around 587 nm as shown in Figure 2.12a. In the case of dansyl boronic acid (**DA**), it exhibited a weak fluorescence signal around 550 nm in aqueous solution.

Upon encapsulation in the nanomicelles, this emission band of **DA** incorporated nanomicelles showed a very strong emission band. In comparison to **SD** and **TD**, the significant increase of emission band of **TSD** at 528 nm was observed in Figure 2.12b. Taking on broad of these micellar systems, the observation of the strong fluorescence spectra implied that Triton-X 100 and **S2** formed a well-constructed assembled micelle to effectively encapsulate both fluorescence dyes (**Cur-BF_2** and **DA**). According to the visual study in inset of Figure 2.12a and 2.12b, particular **TSC** and **TSD** systems demonstrated the red and green brightness, respectively, that was consistent of the fluorescence spectral results.

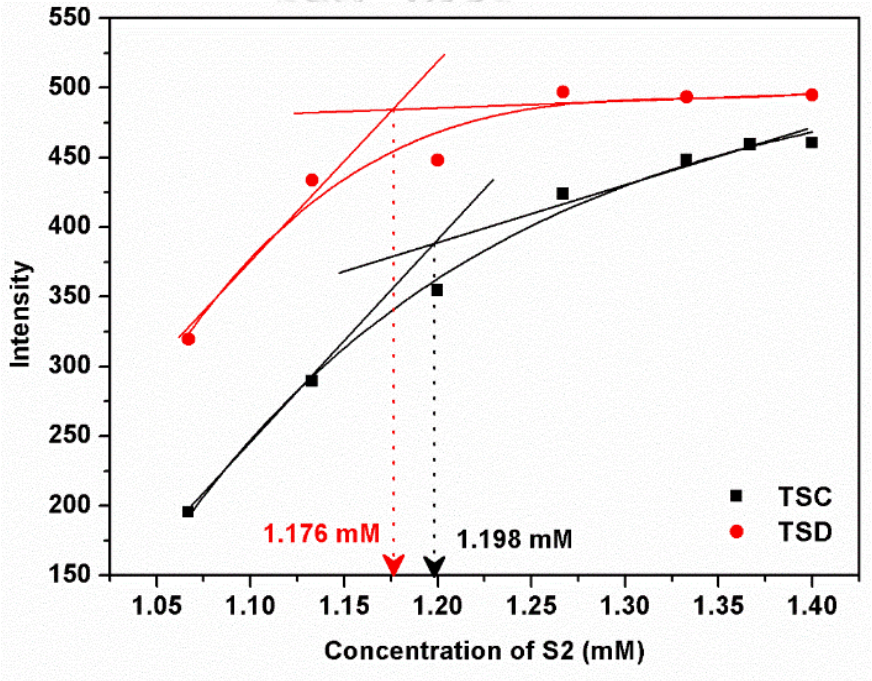

Figure 2.11. The determination of CMC value of **TSC** (■) and **TSD** (●) in the presence of Triton-X 100 0.33 mM in the 2.5% DMSO/PBS solution with various the concentration of **S2** in the range of 1.067 - 1.4 mM.

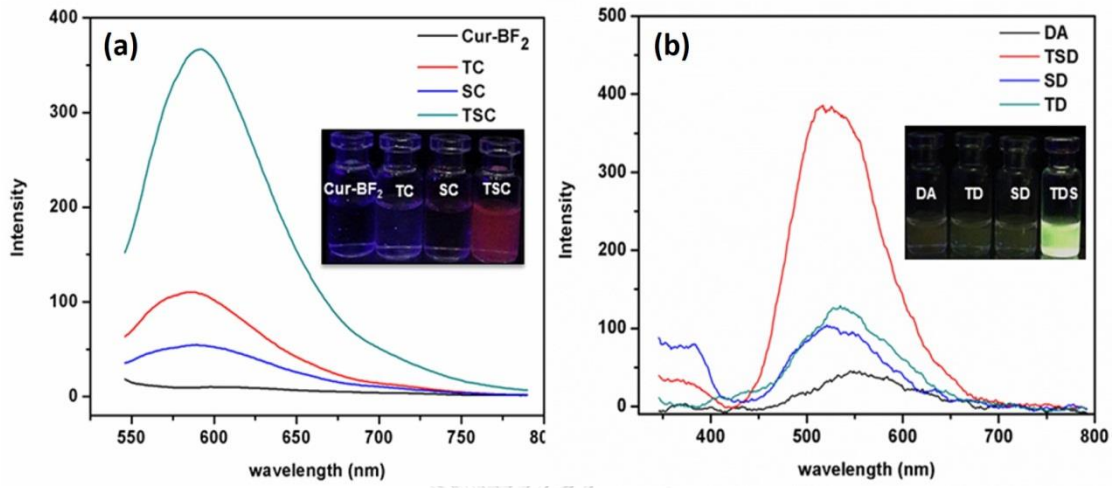

Figure 2.12. Comparison of fluorescence spectra and typical photograph for the different system of **Cur-BF$_2$** (a) and **DA** (b) in 2.5% DMSO/PBS solution.

According to GSH sensing, the amount of **S2** on the nanomicelles sensing approach is reliably important because S2 is a control compound based on the disulfide-cleavage trigger reaction. Therefore, the formation of **TSC** and **TSD** was reliably regarded to the optimization of a suitable concentration of **S2**. The efficient amount of **S2** towards a well-detected approach of the micellar system had been also studied by varying the amount of **S2** (1.06-1.36 mM) in the presence of GSH. Figure 2.13 showed the highest values of 30-35% fluorescent quenching of both systems at the approximately similar concentration of 1.26 mM of **S2**. The proper amount of **S2** was determined in the % quenching of micelle after adding the GSH (6.67 μM) by calculation in the equation 1 as shown in topic of 2.3.3.5. The fluorescence response of both micellar systems (**TSC** and **TSD**) gradually increased at the low concentration of **S2** until to 1.26 mM. After that the concentration of **S2** over 1.26 mM induced the decrease of fluorescent intensity due to the precipitate of an insoluble **S2** (Figure 2.13). The results revealed that the suitable concentration of Triton-X 100 at 0.33 mM and **S2** at 1.26 mM regarding to the ratio of 1:3.8 induced the highest % quenching of micelles in the presence of GSH. Therefore, this concentration of **S2** was suitable for further studying the GSH sensing approach.

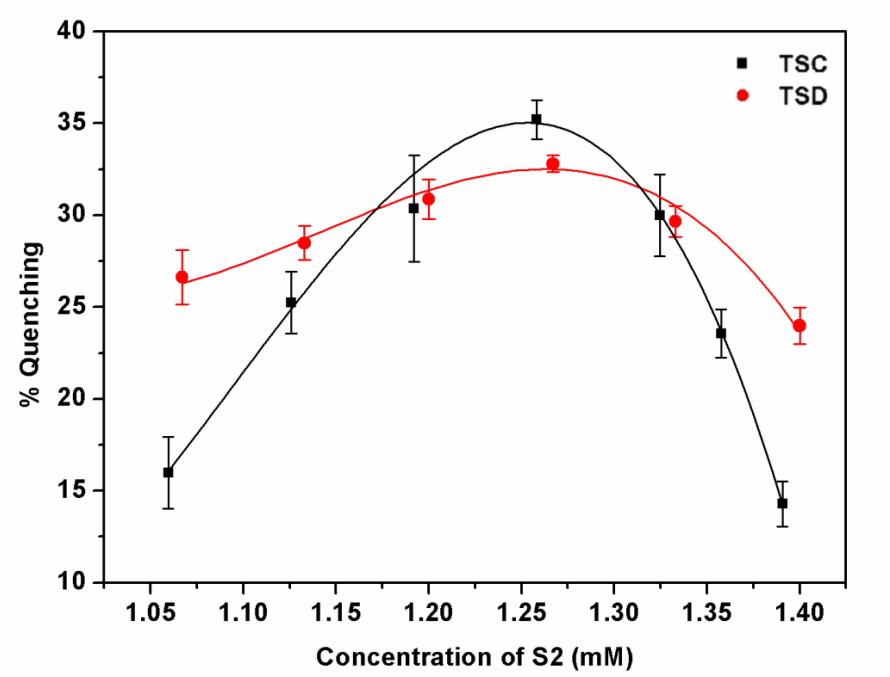

Figure 2.13. Determination of % Quenching of **TSC** (■) and **TSD** (●) in the presence of GSH (6.67 μM) in nanomicellar system of 0.33 mM Triton-X 100 and various concentration of **S2** under excitation at 517 nm

2.4.3. The stability of nanomicelle platform

Particular stability of materials has been realized for sensing purpose under various period of time by the fluorescence spectroscopy. The fluorescence intensity of **TSC** and **TSD** micelle at 587 nm and 525 nm also remained unchanged until at least 24 h (Figure 2.14). These results indicated that the development-encapsulated materials demonstrated the superior stability of fluorescent dyes (**Cur-BF_2** and **DA**) in aqueous solution.

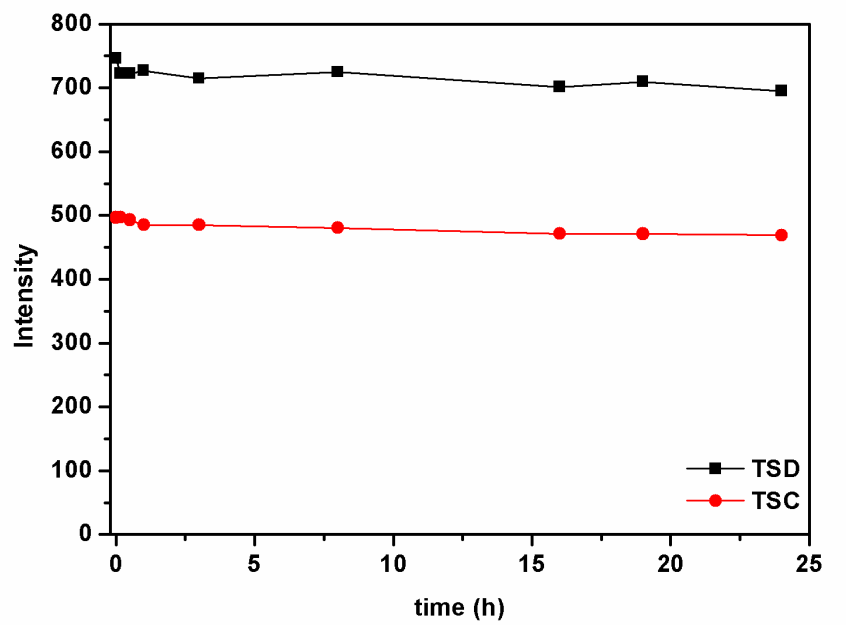

Figure 2.14. Fluorescence intensity of **TSC** (black line) and **TSD** (red line) monitored at the emission bands of 587 nm and 528 nm, respectively, under various period of time for 1 day.

2.4.4. Optimization of sensing condition of TSC and TSD toward GSH

Due to a large fluorescence change of both nanomicelles (**TSC** and **TSD**), it urged us to focus on the sensing properties of these nanomicelles toward GSH. First, the proper condition for sensing purpose is of grate criteria. Apart from the reducing agent properties of GSH, it is well-known to convert disulfide bond to thiol moieties under a redox reaction with a respect amount of H^+ and e^- which are an important factor on charge properties of GSH. Deeply considering of pH profiles, the decrease of fluorescence intensity of dye-dope nanomicelles was observed after adding GSH. There were three possibilities of the processes:

i) The proton may induce the demicellization,

ii) The proton may react with dye which was loaded in micelle and

iii) The concentration of proton possibly increased the GSH activity.

To clarify these hypotheses, the micellar systems of **Cur-BF_2** and **DA** were performed in the absence of GSH with various pH in the range of 3 – 10 and the result was monitored by using fluorescence spectroscopy. Figure 2.15 illustrated the strong fluorescence intensity of nanomicelle platforms. The fluorescence intensity of **TSC**

showed a slightly change in the range pH of 6-8. Compared to the fluorescence feature of **Cur-BF$_2$**, in the aqueous media, the fluorescence intensity of **Cur-BF$_2$** was completely quenched in the pH of 3-10. From the pH effect of **TSC** and **Cur-BF$_2$**, it could be concluded that the micelle was stable in the range of pH from 3 to 8. In the case of **TSD**, the fluorescence signal was increased upon increasing pH from 3 to 8 and then the intensity was quenched in the pH higher than 8 as shown in Figure 2.15. Interestingly, the fluorescence intensity of **DA** was increased upon increasing the basicity of aqueous media (Figure 2.16). The fluorescent behavior of **TSD** and **DA** in the various pH revealed that micelle was stable in pH < 8.

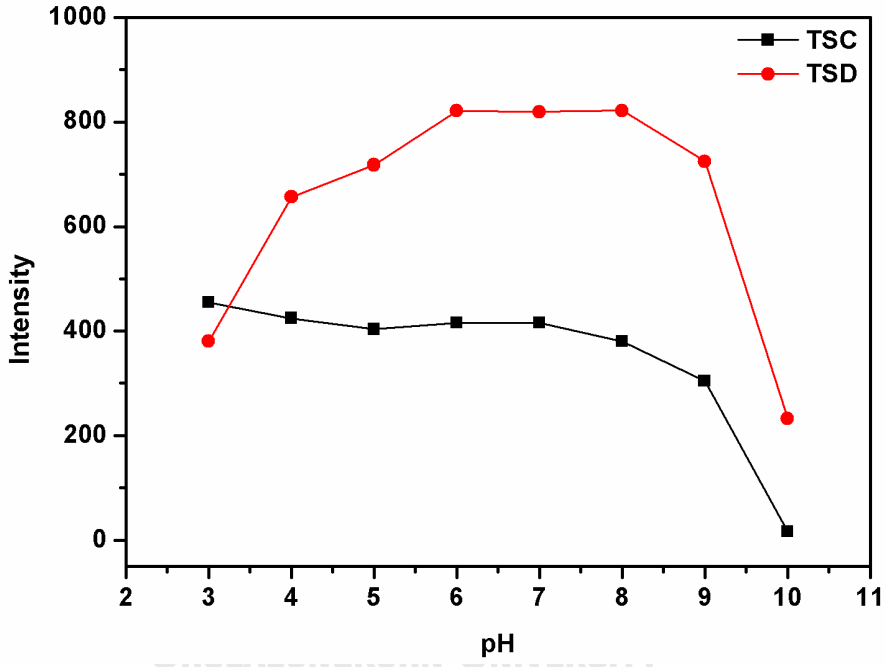

Figure 2.15. The fluorescent responses of micellar system of **TSC** (■) and **TSD** (●) in the pH ranged 3-10. The pH ranged 3-5 prepared from citric acid buffer solution, pH 6-7 from phosphate buffer solution and pH 8-10 from a borate buffer solution.

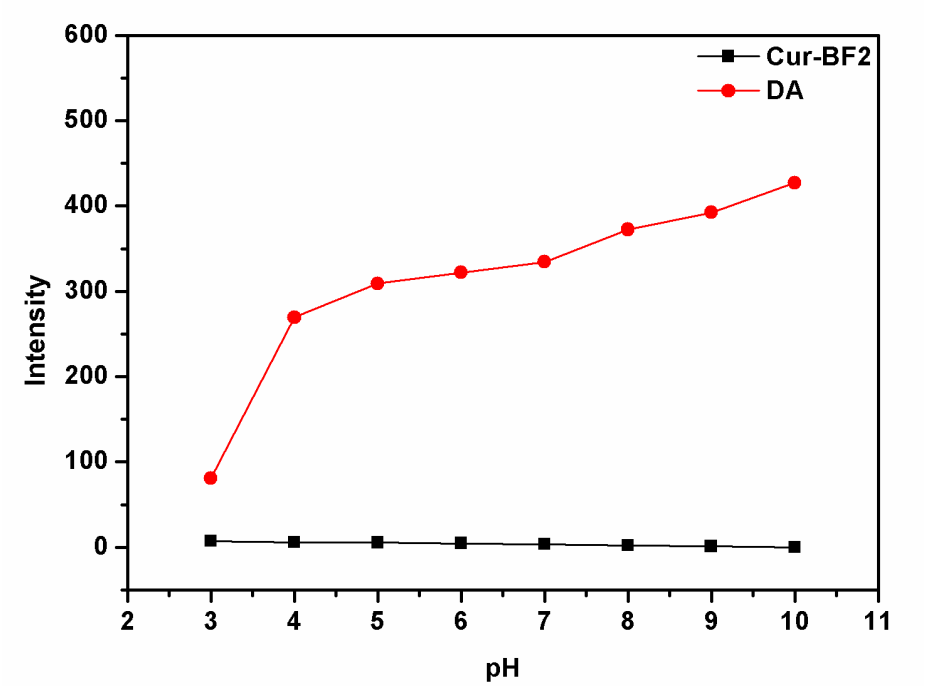

Figure 2.16. Fluorescent responses of **Cur-BF_2** (■) and **DA** (●) in pH ranged 3-10. The pH range 3-5 was prepared from citric acid buffer solution, pH 6-7 from phosphate buffer solution and pH 8-10 from borate buffer solution.

Due to the consistency of high emission band and a large quenching of fluorescence in the presence of GSH for **TSD** and **TSC** nanomicelles, these studies reliably satisfied the appropriated pH for this sensing purpose of nanomicelles at pH 6.0 which was chosen for further sensing studies.

2.4.5. Fluorescent sensing of TSC and TSD toward GSH

The micelle of **TSC** and **TSD** was applied to detect GSH in PBS buffer pH 6. In the case of **TSC**, the strong fluorescent intensity around 587 nm was observed under the excitation wavelength at 517 nm. In the presence of GSH, a large quenching of this emission band was observed as shown in Figure 2.17a. This result indicated that the GSH can reduce disulfide bond of **S2** to provide the demicellization of **TSC** nanomicelles and then the encapsulated fluorescent dye might be released into aqueous media inducing the fluorescent quenching. Similarly, the feature of fluorescence spectra in the case of **TSD** showed the identical behavior to **TSC** due to the same disulfide-cleavage triggered reaction (Figure 2.17b). Moreover, the

brightness of luminescence for **TSC** or **TSD** nanomicelles was investigated under UV light at 256 nm. The visual luminescence of **TSC** and **TSD** changed from red and green brightness to non-bright solution in the presence of GSH, respectively.

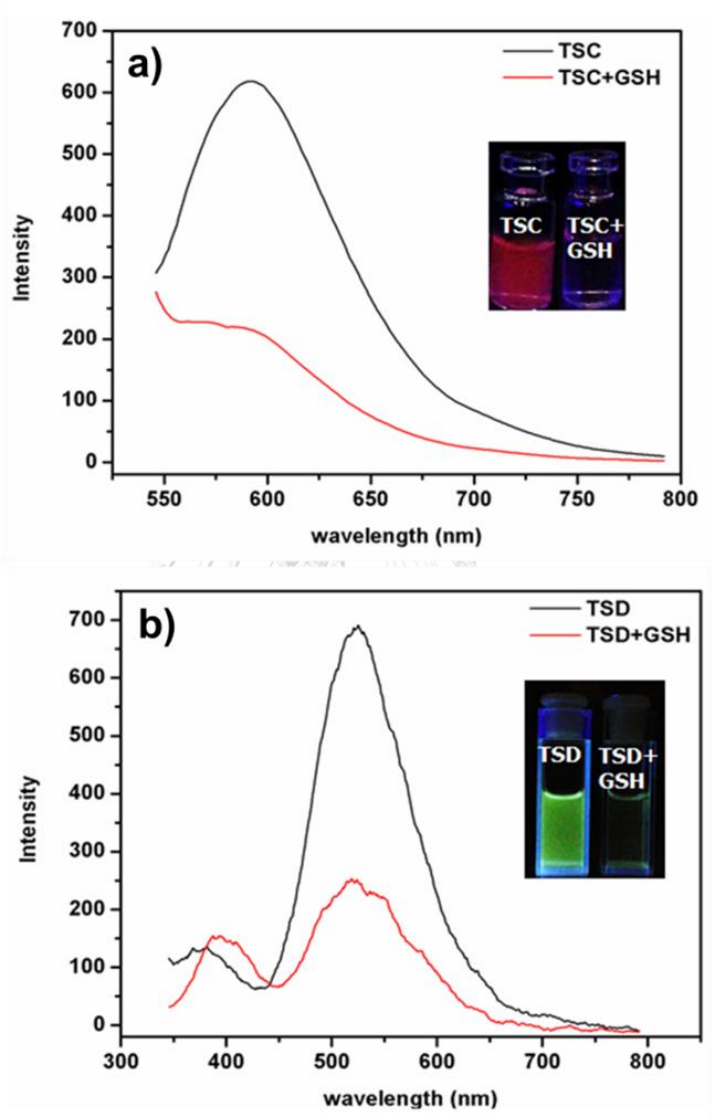

Figure 2.17. The fluorescence spectra and inset: the visual fluorescent change of **TSC** (a) and **TSD** (b) after adding 6.67 μM GSH in 2.5%DMSO/PBS (0.5 mM) buffer solution pH 6.

To prove the hypotheses of demicellization, the absorption bands of **TSC** and **TSD** were measured to determine the demicellization by using UV-Visible spectroscopy. The maximum absorption bands for **TSC** and **TSD** around 517 nm and

350 nm were appeared upon the addition of GSH corresponding to **Cur-BF_2** and **DA**, respectively (Figure 2.18). These results confirmed that the micelle was collapsed by GSH and free dyes were released in aqueous media.

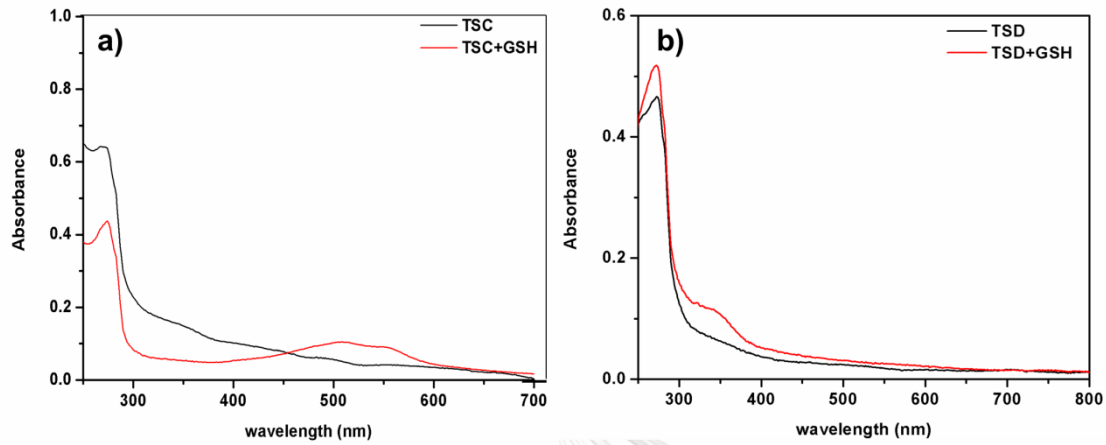

Figure 2.1 8 . The absorption spectra of **TSC** (a) and **TSD** (b) upon the addition of GSH for 20 minutes at pH 6.0 in 2.5%DMSO/PBS

Moreover, TEM images were used to study the sensing process. Figure 2.19, the TEM analysis revealed that the self-aggregation of micelle exhibits a hydrophobic surface of nanosphere with the average diameter of approximately 200 nm for **TSD.** Deeply considering the inside nanosphere, there are several small micelles with a particle size of 10-30 nm. Upon the addition of GSH in the solution, the hydrophobic surface of a spherical structure aggregated nanomicelles was collapsed. This evidence indicated that the reduction of disulfide bond based nanosphere by GSH led to the demicellization and destroyed the hydrophobic surface of aggregation nanomicelle.

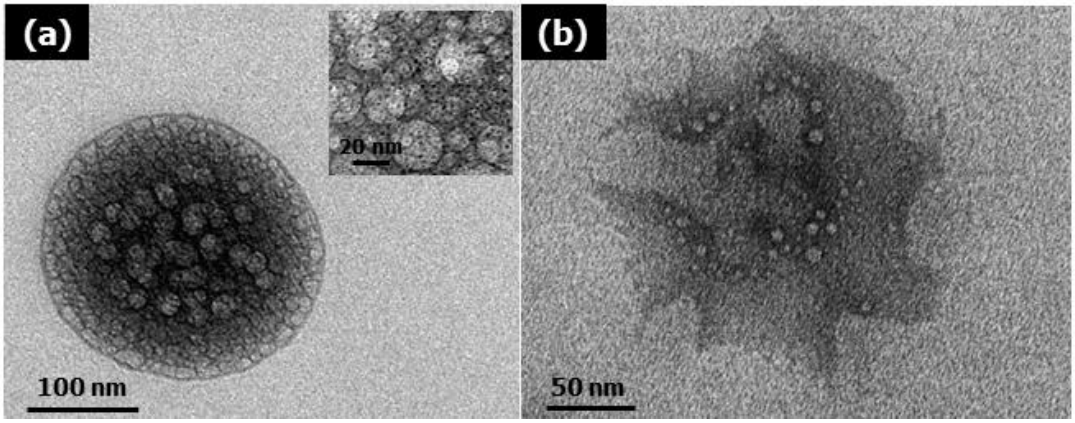

Figure 2.19. HR-TEM images of **TSD** micelle before (a) and after (b) adding GSH in 2.5%DMSO/PBS (0.5 mM) buffer solution pH 6

Moreover, the particles sizes of micelle in solution were also investigated by using dynamic light scattering (DLS) as shown in Figure 2.20. The average diameter of **TSC** in a 2.5% DMSO/PBS in the presence of GSH increased significantly from 164.2 to 531.2 nm, indicating the formation of a large aggregated nanomicelle. Similarly, the **TSD** micelle showed a negligible change from 190.1 to 825.0 nm. The phenomenon of size was increased by GSH- cleavage trigger of disulfide bonds. As a result of collapsing the aggregration nanomocelle by the disulfide-cleavage trigger behavior, water diffused into the collapsed nanomicelles leading to the swelling of particles. The TEM and DLS data clearly confirmed that the demicellization of **TSC** and **TSD** occurred via reduction of disulfide bond by GSH corresponding to the fluorescence quenching behavior.

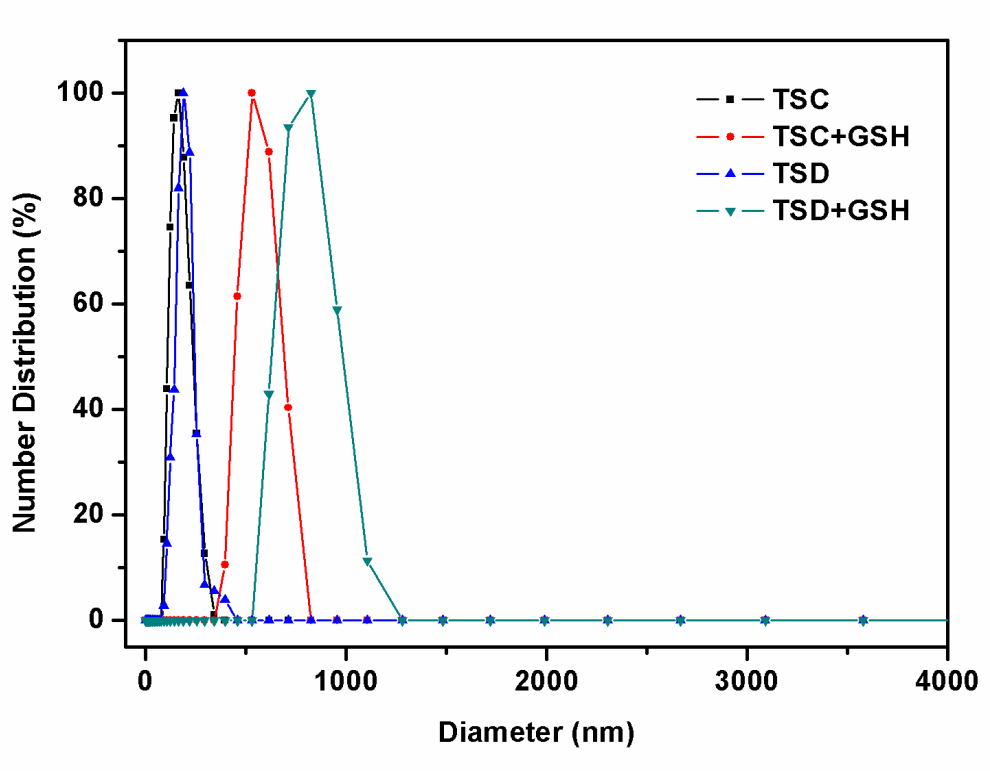

Figure 2.20. Determination of size distribution of **TSC** and **TSD** in the presence of GSH

2.4.6. The time release for GSH sensing

Apart from interesting properties of a new nanomicelle for sensing approaches, we hypothesized that the incubation time-dependent demicellization is an important factor. After adding GSH, the quenching fluorescent feature of **TSC** and **TSD** exhibited as a function of time as shown in Figure 2.21. The result showed a significant decrease in fluorescence signal of **TSC** and **TSD** in the presence of GSH in the period of 0 - 200 min. This suggested that the demicellization of nanomicelles strongly depended on incubation time.

However, the constant fluorescence quenching of incubation time for demicellization is approximately 3 h which is ineffectively for real time detection. Incubation time at 20 min demonstrated the large fluorescence quenching as shown in the inset of Figure 2.21. Thus, the measurement time at 20 min was chosen for all further manipulation.

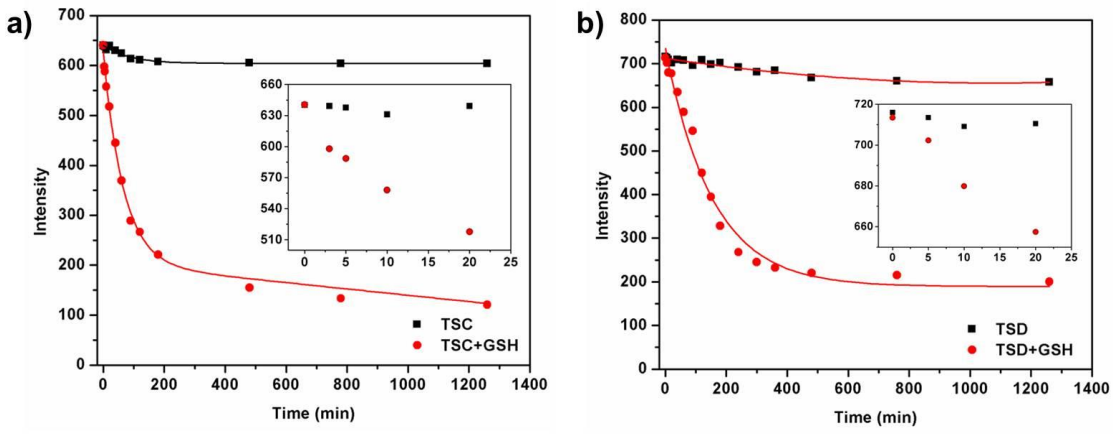

Figure 2.21. Time release profile of **TSC** (a) and **TSD** (b) in the absence (■) and presence GSH 6.67 μM (●) in 2.5%DMSO/PBS (0.5 mM) buffer solution pH 6. Inset showed the expansion graph of time release in the range of 0-20 min after adding GSH.

2.4.7. Selectivity and sensitivity of micellar self-assembly of TSC and TSD for GSH sensing

After the optimized conditions of GSH sensing, the fluorescence response of the micelles (**TSC** and **TSD**) with the other amino acids was also determined to clarify the point of selectivity. The relative fluorescent intensity was monitored and experimental result exhibited insignificant change of fluorescent intensity upon the addition of Leu, Met, Thr, Cys, Phe, Lys, Ala, Gly and Hcy into the solution of **TSC** and **TSD**. Interestingly, the fluorescent intensity of **TSC** and **TSD** were significantly quenched after adding GSH as shown in Figure 2.22. This evidence suggested that **TSC** and **TSD** have high selectivity toward GSH via S-S bond cleavage mechanism.

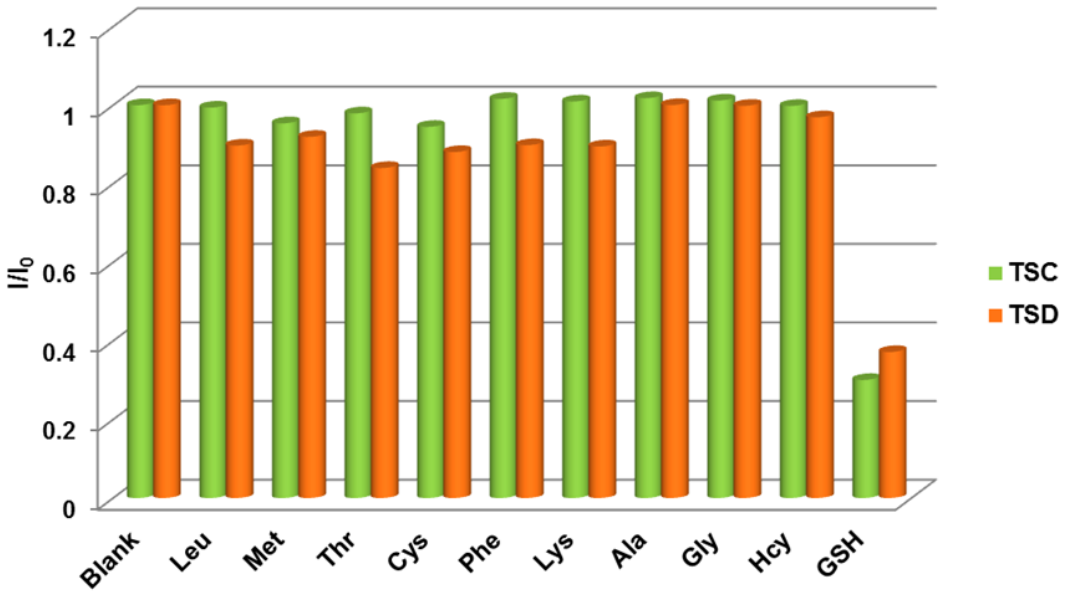

Figure 2.22. The fluorescence responses of **TSC** and **TSD** towords GSH and other amino acids under excitation wavelength 587 nm and 525 nm, respectively. The concentration of other interferences (Leu, Met, Thr, Cys, Phe, Lys, Ala, Gly and Hcy) are 0.15 mM in the 2.5% DMSO/PBS solution

Furthermore, the fluorescent titration of **TSC** and **TSD** was performed to figure out the limit of detection (LOD) in 2.5% DMSO/PBS (0.5 mM) pH 6.0 (Figure 2.23 and 2.25). The result showed that fluorescent intensity at 587 nm corresponding to **TSC** was gradually quenched upon the increment of GSH. The quenching efficiency (I_0/I) toward GSH concentration provided a good linear range between 20 to 200 µM with the correlation coefficient (R^2) of 0.9852 and LOD of 2.24 ppm (7.3 µM) as shown in Figure 2.24. In the case of **TSD** nanomicelles, the fluorescent titration was performed by monitoring an emission band at 525 nm. The calibration curve for quantitative analysis of GSH was calculated and a result showed a linearity of detection from 20-200 µM with R^2 = 0.98629 (Figure 2.26). From the calibration curve, the LOD of **TSC** toward GSH was 2.83 ppm (9.2 µM). The summarized analysis data of **TSD** and **TSC** nanomicelles with GSH was listed in the Table 2.12.

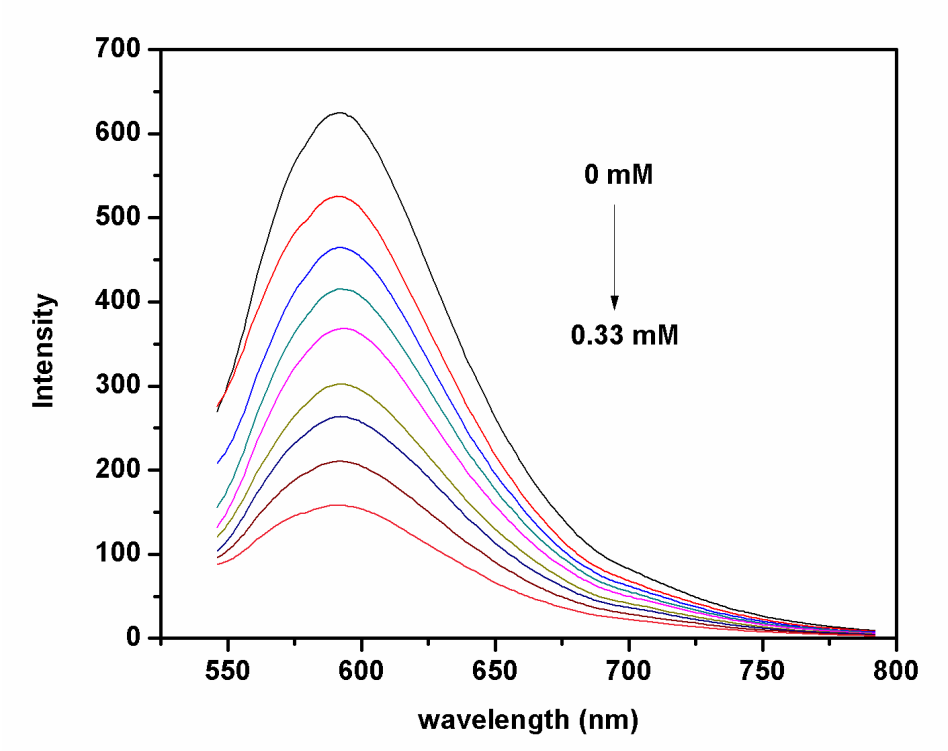

Figure 2.23. Fluorescence spectra of **TSC** in 2.5% DMSO of 0.5 mM phosphate buffer pH 6.0 upon addition of different concentration of GSH (0-0.33 mM) under excitation wavelength at 517 nm

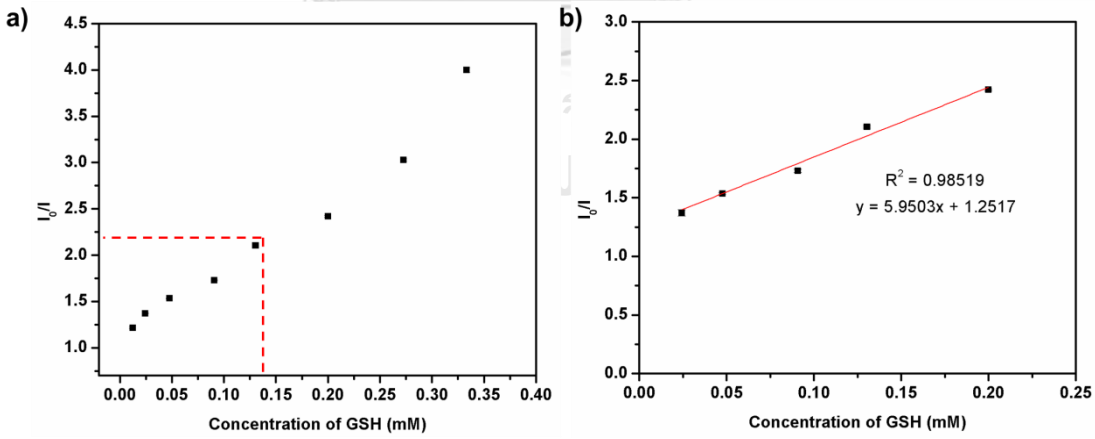

Figure 2.24. The relative intensity of **TSC** at different concentration of GSH (0.01-0.33 mM) (a) and linear plot between relative intensity of **TSC** at 587 nm and concentration of GSH (0.02-0.2 mM) (b)

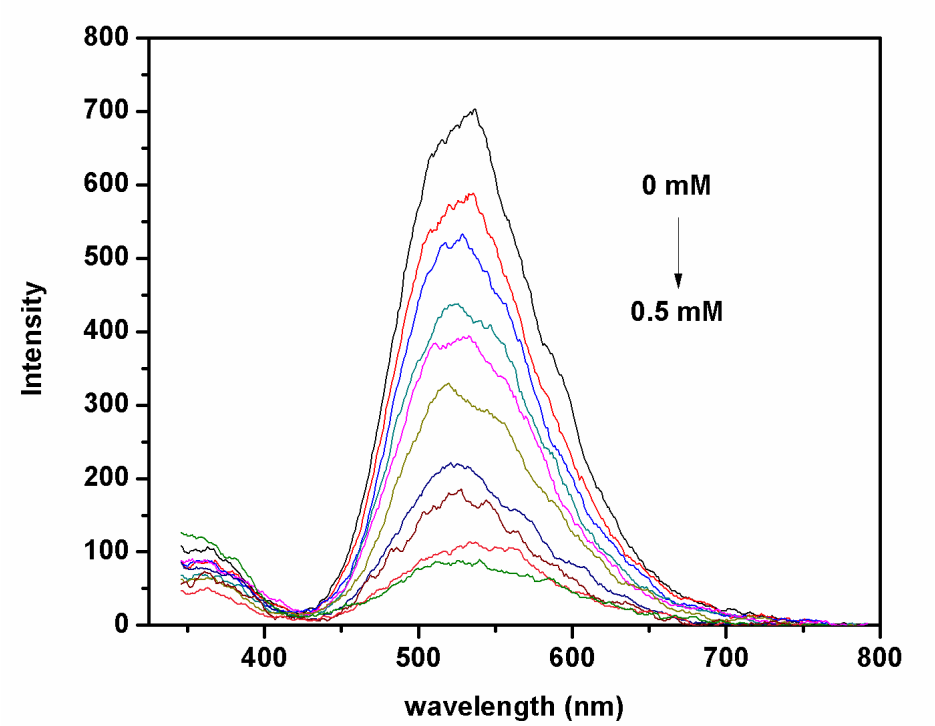

Figure 2.25. Fluorescence spectra of **TSD** in 2.5% DMSO of 0.5 mM phosphate buffer pH 6.0 upon addition of different concentration of GSH (0-0.5 mM) under excitation wavelength at 327 nm

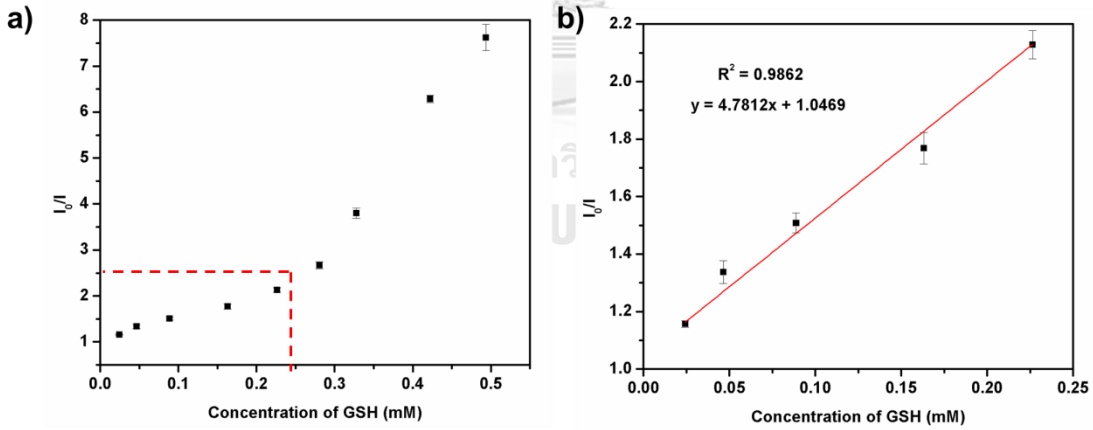

Figure 2.26. The relative intensity of **TSD** at different concentration of GSH (0.01-0.5 mM) (a) and linear plot between relative intensity of **TSD** at 528 nm and the concentration of GSH (0.02-0.22 mM) (b)

Table 2.12. Summarizes results of the GSH detection in 2.5% DMSO of 0.5 mM phosphate buffer pH 6.0

Sensor materials	GSH (ppm)	Found (ppm)	%Recovery	Linearity (ppm)	LOD (ppm)
TSC	27.6	27.49±0.01	99.63	6.15-61.46	2.24
	30.7	30.83±0.01	100.45		
TSD	27.6	27.43±0.02	99.41	6.15-67.61	2.83
	30.7	31.23±0.02	101.73		

2.4.8. Analytical application by 3D microfluidic paper based

For practical and portable device, **TSD** nanomicelle was applied in GSH quantitative detection under distance-based assays. To gain a well-spread deposit of nanosensor on the detecting zone, the paper on detecting zone was cut off and soaked in the sensor solution under sonication for 2 min. Once the reagent deposited on detecting zone was dried. It was reassembled on the detection zone of device. As anticipated, a poor diffusion of sample solution from reservoir to the detecting zone in 2D µPAD would be occurred due to a space between the loading zone and detecting zone. To raise a high efficacy for quantitative analysis, three-dimension (3D) paper-based microfluidic device (3D-µPAD) was constructed as shown in Figure 2.27. The assay was conducted in a three-dimensional (3D) paper-based microfluidic device comprising of (i) stacked and alternating layers of paper that has been patterned with wax into hydrophilic and hydrophobic regions, and (ii) double-sided adhesive tape. All holes in each layer were patterned by using a CO_2 laser cutter. The holes in the tape were filled with disk of paper. The µPAD consists of loading zone and detecting zone for quantitative visual detection of GSH, corresponding to the fluorescence darkness on the surface of the detecting zone. The **TSD** micelle was chosen to determine the amount of GSH in paper based device due to a strong green brightness under UV light at 256 nm.

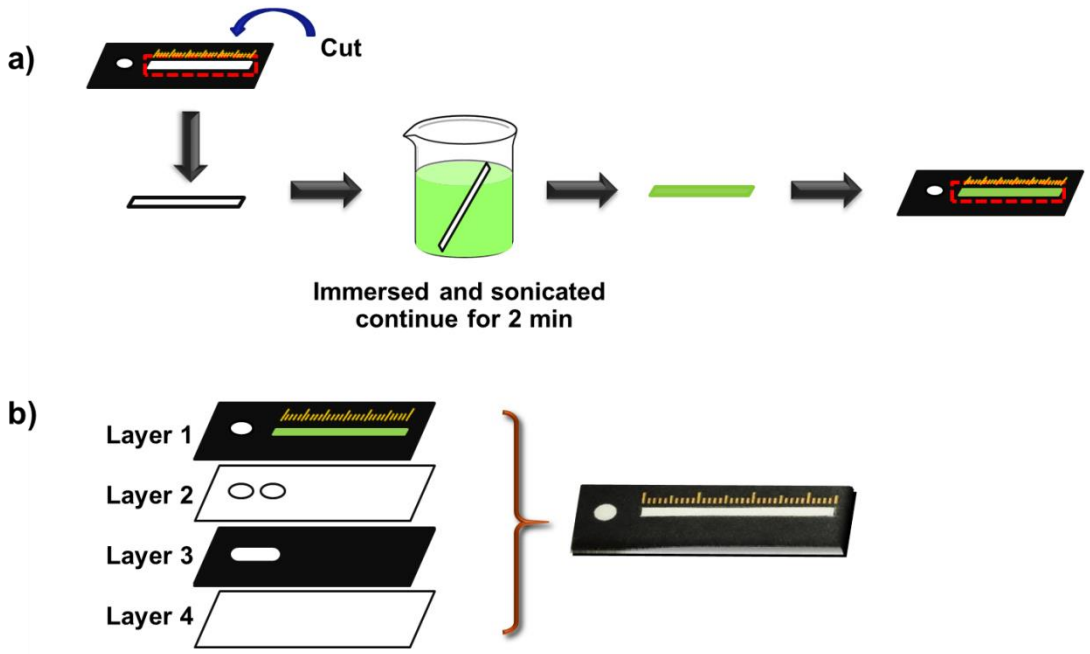

Figure 2.27. The preparation **TSD** sensor on paper device (a) and construction of 3D paper-based microfluidic devices (3D-μPAD) for determination of GSH concentration (b)

The **TSD** nanomicelle was deposited on the detection zone on the layer 1 for reacting with sample. Upon the addition of 60 μL GSH solution on the loading zone on the layer 1, the GSH solution passed down through z direction of the device into layer 4 by gravity force. After that the direction of sample solution flowed up to layer 1 by capillary force. In the layer 1 of the device, the GSH demonstrated the good performance of the disulfide-cleavage trigger reaction in the aggregation nanomicelles resulting in the fluorescent quenching of **TSD** (Figure 2.28). Each concentration of sample in analysis was repeated for 20 times to validate the precision and accuracy of detection. For quantitative assay, the amount of GSH was determined by measurement of the distance of darkness on the detection zone (Table 2.13).

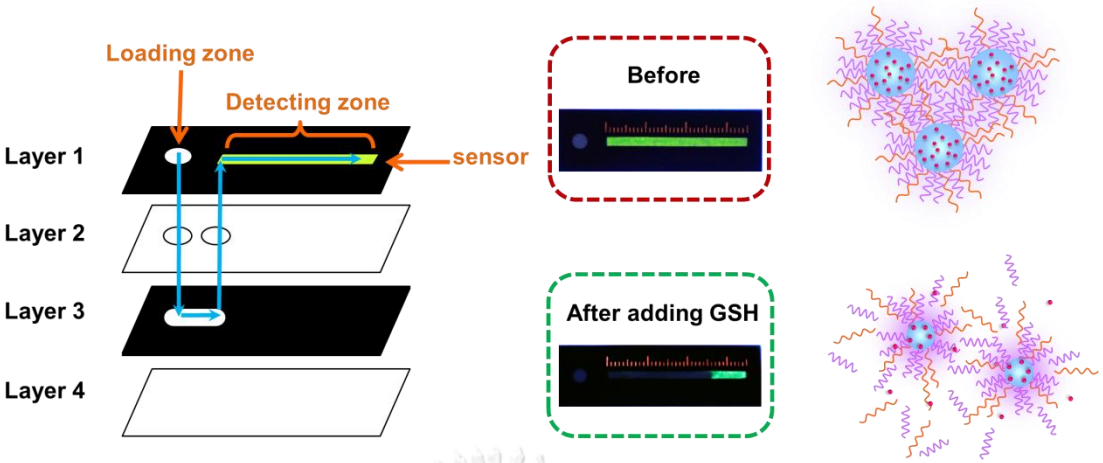

Figure 2.28. The operation of paper-based microfluidic devices (3D-μPAD) for determination of GSH concentration by the photo of prepared 3D paper under UV lamp at 254 nm

Table 2.13. The distance of darkness on detection zone for paper-based analytical device with various concentration of GSH (0 - 6 mg/mL)

Distance of darkness (mm)	Concentration of GSH (mg/mL)									
	0	**0.3**	**0.5**	**0.8**	**1**	**1.5**	**3**	**4**	**5**	**6**
	0	7	6	17	25	25	25	30	34	35
	0	0	4	17	17	31	27	35	33	35
	0	2	11	9	20	25	30	27	34	35
	0	3	10	11	22	27	34	32	35	35
	0	4	12	17	19	25	34	35	33	35
	0	2	8	13	19	26	35	35	34	35
	0	8	6	10	27	27	34	34	35	35
	0	6	7	17	22	25	35	35	35	35
	1	4	6	10	25	27	35	35	34	35
	1	0	9	14	20	29	35	35	35	35
	0	6	12	18	17	29	35	35	35	35
	0	3	9	12	25	30	29	33	35	35
	1	2	6	15	24	30	35	35	35	35
	0	3	14	10	20	31	25	35	35	35
	0	7	10	9	18	30	30	35	35	35
	0	3	14	15	18	30	35	30	30	35
	0	4	9	18	24	30	28	30	34	35
	1	8	11	20	17	27	31	32	33	35
	0	5	14	14	27	27	27	30	34	35
	0	5	12	20	31	33	35	33	33	35
mean	**0.2**	**4.1**	**9.5**	**14.3**	**21.85**	**28.2**	**31.7**	**33.05**	**34.05**	**35**

The relationship between amounts of GSH and distance of darkness was investigated as shown in Figure 2.29. These results suggested that distance of darkness on the top of the layer was correlated to the concentration of GSH. The band-length darkness was increased in the proportion to the GSH concentration with the detection limit of 0.06 mg/mL under linear range of 0.30 - 1.50 mg/mL which gave good analytical characteristics of the GSH detection. Interestingly, these

nanomicelles exhibited highly selective and were also applied to determine the amount of GSH on the paper-based device which encourages the short time operation and easy for use.

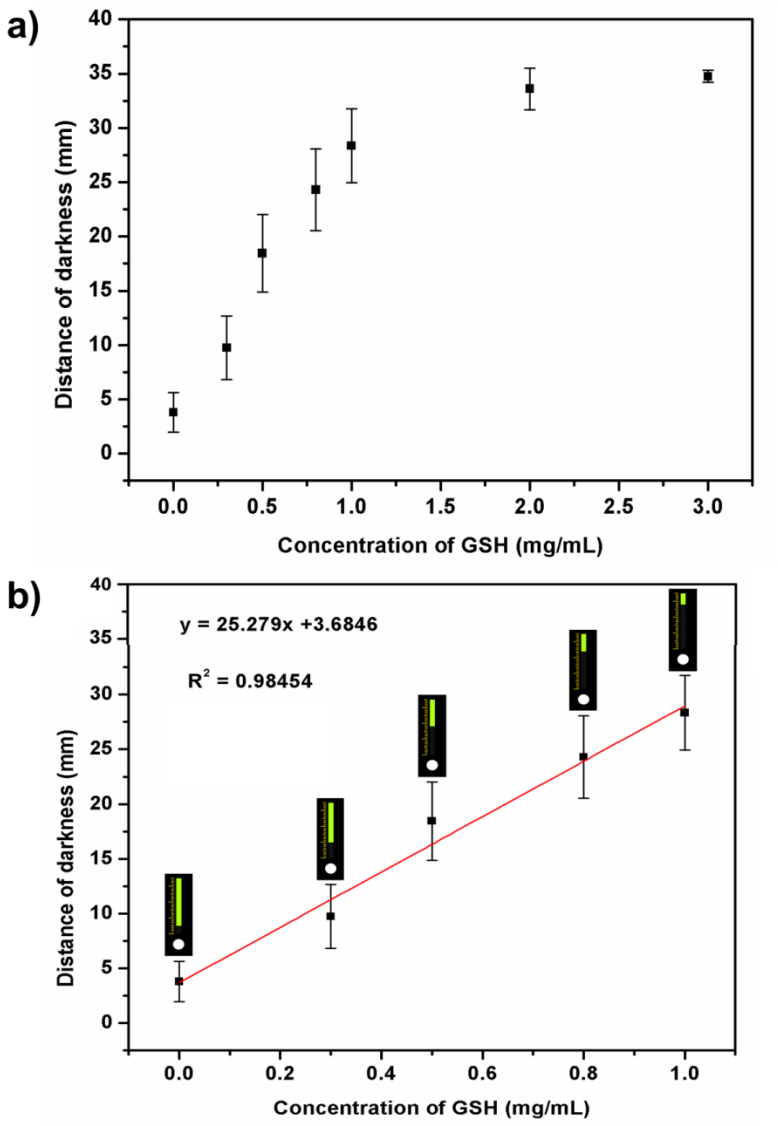

Figure 2.29. The distance of darkness of 3D-μPAD at different concentration of GSH (0 - 6 mg/mL) (a) and linear plot between distance of darkness and concentration of GSH (0.30 - 1.50 mg/mL) (b)

Furthermore, this 3D-μPAD assay was also investigated in the selectivity against other biothiol compounds (Cys and Hcy). Figure 2.30 showed the photograph of distance of darkness for 3D-μPAD toward other biothiols at 0.5 mg/mL. It was found that the minor darkness of the detection zone on layer 1 was observed after loading the Cys and Hcy while a large darkness of the detection zone was addressed in the case of GSH in the same concentration. These satisfied that Cys and Hcy did not interfere to the determination of GSH in the paper based device.

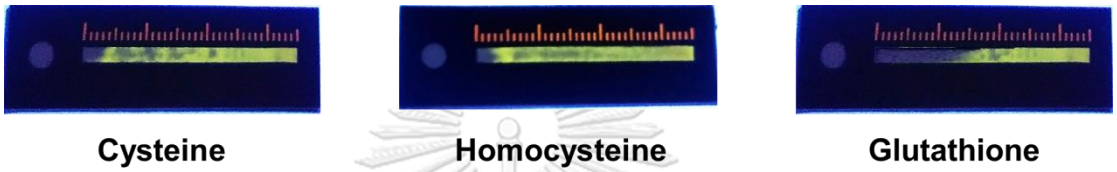

Figure 2.30. The visual color of distance of darkness of 3D-μPAD toward other biothiols at 0.5 mg/mL

Chapter III
Cysteine sensing

3.1. Introduction

Amino acids are essential molecules for biological systems for example, it plays a pivotal of building block in protein synthesis [2, 40], crucial role in maintaining cellular redox environments and mitigating damage from free radicals and toxins, moreover, the balancing nervous system to maintain in human body [41]. Importantly, two amino acids (Cys and Lys) are necessarily needed to infants and human health.

Cysteine (Cys) is a semi-essential α-amino acid which can be biosynthesized in humans. Cys acts as a reagent in many catalytic reactions in biological system and plays a pivotal role in inducible, endogenous detoxification mechanisms in organs [42, 43]. The abnormal level of Cys is responsible for many diseases involving liver damage, skin lesions, slow growth in the children and lethargy [44].

L-lysine is a significant essential amino acid for human body. It exhibits the key role in the carnitine product that is a nutrient for converting the fatty acids into energy and helping lower cholesterol, a substance important for bones and connective tissues including skin, tendons, and cartilage [45]. The deficiency of Lys is involved in fatigue, loss of appetite, slow growth, anemia and reproductive disorders [46].

Therefore, those amino acids are important parameter for various kinds of difference diagnosis diseases [47, 48]. The analytical methods to detect Cys and Lys have been reported, especially in chemiluminescence [49, 50], chromatography [51-54] and electrochemistry [54]. All of techniques that mentioned above, they have the high sensitivity but also had many disadvantages of high costs and time-consuming steps. Nowadays, the nanomolecular sensors have been developed to detect biomedical molecules due to chemical stability, biocompatibility and easies surface modification [55, 56].

The biosensing applications of gold nanoparticles (AuNPs) have been reported in a range of biological environment. The sulfhydryl (thiol) and amine side chain of amino acids could covalently bound with AuNPs to induce an aggregation of AuNPs

resulting in color change from red to blue upon concentration of amino thiol molecules. Gold nanoparticles could be applied to measure concentration of amino acids, however, the small biothiol molecules such as glutathione (GSH) and homocysteine (Hcy) can interfere the amino detection due to containing the similar thiol group containing structure [3, 57, 58].

In the past decades, Luminescent quantum dots (QDs) and gold nanoparticles (AuNPs) have been developed to be a sensor via energy transfer process [27-29]. This process has been motivated by the potential that these materials offer in sensor development both in vitro and in vivo [30, 31], and by recent advances in engineering a variety of nanoparticles with several unique optical and physical properties. Although, these materials were applied to form nanohybrid between QDs and AuNPs in biomedical application, however, there are very few reports to construct the nanomaterials by combining both of AuNPs and QDs for detection of amino acids. We expected that the energy transfer between AuNPs and QDs will be well-defined nanosensor.

3.2. Conceptual design

In this research we attempt to design the multi-function for detection of amino acids. We designed the graphene quantum dots fabricated on the surface of AuNPs. Detection mechanism was expectedly demonstrated in two difference processes; (i) self-aggregation mechanism was occurred by the utilization of thiol moiety bound covalently with AuNPs. This aggregation could be used to measure concentration of Cys by UV-Visible spectroscopic method, (ii) the displacement process of GQDs on AuNPs surface was occurred by turn-on fluorescent in the presence of Lys. From the different method of detection, the **GQDs/AuNPs** could be used to measure the concentration of Lys and Cys with no interfere together as shown in Scheme 3.1.

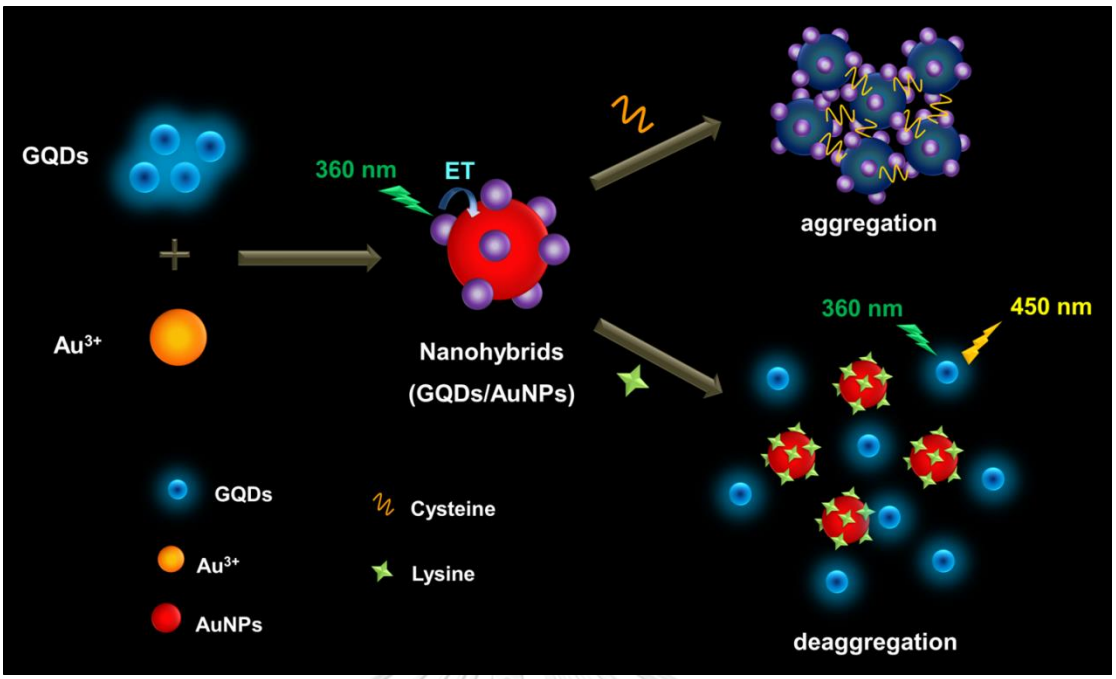

Scheme 3.1. The conceptual design of multifunction sensor for bio compounds detection

3.3. Experimental Analysis

3.3.1. General procedure

3.3.1.1. Reagents and Materials

Citric acid monohydrate ($C_6H_8O_7.H_2O$) was purchased from Merck. Sodium tetrachloroaurate (III) dihydrate ($NaAuCl_4.2H_2O$ 99%) and all amino acids (Cys, Lys, Hcy, Gly, Thr, Phe, Ala, Leu and Met) were brought from Sigma Aldrich. L-glutathione (GSH, reduced > 98%) was received from Calbiochem. Dialysis sacks in MWCO 2000 Da was purchased from Sigma Aldrich. Milli-Q ultrapure water was used for experimental analysis.

3.3.1.2. Instrumentation

Absorption spectra were measured on a Varian Cary 50 UV-Vis spectrophotometer. Fluorescence spectra were performed on a Varian spectrofluorometer by personal computer data processing unit. The nano-hybrid

materials were characterized by High Resolution Transmission Electron Microscopy (HR-TEM) on an accelerating voltage of 100 kV. The microscopic charge states of nanosensors were measured by Malvern Zetasizer Nano. The size distribution of particles was performed by dynamic light scattering (DLS) analysis. All nanomaterials were separated a Eppendorf centrifuge 5804R prior to analysis.

3.3.2. Preparation of nanocomposite

3.3.2.1. Synthesis pathway of graphene quantum dots, ***GQDs***

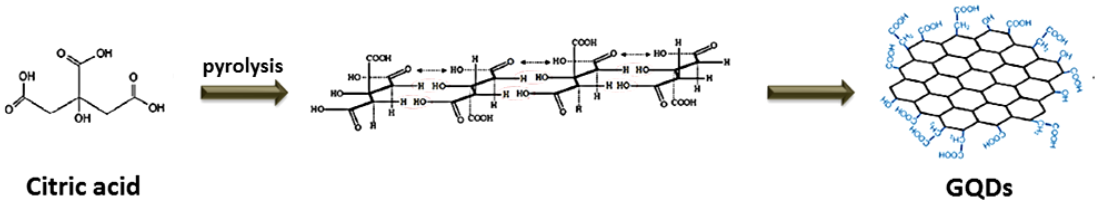

A typical procedure of **GQDs** is described for synthesis as a previously reported method [22, 29]. The 5 g citric acid was melted at 225 ºC and the colorless clear solution was changed to be pale yellow. The reaction was continuously stirred until the solution was returned to colorless again, implying the formation of **GQDs**. After the reaction complete, 2.5 M NaOH (20 mL) was immediately added to quench reaction and the pH of solution was adjusted to be pH 7 with 1.0 M HCl under vigorously stirring. The solution of **GQDs** was purified by dialysis sacks (MWCO 2000 Da) with 500 mL milli-Q water for 3 h to remove the inorganic salts.

3.3.2.2. Synthesis of nanosensor hybrid ***GQDs/AuNPs***

Typically, the 0.01 M stock solution of $NaAuCl_4.2H_2O$ in milli-Q water was prepared in 5 mL volumetric flask. Aqueous solution of $NaAuCl_4.2H_2O$ (0 - 0.33 mM) was rapidly added (Table 3.1) into the 200 μL of **GQDs** solution (64.06 mg/mL) and the pH of reaction was maintained by adding 3 mL of 1 mM PBS buffer (pH 7.4). The reaction was vigorously stirred at ambient temperature for 5 min and then the yellow solution was turned to red. The reaction was further stirred for 20 min to ensure the complete reaction. A ruby red color solution was centrifuged at 5000 rpm

for 5 min to remove the inorganic residues and the hybrid **GQDs/AuNPs** products were redispersed in 3 mL of 1 mM PBS solution (pH 7.4).

Table 3.1. The amount of $NaAuCl_4.2H_2O$ was used for synthesis of the **GQDs/AuNPs** hybrid material

Entry	V of GQDs (mL)	V of $NaAuCl_4.2H_2O$ (mL)	[$NaAuCl_4.2H_2O$] (mM)	Total V (mL)
1	0.200	0.010	0.033	3.000
2	0.200	0.015	0.050	3.000
3	0.200	0.020	0.067	3.000
4	0.200	0.040	0.133	3.000
5	0.200	0.060	0.200	3.000
6	0.200	0.080	0.267	3.000
7	0.200	0.100	0.333	3.000

3.3.3. Determination of cysteine and lysine using UV-Vis and fluorescence titration

Typically, a stock solution (1 mM) of Cys and Lys was prepared in 1 mM PBS buffer solutions (pH 7.4). The nanohybrid **GQDs/AuNPs** was evaluated by using the following in the topic of 3.3.2.2. To investigate the sensing properties of **GQDs/AuNPs** toward cysteine, the various concentrations of Cys (0 - 0.5 mM) was added into 200 μL of **GQDs/AuNPs** solution (64.06 mg/mL) and the volume of solution was adjusted to 2 mL by 1 mM PBS buffer solution pH 7.4 as shown in Table 3.2. The mixture was stirred for 2 min before measurement of the absorption spectrum in the range of 200-800 nm.

In the case of Lys detection, the various concentration of Lys (0 - 0.8 mM) was added into 200 μL of **GQDs/AuNPs** solution (64.06 mg/mL) and the volume of solution was adjusted to 2 mL by 1 mM PBS buffer solution at pH 7.4 as shown in Table 3.3. The mixture was stirred for 2 min before measurement of the fluorescence spectrum under excitation wavelength at 360 nm.

Table 3.2. The amount of Cys was used for absorption titration studies

Entry	V. of Cys (mL)	[Cys] mM	V total (mL)	Abs. at 645 nm
1	0.000	0.000	2.000	0.02184
2	0.010	0.005	2.000	0.02905
3	0.020	0.010	2.000	0.03419
4	0.050	0.025	2.000	0.03938
5	0.100	0.050	2.000	0.04771
6	0.200	0.100	2.000	0.06415
7	0.500	0.250	2.000	0.07363
8	0.800	0.400	2.000	0.07162
9	1.000	0.500	2.000	0.07191

Table 3.3. The amount of Lys was used for absorption titration studies

Entry	V. of Lys (mL)	[Lys] mM	V total (mL)	Int. at 450 nm
1	0.000	0.000	2.000	66.12088
2	0.010	0.005	2.000	70.94397
3	0.020	0.010	2.000	80.19742
4	0.050	0.025	2.000	100.3287
5	0.100	0.050	2.000	111.2455
6	0.200	0.100	2.000	139.743
7	0.500	0.250	2.000	207.4075
8	0.800	0.400	2.000	237.3557
9	1.000	0.500	2.000	253.3132

3.3.4. The interference effect from other amino acid toward cysteine and lysine determination by using UV-Vis and fluorescence spectroscopy

The 0.01 M stock solution of amino acids (Cys, Lys, GSH, Gly, Thr, Phe, Ala, Leu and Met) was prepared in 5 mL volumetric flask. In the interference study toward Cys, the 10 equiv of other amino acid was directly added into each portion of **GQDs/AuNPs** and Cys. The total volume of solution was adjusted to 2 mL by 0.1 mM PBS buffer solution pH 7.4 and the mixed solution was stirred for 2 min prior to

measurement of the absorption spectra by UV-Vis technique from 200 to 800 nm (as shown in Table 3.4).

For interference studies of Lys sensing, the 10 equiv of other amino acid was directly added into each portion of **GQDs/AuNPs** and Lys. The total volume of solution was adjusted to 2 mL by 0.1 mM PBS buffer solution pH 7.4 and the mixed solution was stirred for 2 min prior to measurement of the fluorescence spectra under excitation wavelength at 360 nm (as shown in Table 3.5).

Table 3.4. The amount of Cys was used for interference studies

Amino acid	**Cys : amino acid**	**[Cys] mM**	**[Amino acid] mM**	**A_{525}**	**A_{645}**
GQDs/AuNPs	0	0.00	0.00	0.06474	0.02031
Cys	1 : 0	0.05	0.00	0.0558	0.0399
Cys +Thr	1 : 10	0.05	0.50	0.05256	0.04112
Cys +Phe	1 : 10	0.05	0.50	0.05293	0.03945
Cys +Lys	1 : 10	0.05	0.50	0.05926	0.05065
Cys +Glu	1 : 10	0.05	0.50	0.05159	0.04195
Cys +Met	1 : 10	0.05	0.50	0.05412	0.04912
Cys +Leu	1 : 10	0.05	0.50	0.05117	0.0401
Cys +Ala	1 : 10	0.05	0.50	0.05253	0.03843
Cys +GSH	1 : 10	0.05	0.50	0.05249	0.04339
Cys +Gly	1 : 10	0.05	0.50	0.05321	0.04865

Table 3.5. The amount of Lys was used for interference studies

Amino acid	Lys : amino acid	[Lys] mM	[Amino acid] mM	I_{450}
GQDs/AuNPs	0	0.00	0.00	49.81566
Lys	1 : 0	0.05	0.00	254.2836
Lys +Thr	1 : 10	0.05	0.50	41.21601
Lys +Phe	1 : 10	0.05	0.50	42.33438
Lys +Cys	1 : 10	0.05	0.50	40.23609
Lys +Glu	1 : 10	0.05	0.50	47.54444
Lys +Met	1 : 10	0.05	0.50	38.53481
Lys +Leu	1 : 10	0.05	0.50	48.26735
Lys +Ala	1 : 10	0.05	0.50	41.97398
Lys +GSH	1 : 10	0.05	0.50	50.31585
Lys +Gly	1 : 10	0.05	0.50	44.56982

3.3.5. Determination of Cys and Lys in biological samples

3.3.5.1. Preparation of Cys in urine sample

Firstly, the synthetic urine was prepared [59-61] as indicated in Table 3.6. Urine samples were collected from the three people and kept at -20 ^{o}C for 24 h to obtain the protein residue precipitate. The sample was melted at room temperature and centrifuged at 10000 rpm 10 min for separation of the protein residues. The standard addition method was used to explore the efficacy of Cys detection. Briefly, a various concentration of Cys (0 - 0.029 mM) was separately added into the mixture solution of 200 μL **GQDs/AuNPs** and 200 μL urine sample. The mixture was diluted to be 2 mL by PBS buffer solution at pH 7.4 (Table 3.7) and then stirred at ambient temperature for 2 min. The absorption spectra were recorded in the range of 200-800 nm.

3.3.5.2. Preparation of Lys in milk sample

Milk and soybean milk were used for Lys detection. The 5 g of samples were accurately weigh and dissolved in 20 mL milli-Q water and were stirred until

homogeneous solution. The samples were centrifuged under 10000 rpm for 10 min to obtain a clear solution. The 0.01 M stock solution of Lys was added into 200 μL milk sample with 200 μL **GQDs/AuNPs**. The mixture was adjusted to be 2 mL by PBS buffer solution at pH 7.4 as shown in Table 3.8 - 3.9. The reaction mixture was stirred for 2 min before measurement of fluorescence spectra under excitation wavelength at 360 nm.

Table 3.6. Composition of synthetic urine

Species	**Concentration (gL^{-1})**
$CaCl_2.H_2O$	0.65
$MgCl_2.6H_2O$	0.651
NaCl	4.6
Na_2SO_4	2.3
$Na_3C_6H_8O_7.2H_2O$	0.65
Na_2CO_3	0.020
KH_2PO_4	2.8
KCl	1.6
NH_4Cl	1
$CO(NH_2)_2$	25
$C_4H_7N_3O$	1.1

Table 3.7. The amount of Cys was added for urine sample

Entry	V of Cys (mL)	[Cys] mM	V total (mL)	A_{645}/A_{525}	SD
1	0.000	0.000	2	0.4221	0.0178
2	0.010	0.005	2	0.5068	0.0135
3	0.020	0.010	2	0.6306	0.0298
4	0.030	0.015	2	0.7838	0.0253
5	0.040	0.020	2	0.9216	0.0349
6	0.050	0.024	2	1.0721	0.0499
7	0.060	0.029	2	1.1874	0.0198

Table 3.8. The amount of Lys was added for milk sample

No.	V of Lys (mL)	[Lys] mM	V total (mL)	I_{450}	SD
1	0.00	0.00	2	16.1343	1.0421
2	0.10	0.05	2	32.1214	2.2492
3	0.20	0.10	2	41.3688	4.8886
4	0.40	0.20	2	71.2120	4.6142
5	0.60	0.30	2	92.2097	4.1995
6	0.80	0.40	2	124.3709	3.7127
7	1.00	0.50	2	142.5565	6.1977

Table 3.9. The amount of Lys was added for soybean milk sample

No.	V of Lys (mL)	[Lys] mM	V total (mL)	I_{450}	SD
1	0.00	0.00	2	35.1176	1.49483
2	0.10	0.05	2	51.6221	2.60305
3	0.20	0.10	2	67.7199	4.33274
4	0.40	0.20	2	92.9148	3.83503
5	0.60	0.30	2	114.2807	2.59289
6	0.80	0.40	2	141.9774	4.36006
7	1.00	0.50	2	161.2802	3.82639

3.4. Results and discussions

3.4.1. Characterization of GQDs nanocomposite

The synthesis of graphene quantum dots (**GQDs**) were prepared via chemical oxidation process following to previous work [22]. A bottom-up preparation of **GQDs** particles was performed to fabricate a unique form of **GQDs**. The citric acid was pyrolyzed for carbonization under temperature 200 ^{o}C to generate a carbon source for **GQDs** forming. The synthesized product was purified by dialysis to remove an organic residue. The **GQDs** were characterized by Fourier-transform (FT-IR) spectroscopy as shown in Figure 3.1. As a comparision of the IR spectra of citric acid and **GQDs**, the IR spectrum of citric acid showed vibration band at 3323 cm^{-1} corresponding to O-H stretching. This absorption band was shifted to 3250 cm^{-1} when the **GQDs** were formed. Moreover, the characteristic peak of C=O and C-O of citric acid were found at 1720 and 1207 cm^{-1}, respectively. Both of the absorption peaks were also significant changed to 1556 and 1380 cm^{-1} which assigned to be C=O and C-O of **GQDs**, respectively [62, 63]. Interestingly, the typical mode of phenolic of C-OH stretching was attributed at 1078 cm^{-1}. This results showed that the carbonization of citric acid was not completed. It could be implied that **GQDs** were formed under this condition [22].

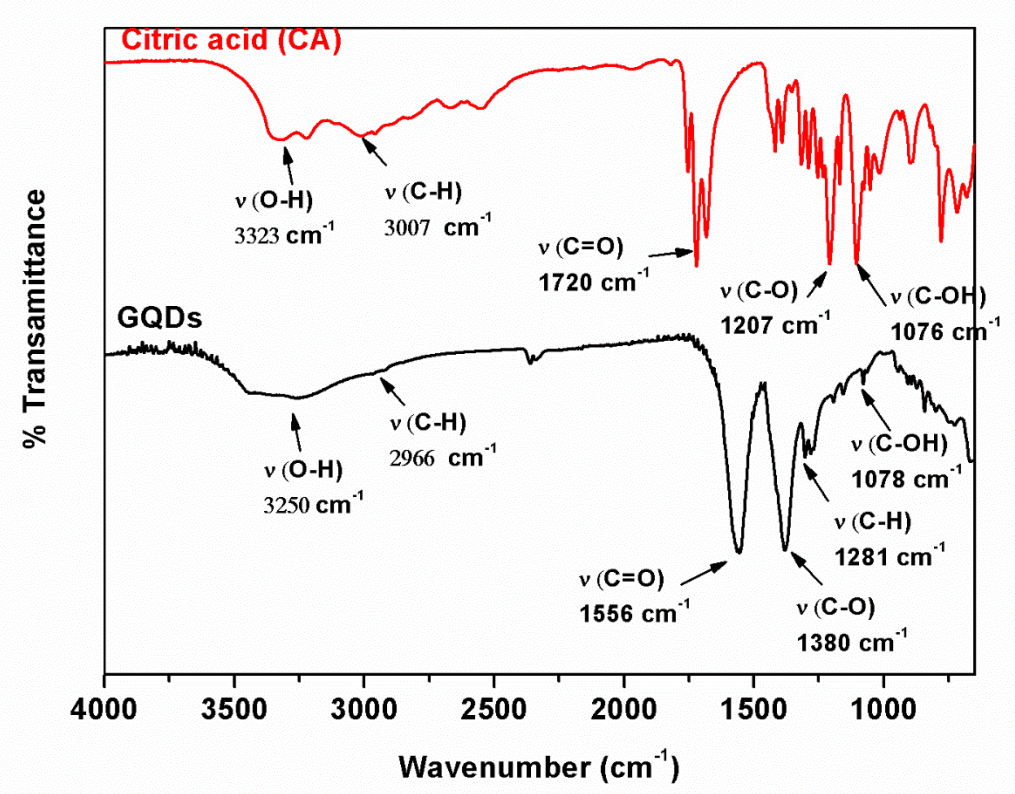

Figure 3.1. FT-IR spectra of citric acid (red line) and **GQDs** nanocomposite (black line)

The structural information of **GQDs** nanomaterials was confirmed by transmission electron microscopy (TEM) and energy-dispersive x-ray spectroscopy (EDX). The average diameter size of **GQDs** was calculated from imageJ software and the results showed 150 particles of **GQDs** had an average size of 5 nm (Figure 3.2).

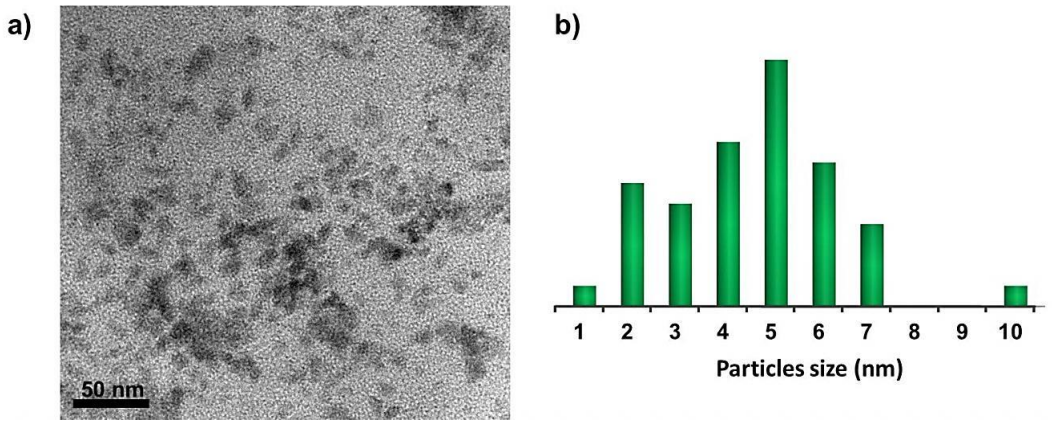

Figure 3.2. The TEM image (a) and particles size (b) of as-prepared **GQDs**

Moreover, the EDX analysis was also evaluated to determine the element composition of **GQDs**. They contained mainly C and O elements due to the pyrolysis of citric acid (Figure 3.3). The as-prepared composition of **GQDs** was determined by using EDX analysis as shown in the Table 3.10. This analysis confirmed that C and O atoms were the main component of **GQDs**.

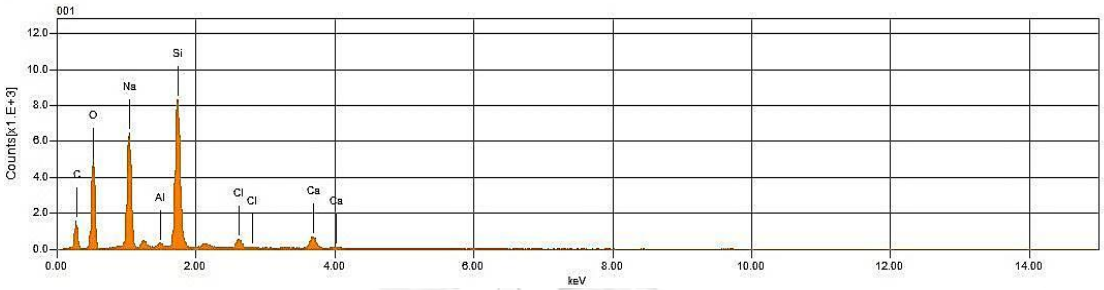

Figure 3.3. The EDX spectrum of **GDQs** nanocomposite

Table 3.10. The percent composition of **GQDs** nanocomposite

Formula	Mass%	Atom%	Surface area
C	26.71	37.49	36793
O	36.72	38.68	130032
Na	17.61	12.91	215176
Al	0.39	0.24	7239
Si	15.61	9.37	332403
Cl	1.14	0.54	23434
Ca	1.81	0.76	37000

3.4.2. Optical properties of GQDs nanocomposite

The optical properties of **GQDs** nanocomposite was characterized by using UV-Visible and fluorescence spectroscopy. The maximum absorption band of **GQDs** was observed at 360 nm, regarding to π to π^* transition of C=C band [64] (Figure 3.4). Apart from photophycical properties, the blue brightness luminescence of **GQDs** (Figure 3.5) exhibited an emission band at 450 nm under various excitation wavelengths (λ_{ex}) from 300 to 440 nm. The fluorescence signal at 450 nm was

increased under excitation in the range of 300-360 nm, except for the decrease of fluorescence in the excitation range of 380-440 nm (Figure 3.5). It clearly indicated that the excitation-independent photoluminescence of **GQDs** may attribute to the uniform size and the surface state of sp^2 hybridization for **GQDs** [65]. The maximum fluorescence intensity was developed under an excitation wavelength at 360 nm. Consequently, the excitation wavelength at 360 nm of as-prepared **GQDs** was chosen for use in further analysis as shown in Figure 3.5.

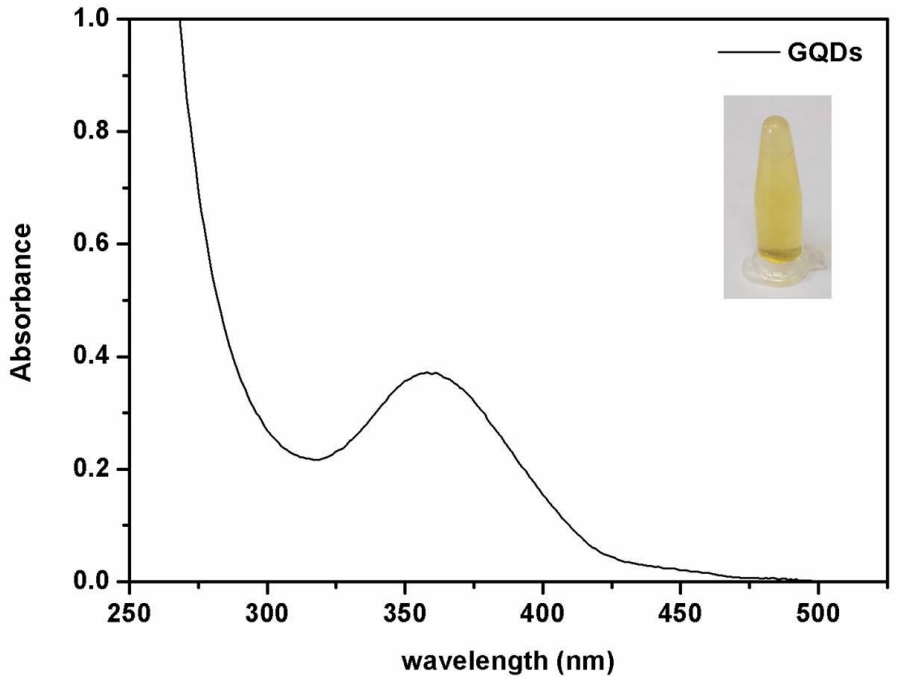

Figure 3.4. The absorption spectrum of as-prepared **GQDs** and inset photographic image of color solution

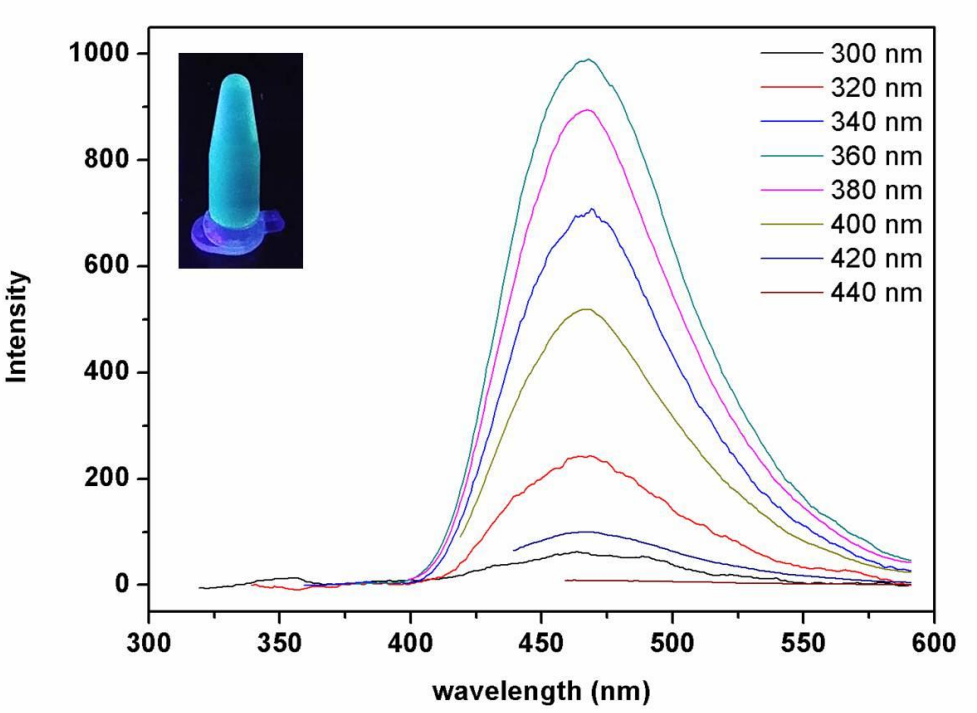

Figure 3.5. The fluorescence spectra of **GQDs** under excitation wavelength of 300-440 nm. Inset showed the blue brightness solution under UV light at 365 nm

3.4.3. Characterization of as-prepared GQDs/AuNPs nanohybrid

The colloidal gold nanoparticles were prepared by redox reaction method by using **GQDs** as the reducing agent and stabilizer. To verify the proper ratio of **GQDs** and $NaAuCl_4$, the UV-visible spectroscopy was carried out with various concentration of $NaAuCl_4$ in the range of 0.03 – 0.33 mM. The absorption spectra of AuNPs at 525 nm were increased upon increasing the concentration of $NaAuCl_4$ and the maximum absorbance was observed upon the addition of AuNPs at 0.22 mM. However, in the higher concentration of AuNPs over 0.13 mM, the new absorption band of aggregation AuNPs was found at 645 nm with a concomitant of the visually color change from red to purple as shown in Figure 3.6. These results suggested that the 0.13 mM of $NaAuCl_4$ in the presence of 200 μL **GQDs** (64.06 mg/mL) is a suitable concentration for sensor application of **GQDs/AuNPs**.

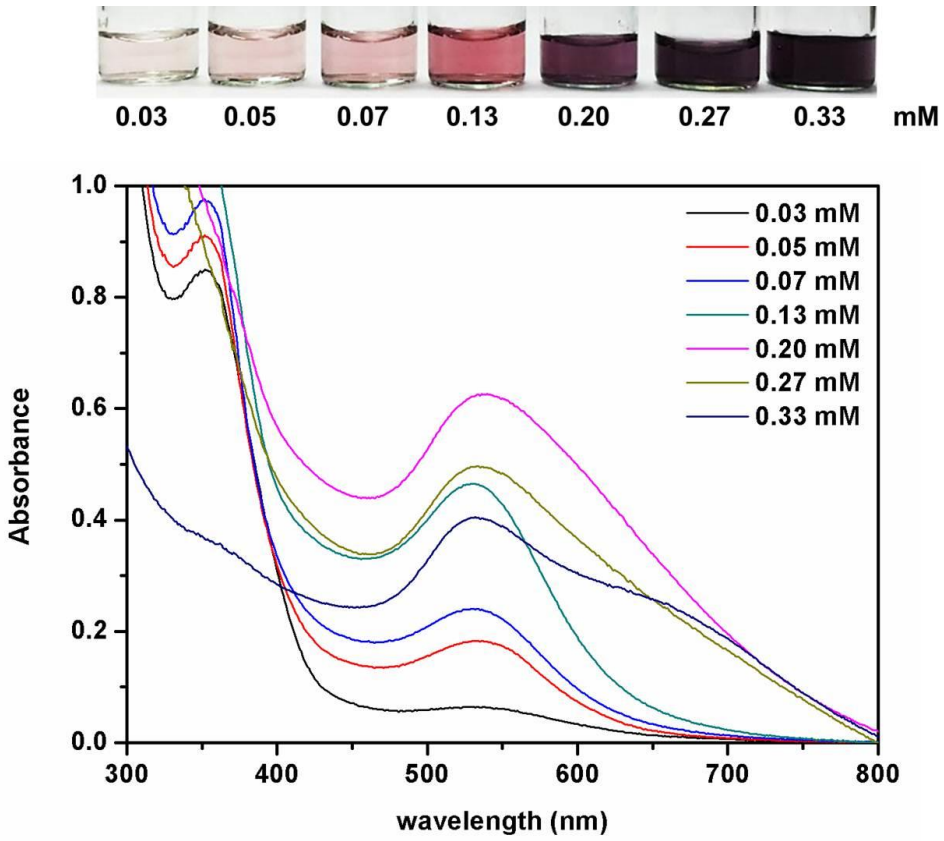

Figure 3.6. Absorption spectra of formation of **GQDs/AuNPs** particles in 1 mM PBS buffer solution (pH 7.4) and inset photographical images with various concentrations of $NaAuCl_4$ in the range of 0.03 – 0.33 mM.

The as-prepared **GQDs/AuNPs** nanohybrid was characterized by Fourier-transform (FT-IR) spectroscopy as shown in Figure 3.7. Comparing the FT-IR spectra of **GQDs** and **GQDs/AuNPs**, the relative intensity of C=O and C-O vibrational absorption slightly increased. It can be explained that GQDs possibly caused by the partial oxidation by $NaAuCl_4$. However, the vibrational absorption of hydroxyl group (-OH) and C-H stretching of **GQDs** was still observed at 3255 cm^{-1} as well as 2965 cm^{-1} and 1281 cm^{-1}, respectively.

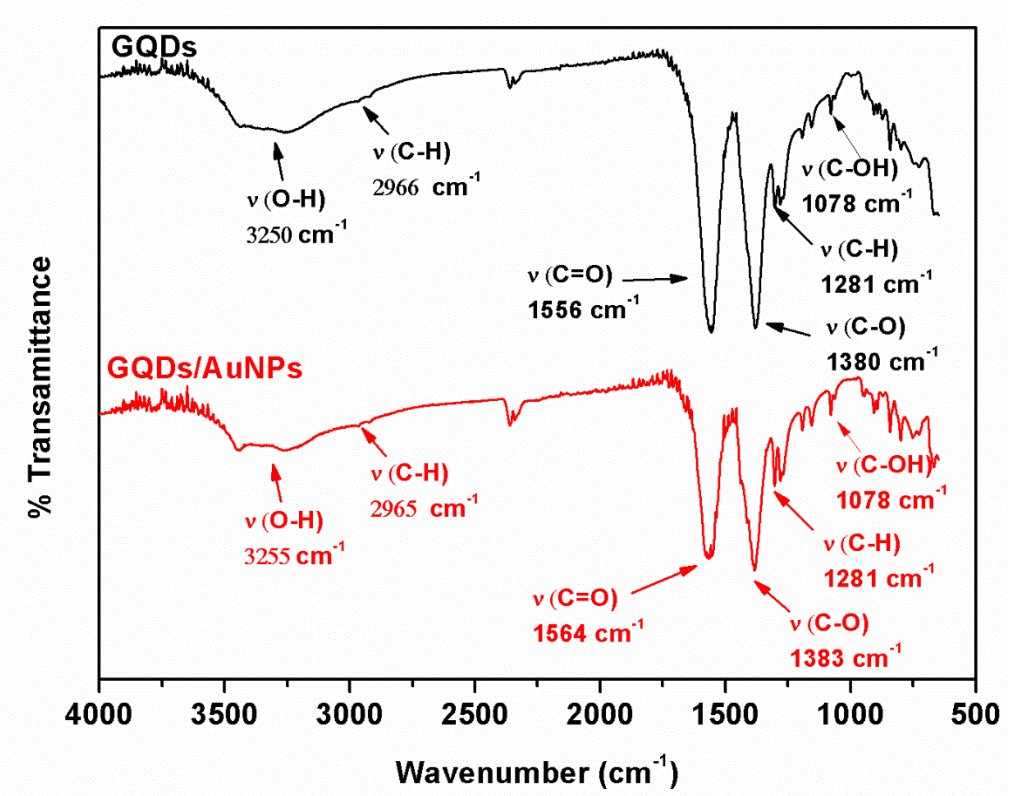

Figure 3.7. FT-IR spectra of **GQDs** (black line) and **GQDs/AuNPs** (red line)

The structural information of **GQDs/AuNPs** nanomaterials was confirmed by TEM and EDX spectra. After adding $NaAuCl_4$, the TEM image of Figure 3.8b exhibited the intense dark particles assigned to AuNPs which was encapsulated by the light shell of **GQDs** nanosheets. Moreover, the results showed the significant increase of an average particle size of **GQDs/AuNPs** nanomaterials from 5 to ~15 nm. A larger average size of as-prepared **GQDs/AuNPs** is due to the possible aggregation of **GQDs** on surface of gold nanoparticles. Besides the different size, the morphologies of TEM images of **GQDs** (in Figure 3.8a) and **GQDs/AuNPs** (in Figure 3.8b) were relatively different.

The EDX analysis was used to evaluate the element composition of **GQDs/AuNPs**. The peak of Au element was observed. These results confirmed that the component of Au was hybrid on the surface of **GQDs** as shown in the Figure 3.8. The percent composition of **GQDs/AuNPs** was determined form EDX analysis as shown in the Table 3.11. These results reasonably revealed that the preparation of the **GQDs/AuNPs** nanomaterials has been achieved.

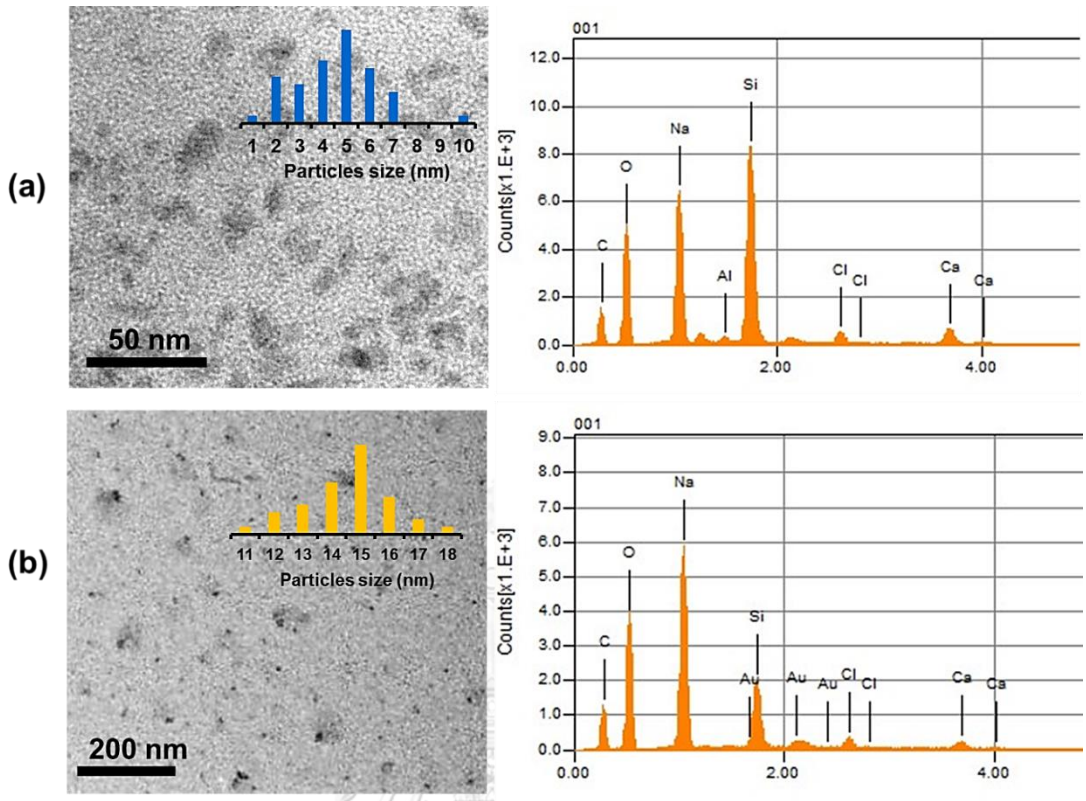

Figure 3.8. Comparison properties of the TEM image and EDX spectra of as-prepared of **GQDs** (a) and **GQDs/AuNPs** (b)

Table 3.11. The percent composition of **GQDs/AuNPs** nanocomposite

Formula	Mass%	Atom%	Surface area
C	23.98	34.04	26317
O	40.81	43.5	112724
Na	19.37	14.37	158393
Mg	0.99	0.7	12898
Al	0.21	0.13	2611
Si	10.05	6.1	141047
Cl	0.98	0.47	13906
K	0.1	0.04	1322
Ca	1.01	0.43	14174
Au	2.49	0.22	15774

3.4.4. Optical properties of AuNPs supported on GQDs (GQDs/AuNPs)

The two absorption bands at 350 nm and 525 nm corresponding to the **GQDs** and AuNPs, respectively, are strong evidence of forming **GQDs/AuNPs**. Moreover, the luminescence feature of **GQDs/AuNPs** was measured by fluorescent spectroscopy under excitation wavelength of 360 nm. A large fluorescence quenching of emission band at 475 nm was observed via energy transfer from **GQDs** to AuNPs as shown in Figure 3.9a and 3.9b. This result indicated that $NaAuCl_4$ was reduced by **GQDs** providing AuNPs fabricated on **GQDs**. In the optical properties of **GQDs** in various concentrations of AuNPs, it revealed the dual functions of **GQDs**. Firstly, **GQDs** acted as a reducing agent to reduce Au^{3+} to be AuNPs. Moreover, the negative charge of carboxylate on the surface of **GQDs** could be a stabilizer for AuNPs by electrostatic repulsion to prevent an aggregation of AuNPs.

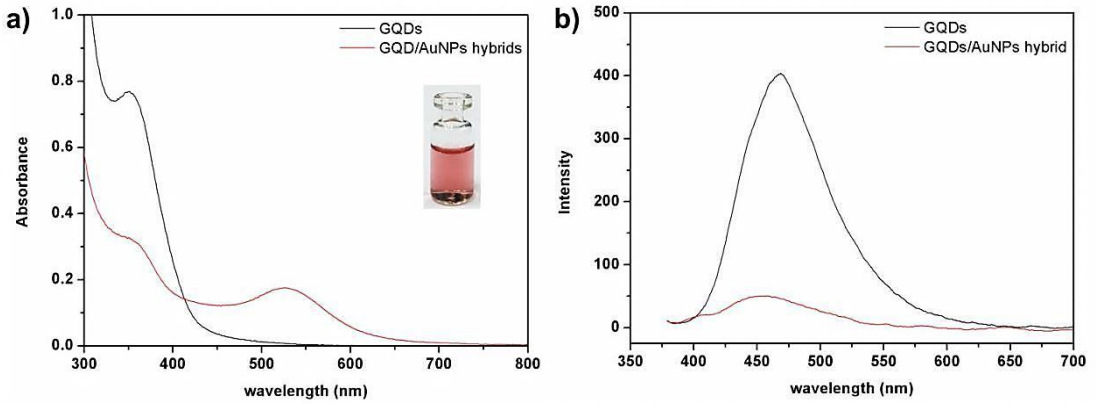

Figure 3.9. The absorption (a) and emission (b) spectra of **GQDs/AuNPs** hybrids in the 1 mM PBS buffer solution (pH 7.4). The nanocomposite of **GQDs/AuNPs** was studies under excitation wavelength at 360 nm

3.4.5. The stability of GQDs/AuNPs hybrids

Taking on board of the benefit of nanocomposite in term of stability, we have particularly compared in stability of nanomaterials before and after centrifuge to remove the inorganic residue by using UV-Vis spectroscopy. The stability of **GQDs/AuNPs** hybrids was measured by absorption peak of **GQDs/AuNPs** at 525 nm. In the unpurified **GQDs/AuNPs,** the aggregation of AuNPs was observed within 2 days. The stability of **GQDs/AuNPs** was improved by centrifugation to remove the inorganic residue and the result showed an aggregation of a purified **GQDs/AuNPs** was retarded over a month as shown in Figure 3.10. These results indicated that **GQDs** served as a good stabilizer of gold nanoparticles to excellently prevent an aggregation of AuNPs nanoparticles based on high negative repulsion of carboxylate moiety in **GQDs**.

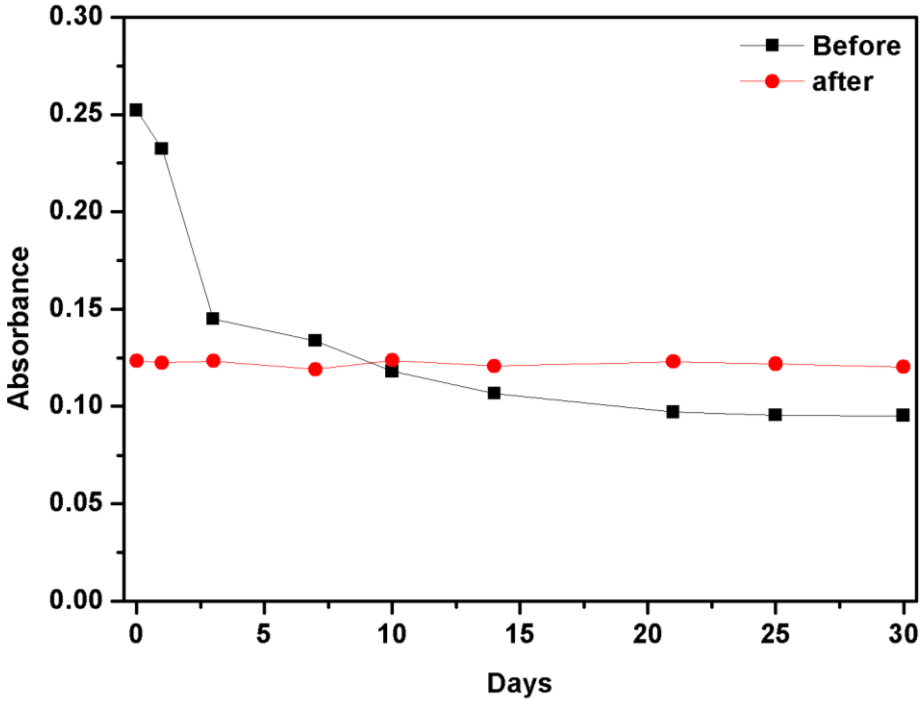

Figure 3.10. The determination of stability of **GQDs/AuNPs** hybrid before (■) and after (●) removing the inorganic residue by monitoring the absorption band at 525 nm

3.4.6. Photophysical properties of nanomaterials with various amino acids

The **GQDs/AuNPs** hybrid materials were screening test with various amino acids in both techniques of UV-visible and fluorescence spectroscopy. In the presence of Cys, the maximum absorption peak of **GQDs/AuNPs** at 525 nm was decreased with a concomitant of a new absorption band around 645 nm. Upon the addition of other amino acid, the absorption spectra of **GQDs/AuNPs** were insignificant changed. In visual response of solution, the color solution of **GQDs/AuNPs** rapidly turned from red to blue in the presence of Cys while the red color solution of **GQDs/AuNPs** remained unchanged in the case of other amino acid.

Particular properties of gold nanoparticles are very well-known that the typical aggregation of gold nanoparticle performs blue color solution and red-shifted absorption band. These phenomenon of **GQDs/AuNPs** with Cys induced dramatically AuNPs aggregation undergone sulfhydryl side chain. The zwitterionic formation of Cys between carboxylate (COO^-) and amine (NH_3^+) moiety can bind with AuNPs with the opposite group of Cys adsorbed on particles leading to the change of the

color solution. Deeply consideration in Figure 3.11a, the absorption peak around 350 nm of **GQDs/AuNPs** was increased in the increment of Lys. Moreover, the **GQDs/AuNPs** particles have been investigated in fluorescence response towards various amino acids in 1 mM PBS pH 7.4. As shown in Figure 3.11b, the strongest emission band at approximately 450 nm was obviously observed in the presence of Lys while other amino acid showed the similar emission band of the **GQDs/AuNPs** nanomaterials. According to the fluorescence properties of **GQDs**, the subsequent photoluminescence recovery of **GQDs** in **GQDs/AuNPs** was appeared and the red color solution remained unchanged (inset of Figure 3.11). These results demonstrated that **GQDs** was probably desorbed on the AuNPs possibly caused by the competition between amino acid group of Lysine and oxygen-containing functional group of **GQDs**. Consequently, Lys performed the stabilizer of AuNPs instead of **GQDs**.

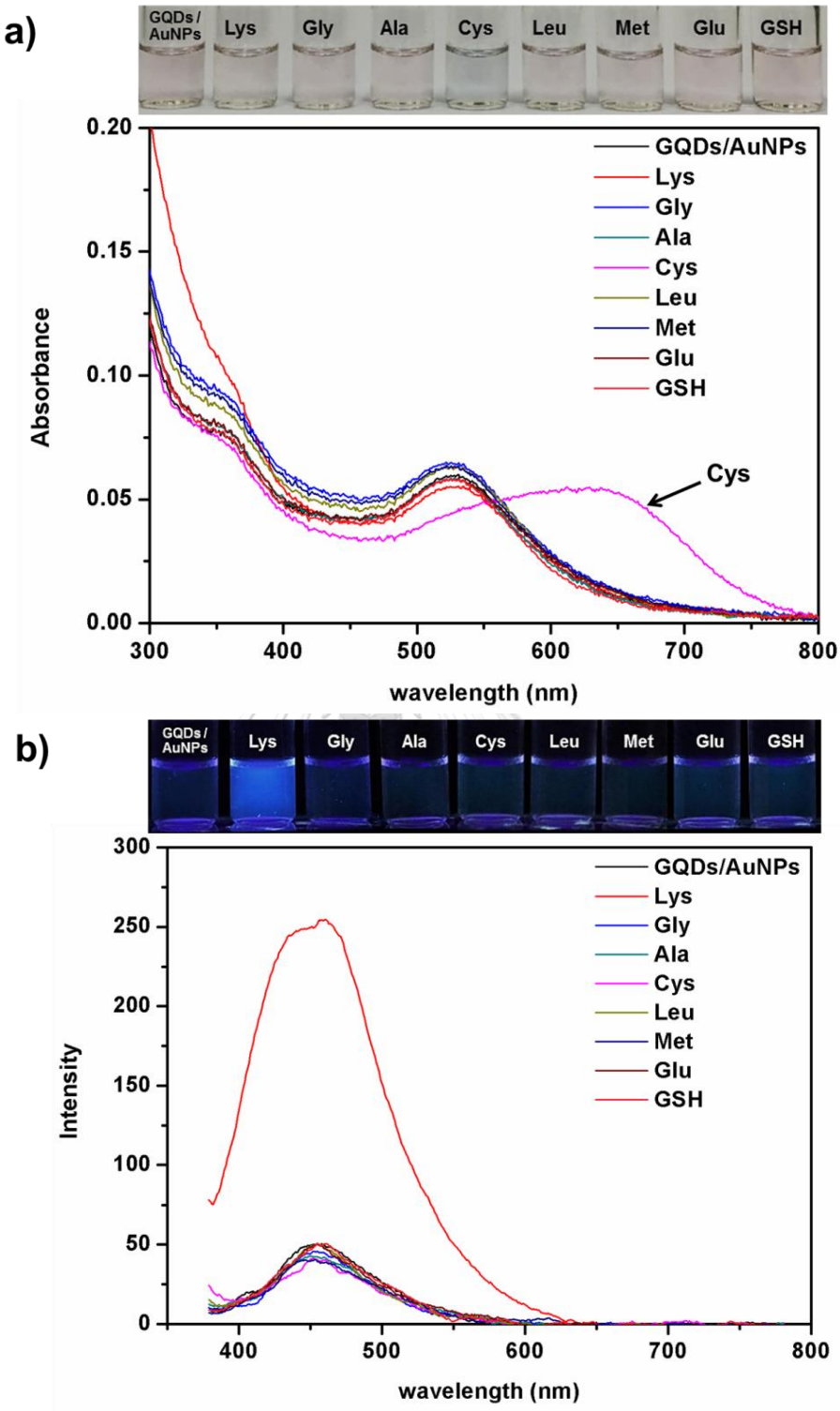

Figure 3.11. The absorption (a) and emission (b) spectra of 0.4 μM **GQDs/AuNPs** nanocomposite with 10 equiv of various amino acids in 1 mM PBS buffer solution (pH 7.4) after stirring 2 min and inset photographical images of the solution under the light and UV light at 365 nm, respectively.

To verify the hypotheses, the zeta-potential (ζ-potential) analysis was used to examine the magnitude of electrostatic charge on surface of particles. The microscopic charge state of **GQDs/AuNPs** particles was about -52 mV ascribing the excellent disaggregation of nanoparticles resulting in the red color solution of **GQDs/AuNPs**. This means the good stabilizer of **GQDs** on AuNPs. While low colloidal stability of AuNPs in the presence of Cys, it was found that Cys induced the slightly shift to the positive charge at -44 mV resulting in the blue color solution with a respect of the aggregation of particles. In the case of Lys, the total charge state exhibited at -32 mV which is more positive charge than free **GQDs/AuNPs** and the mixture solution of **GQDs/AuNPs** and Cys (Figure 3.12). However, the color solution of **GQDs/AuNPs** in the presence of Lys displayed a red solution with an unchanged absorption band at 525 nm and turn-on fluorescence at 450 nm. These results implied the deaggregation of particles. As assumption, it can be explained that the desorption process of **GQDs** on the surface of **GQDs/AuNPs** nanocomposite was occurred and the Lys was assembly bound with the surface of AuNPs and performed as the good stabilizer via positive ions repulsion of primary ammonium ions (NH_3^+) in Lys.

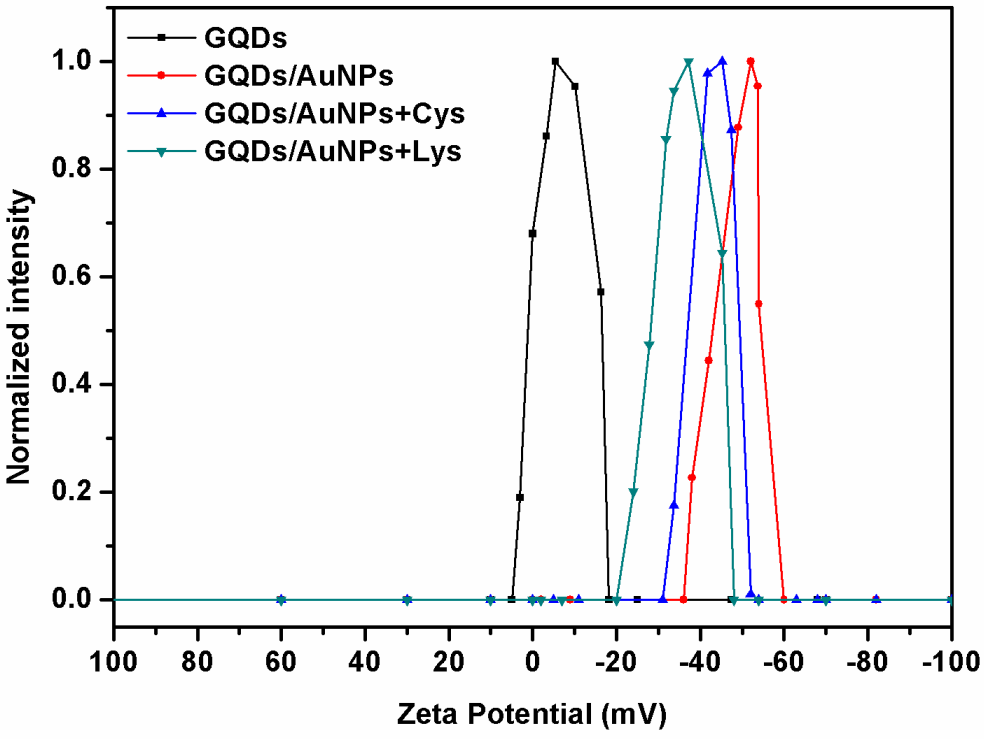

Figure 3.12. Determination of zeta potential of nanohybrids of **GQDs** (black), **GQDs/AuNPs** (red), **GQDs/AuNPs**⊂Cys (blue) and **GQDs/AuNPs**⊂Lys (green)

Furthermore, the TEM image was used to investigate the sensing mechanism of **GQDs/AuNPs**. The morphology of unique colloidal nanosensor was displayed in Figure 3.13 showing an average particles size of 9 nm regarding to a spherical AuNPs which was supported on **GQDs** surface (Figure 3.13a). Upon the addition of Cys into the solution of nanosensors, the self-aggregation of **GQDs/AuNPs**⊂Cys showed an increase of diameter size of AuNPs to be 400 nm as shown in Figure 3.13b. In the case of Lys, the particle sizes of **GQDs/AuNPs**⊂Lys were slightly increased to be 12 nm. In the high magnification of Figure 3.13c inset, the graphene nanosheets were remarkably removed off AuNPs. These TEM images suggested a strong evidence to support that Cys enabled to induce the self-aggregation of **GQDs/AuNPs** while Lys preferred to perform the stabilizer by displacement of **GQDs** sheets resulting in turn-on fluorescence at 450 nm corresponding to **GQDs**.

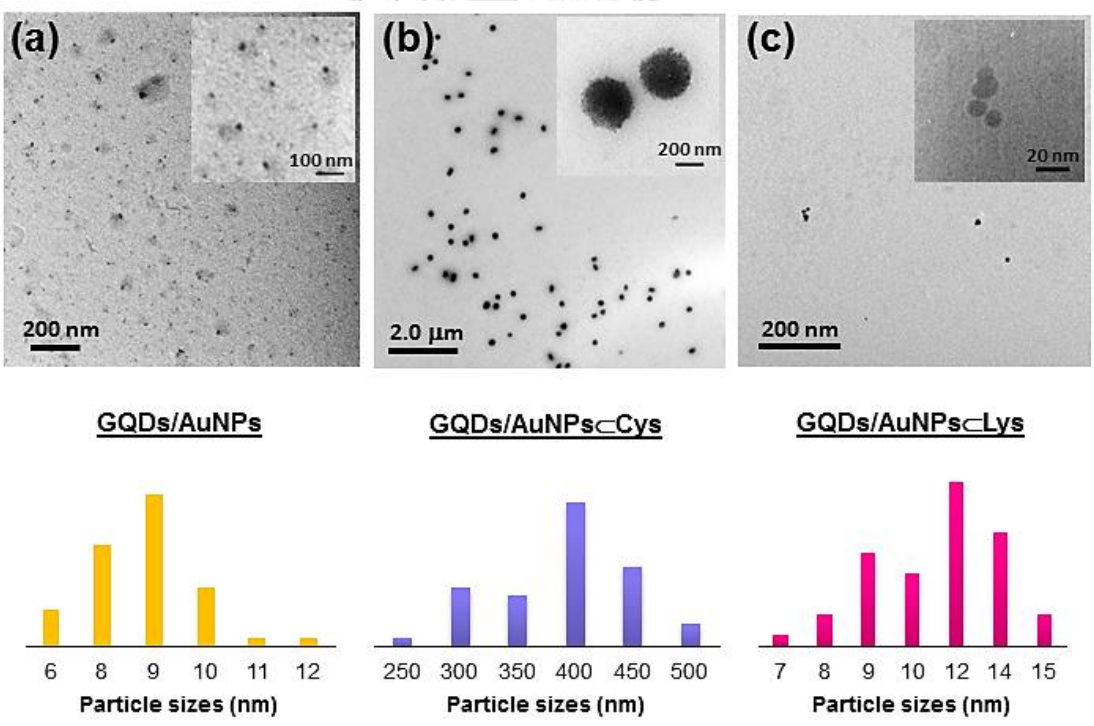

Figure 3.13. TEM images and particle sizes of **GQDs/ AuNPs** (a) , **GQDs/AuNPs**⊂Cys (b), **GQDs/AuNPs**⊂Lys (c) and inserted graphical photograph.

3.4.7. Interference study of GQDs/AuNPs nanomaterial towards amino acids

The interference studies of **GQDs/AuNPs** toward Cys and Lys with 10 equiv of other amino acids were examined by using UV-Visble and fluorometric methods. In the case of Cys, the surface plasmon band of **GQDs/AuNPs** shifted from 525 nm to 645 nm in the presence of Cys. For Cys detection, the absorbance ratio of the absorption band at 525 nm and 645 nm (A_{525}/A_{645}) was monitored to evaluate the interference effect from the other amino acids. In the presence of Cys (**GQDs/AuNPs**⊂Cys), the relative absorbance of A_{525}/A_{645} was still observed at 1.5 in the sample solution with and without the other amino acid (Figure 3.14a). The constant absorbance ratio is a strong support that the other amino acid could not interfere the quantitative analysis of Cys. Then, it could be concluded that **GQDs/AuNPs** has a highly selective detection of Cys without the effect of interference. On the other hand, the interference studies of other amino acid toward Lys had been also monitored in the 1 mM PBS by using fluorescence technique (Figure 3.14b). The relative fluorescent intensity of **GQDs/AuNPs**⊂Lys complexation was similar to that of the addition of 10 equiv other amino acids into **GQDs/AuNPs**⊂Lys. This result revealed that the **GQDs/AuNPs** enable to be the fluorescent probe for determination of Lys with a high selectivity and without interference from the other amino acids. As the advantage of dual detection of **GQDs/AuNPs** toward Lys and Cys, the interference was presumably occurred in each other for detection even in difference techniques. Fascinatingly, the results from UV-Visible and fluorescent methods reliably promoted the high-specific detection of Cys and Lys without interruption of each other.

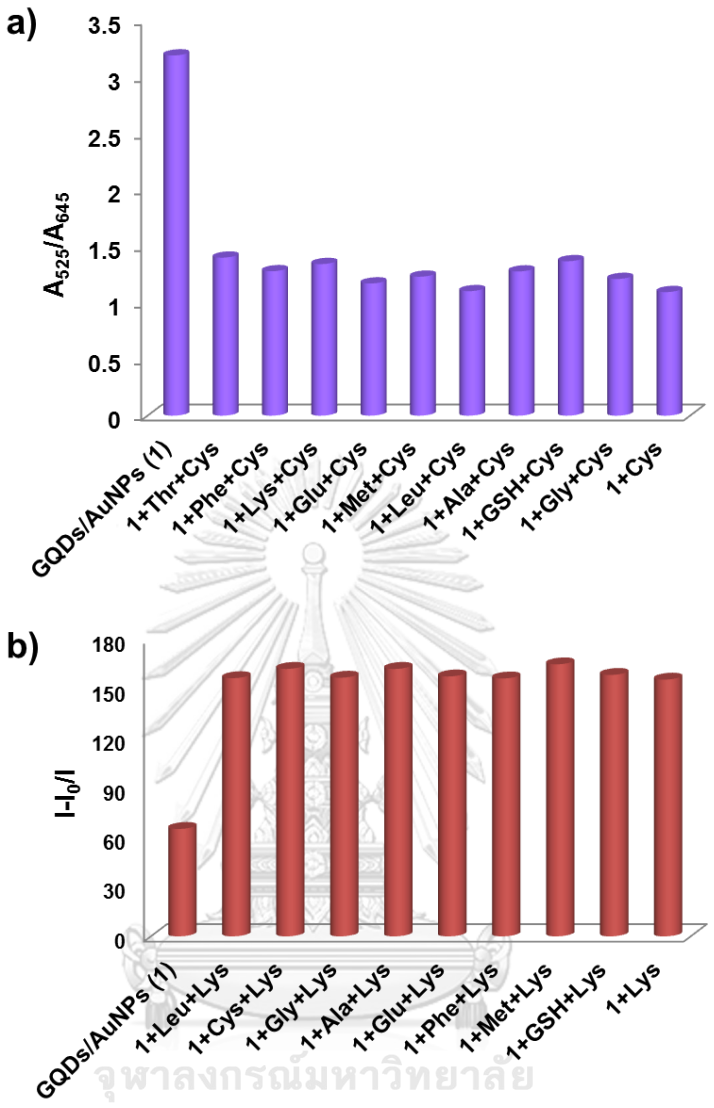

Figure 3.14. Interference studies of **GQDs/AuNPs** (0.4 μM) toward Cys (a) and Lys (b) with 50 equiv other amino acids in 1 mM PBS buffer (pH 7.4)

According to the sensing ability of dual detection of nanomaterials, the limit of detection (LOD) of **GQDs/AuNPs** toward Cys and Lys was evaluated by using UV-Visible and Fluorescence techniques in 1 mM PBS (pH 7), respectively. The gradual increase of an absorption band at 645 nm from UV-visible titration had been utilized to calculate the limit of detection of Cys which provided 5.88 μM in the linear range of 0.005-0.100 mM with R^2 = 0.98 (Figure 3.15a). Whereas the limit of detection of **GQDs/AuNPs** towards Lys was at 16.14 μM in the linear range of 0.047-0.800 mM with R^2 = 0.99 by using fluorescence titration (Figure 3.15b).

Moreover, the visual sensing for Cys and Lys detection by **GQDs/AuNPs** was carried out under light and UV lamp at 365 nm. Figure 3.16 showed a visualized-color change of **GQDs/AuNPs** regarding to an increment of concentration of Cys and Lys. The result exhibited a visual detection limit with Cys was approximately 0.012 mM (1.44 ppm) with the color change from red to blue as shown in Figure 3.16a. In the case of Lys, the increment of Lys concentration provided blue brightness solution under UV lamp and the visual detection limit was examined to be 0.070 mM (10.25 ppm) as shown in inset of Figure 3.16b. Noticeably, **GQDs/AuNPs** offered the powerful visual detection of Cys and Lys in ppm level under the UV light and UV lamp at 365 nm, respectively.

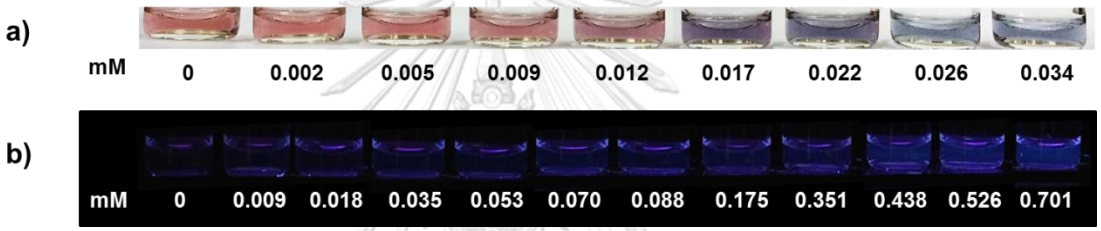

Figure 3.15. The visual changes of **GQDs/AuNPs** (1.68×10^{-5} M) nanomaterials with varying amount of Cys (a) and Lys (b)

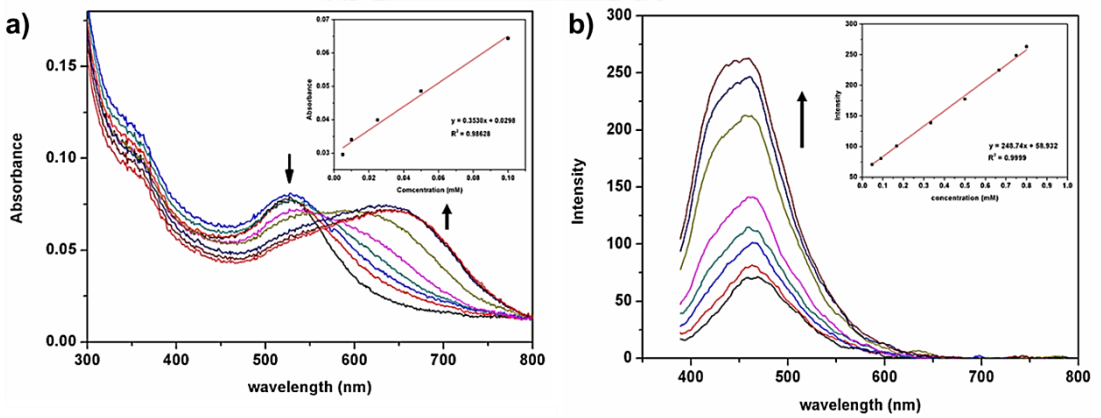

Figure 3.16. The absorption (a) and emission (b) spectra of 0.4 μM **GQDs/AuNPs** hybrids under excitation wavelength 360 nm in the 1 mM PBS solution pH 7.4 upon addition of different concentration of Cys (0.005-0.100 mM) and Lys (0.047-0.800 mM) after stirring for 2 min

3.4.8. Monitoring in real sample

To verify the accuracy and reliability of the dual detection for **GQDs/AuNPs**, the real samples of urine and milk were utilized for measurement of Cys and Lys, respectively. Apart of Cys detection, the real samples of urine were collected from three people. The urine sample was applied to evaluate the capability of **GQDs/AuNPs** for detection of Cys. The average % recoveries of the spiked samples of Cys to the solution of nanohybrid sensor of **GQDs/AuNPs** were calculated from calibration curve as seen in Figure 3.17. In the determination of Lys, the **GQDs/AuNPs** sensor was applied to determine the amount of Lys in food samples (milk and soybean milk) and the %recoveries of the spiked samples of Lys were calculated from calibration curve as seen in Figure 3.18 (for milk) and Figure 3.19 (for soybean milk). As shown in Table 3.12 and 3.13, % recovery of Cys and Lys were measured by using **GQDs/AuNPs** and the result exhibited the linear range from 101.60 -105.83 and 103.49-105.47, respectively. The RSD is very low values indicating a good accuracy and repeatability of the developed method in real sample analysis. The results suggested that our strategy has potential for highly selective quantification of Cys and Lys in real samples.

Table 3.12. Determination of cysteine in urine samples

Samples	Added /μM	Found /μM	%recovery	RSD[a]
1	25	25.76±4.27	103.05	0.1658
2	25	26.45±2.99	105.83	0.1132
3	25	25.42±3.99	101.68	0.1571

[a] Relative standard deviation (RSD) for recovery (n = 5)

Table 3.13. Determination of Lys in milk samples

Samples	Added /mM	Found /mM	%recovery	RSD[a]
Milk	1.50	1.55±1.36	103.49	0.0237
Soybean milk	1.50	1.58±4.22	105.47	0.0530

[a] Relative standard deviation (RSD) for recovery (n = 5)

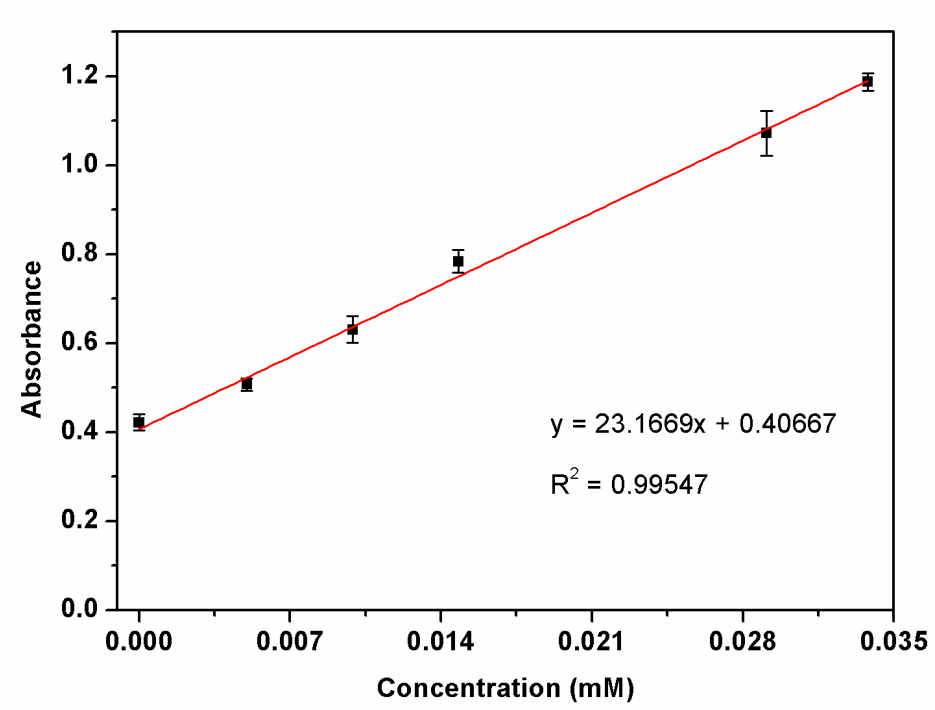

Figure 3.17. Determination of **GQDs/AuNPs** (0.4 μM) upon the addition of Cys (0-0.035 mM) in the 1 mM PBS solution pH 7.4 of urine sample upon stirring for 2 min

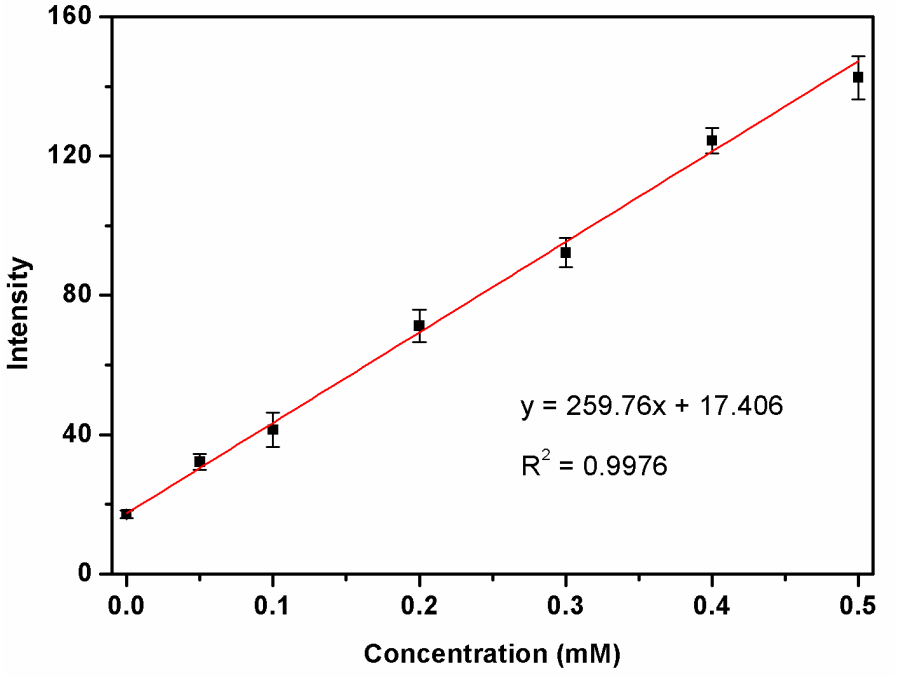

Figure 3.18. Determination of **GQDs/AuNPs** (0.4 μM) upon the addition of Lys (0-0.5 mM) in the 1 mM PBS solution pH 7.4 of milk sample upon stirring for 2 min. The fluorescence spectra were recorded under excitation wavelength at 360 nm.

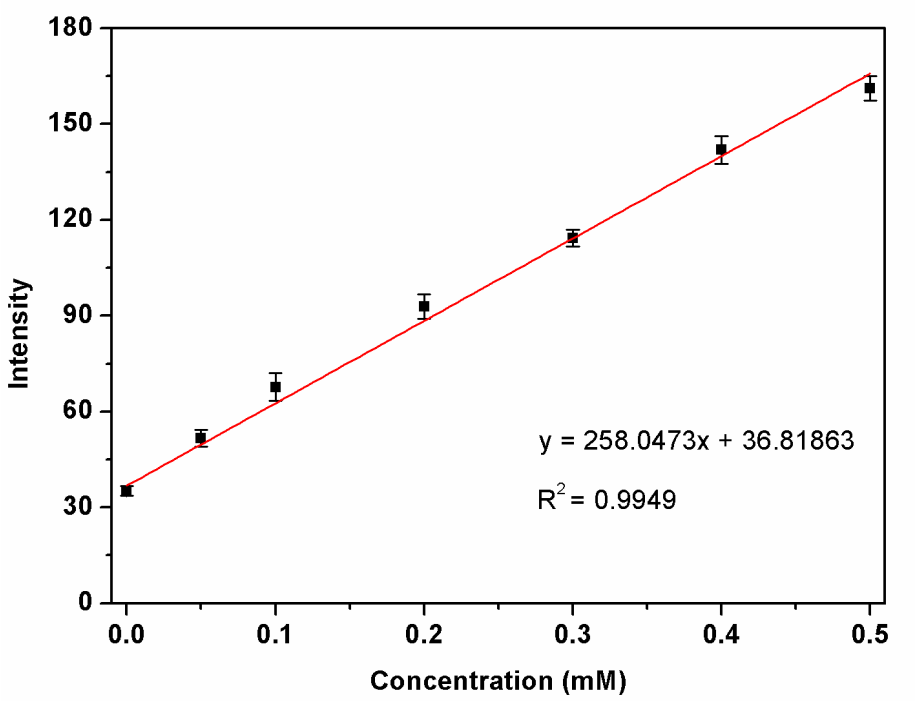

Figure 3.19. Determination of **GQDs/AuNPs** hybrids (0.4 μM) upon the addition of Lys (0-0.5 mM) in the 1 mM PBS solution pH 7.4 of soybean milk sample upon stirring for 2 min. The fluorescence spectra were recorded under excitation wavelength at 360 nm.

Chapter IV
Conclusion

With the recognition of biothiol compounds in aqueous system, we have successfully developed the new nanomaterial sensors. This dissertation has reported two different strategies of sensing. For first sensing approach, the self-assembly nanomicelle has been designed to be a nanosensor for detection of GSH based on disulfide cleavage in the micelle. The micellar system was constructed by self-assembled of dual surfactants of Triton-X 100 and bis(6-hydroxyhexyl) disulfide (**S2**) which acts as a co-surfactant and a reactive site under the disulfide-cleavage trigger in the micelle. Curcumine-BF_2 (**Cur-BF_2**) and dansyl boronic acid (**DA**) were chosen as a fluorescent probe in the system of aggregation nanomicelle bearing Triton–X and **S2** assigned to **TSC** and **TSD**, respectively, with a particle size of approximately 200 nm. In the challenging task for the disulfide-cleavage triggered aspect, the optimization of the ration between Triton-X 100 and **S2** for studying the GSH sensing approach in both systems was 1:3.8 which provides a large fluorescence quenching in the presence of GSH. The fluorescence spectrum of **TSC** and **TSD** platform showed highly fluorescent intensity around 587 nm and 528 nm, respectively. Based on disulfide-cleavage trigger, the disulfide bond in **TSC** and **TSD** would be easily reduced by specific GSH in 2.5% DMSO/PBS at pH 6 inducing the collapse of aggregation nanomicelles which were monitoring from the fluorescence quenching. These nanomicelles showed high selectivity and rapid detection of GSH with the detection limit of 2.24 ppm and 2.83 ppm for **TSC** and **TSD**, respectively, under linear range of 0.02-0.22 mM. In addition, **TSD** was successfully developed to be non-bright distance based 3D paper analytical device (3D-µPAD) for the detection of GSH under the visualized fluorescence response. The distance of fluorescence darkness on paper is proportional to the amount of GSH with the detection limit of 0.06 mg/mL under linear range of 0.30 - 1.50 mg/mL.

The second sensing approach, we have been successfully designed and engineered the nanohybrids to detect amino acid in PBS buffer pH 7.4. The sensor **GQDs/AuNPs** have been designed and prepared by using **GQDs** as a reductant and

stabilizer for the AuNPs. The **GQDs/AuNPs** were prepared via *in situ* growth of AuNPs on the surface of **GQDs**. This nanohybrid material is extremely stable in aqueous medium with an intensive surface plasma band at 525 nm. The **GQDs/AuNPs** was found to be dual detection of Cys and Lys based on the UV-visible and fluorescence techniques, respectively. In the case of Cys, the self-aggregation of **GQDs/AuNPs** has been demonstrated by the observation of color change from red to blue and the red shift of absorption band from 525 nm and 645 nm. Moreover, this material was found to determine Lys by "turn-on" fluorescent at 450 nm with a respect to emission band of free GQDs. This manner underwent the displacement process between **GQDs** sheets and Lys on AuNPs surface. The nanocomposite of **GQDs/AuNPs** can be used to measure the concentration of Cys and Lys without interference in the detection limit of 5.88 μM and 16.14 μM under linear range of 0.05-0.5 mM and 0.047-0.8 mM, respectively. Furthermore, **GQDs/AuNPs** highlighted a promising quantitative determination of Cys in urine samples and Lys in milk samples with real time analysis and the acceptable %recovery in the range of 101.68 - 105.83 %.

REFERENCES

[1] Wood, Z.A., Schröder, E., Robin Harris, J., and Poole, L.B. Structure, mechanism and regulation of peroxiredoxins. Trends in Biochemical Sciences 28(1) (2003): 32-40.

[2] Yuan, X., Tay, Y., Dou, X., Luo, Z., Leong, D.T., and Xie, J. Glutathione-Protected Silver Nanoclusters as Cysteine-Selective Fluorometric and Colorimetric Probe. Analytical Chemistry 85(3) (2013): 1913-1919.

[3] Zhang, H., et al. A minimalist fluorescent probe for differentiating Cys, Hcy and GSH in live cells. Chemical Science 7(1) (2016): 256-260.

[4] Boubakari, Bracht, K., Neumann, C., Grünert, R., and Bednarski, P.J. No Correlation between GSH Levels in Human Cancer Cell Lines and the Cell Growth Inhibitory Activities of Platinum Diamine Complexes. Archiv der Pharmazie 337(12) (2004): 668-671.

[5] Niu, L.-Y., Guan, Y.-S., Chen, Y.-Z., Wu, L.-Z., Tung, C.-H., and Yang, Q.-Z. BODIPY-Based Ratiometric Fluorescent Sensor for Highly Selective Detection of Glutathione over Cysteine and Homocysteine. Journal of the American Chemical Society 134(46) (2012): 18928-18931.

[6] He, L., Xu, Q., Liu, Y., Wei, H., Tang, Y., and Lin, W. Coumarin-Based Turn-On Fluorescence Probe for Specific Detection of Glutathione over Cysteine and Homocysteine. ACS Applied Materials & Interfaces 7(23) (2015): 12809-12813.

[7] Zhu, B., Zhang, X., Li, Y., Wang, P., Zhang, H., and Zhuang, X. A colorimetric and ratiometric fluorescent probe for thiols and its bioimaging applications. Chemical Communications 46(31) (2010): 5710-5712.

[8] Tang, F., Li, L., and Chen, D. Mesoporous Silica Nanoparticles: Synthesis, Biocompatibility and Drug Delivery. Advanced Materials 24(12) (2012): 1504-1534.

[9] Cui, Y., Dong, H., Cai, X., Wang, D., and Li, Y. Mesoporous Silica Nanoparticles Capped with Disulfide-Linked PEG Gatekeepers for Glutathione-Mediated Controlled Release. ACS Applied Materials & Interfaces 4(6) (2012): 3177-3183.

[10] Pileni, M.-P. The Role of Soft Colloidal Templates in Controlling the Size and Shape of Inorganic Nanocrystals. Vol. 2, 2003.

[11] Agubata, C., Nzekwe, I., Obitte, N., Elochuhukwu, C., Attama, A., and Onunkwo, G. Effect of Oil, Surfactant and Co-Surfactant Concentrations on the Phase Behavior, Physicochemical Properties and Drug Release from Self-Emulsifying Drug Delivery Systems. Vol. 1, 2014.

[12] Khoshnood, A., Lukanov, B., and Firoozabadi, A. Temperature Effect on Micelle Formation: Molecular Thermodynamic Model Revisited. Langmuir 32(9) (2016): 2175-2183.

[13] Kovalenko, A., Polavarapu, P., Pourroy, G., Waton, G., and Krafft, M.P. pH-Controlled Microbubble Shell Formation and Stabilization. Langmuir 30(22) (2014): 6339-6347.

[14] Xu, Z., Liu, S., Kang, Y., and Wang, M. Glutathione-Responsive Polymeric Micelles Formed by a Biodegradable Amphiphilic Triblock Copolymer for Anticancer Drug Delivery and Controlled Release. ACS Biomaterials Science & Engineering 1(7) (2015): 585-592.

[15] Ko, N.R. and Oh, J.K. Glutathione-Triggered Disassembly of Dual Disulfide Located Degradable Nanocarriers of Polylactide-Based Block Copolymers for Rapid Drug Release. Biomacromolecules 15(8) (2014): 3180-3189.

[16] Ni, P., et al. Highly sensitive and selective colorimetric detection of glutathione based on Ag [I] ion–3,3′,5,5′-tetramethylbenzidine (TMB). Biosensors and Bioelectronics 63 (2015): 47-52.

[17] Kumar, S., Rhim, W.-K., Lim, D.-K., and Nam, J.-M. Glutathione Dimerization-Based Plasmonic Nanoswitch for Biodetection of Reactive Oxygen and Nitrogen Species. ACS Nano 7(3) (2013): 2221-2230.

[18] Acres, R.G., Feyer, V., Tsud, N., Carlino, E., and Prince, K.C. Mechanisms of Aggregation of Cysteine Functionalized Gold Nanoparticles. The Journal of Physical Chemistry C 118(19) (2014): 10481-10487.

[19] Reimann, S.M. and Manninen, M. Electronic structure of quantum dots. Reviews of Modern Physics 74(4) (2002): 1283-1342.

[20] M G Bawendi, M L Steigerwald, a., and Brus, L.E. The Quantum Mechanics of Larger Semiconductor Clusters ("Quantum Dots"). Annual Review of Physical Chemistry 41(1) (1990): 477-496.

[21] Yoffe, A.D. Semiconductor quantum dots and related systems: Electronic, optical, luminescence and related properties of low dimensional systems. Advances in Physics 50(1) (2001): 1-208.

[22] Dong, Y. Blue luminescent graphene quantum dots and graphene oxide prepared by tuning the carbonization degree of citric acid. Carbon v. 50(no. 12) (2012): pp. 4738-4743-2012 v.50 no.12.

[23] Yang, S.-T., et al. Carbon Dots for Optical Imaging in Vivo. Journal of the American Chemical Society 131(32) (2009): 11308-11309.

[24] Nurunnabi, M., et al. In Vivo Biodistribution and Toxicology of Carboxylated Graphene Quantum Dots. ACS Nano 7(8) (2013): 6858-6867.

[25] Ju, J. and Chen, W. In Situ Growth of Surfactant-Free Gold Nanoparticles on Nitrogen-Doped Graphene Quantum Dots for Electrochemical Detection of Hydrogen Peroxide in Biological Environments. Analytical Chemistry 87(3) (2015): 1903-1910.

[26] Zhang, L., Zhang, Z.-Y., Liang, R.-P., Li, Y.-H., and Qiu, J.-D. Boron-Doped Graphene Quantum Dots for Selective Glucose Sensing Based on the "Abnormal" Aggregation-Induced Photoluminescence Enhancement. Analytical Chemistry 86(9) (2014): 4423-4430.

[27] Jongjinakool, S., Palasak, K., Bousod, N., and Teepoo, S. Gold Nanoparticles-based Colorimetric Sensor for Cysteine Detection. Energy Procedia 56 (2014): 10-18.

[28] Zhou, Y., Yang, Z., and Xu, M. Colorimetric detection of lysine using gold nanoparticles aggregation. Analytical Methods 4(9) (2012): 2711-2714.

[29] Rawat, K.A. and Kailasa, S.K. Visual detection of arginine, histidine and lysine using quercetin-functionalized gold nanoparticles. Microchimica Acta 181(15) (2014): 1917-1929.

[30] Tang, Z., Lin, Z., Li, G., and Hu, Y. Amino Nitrogen Quantum Dots-Based Nanoprobe for Fluorescence Detection and Imaging of Cysteine in Biological Samples. Analytical Chemistry 89(7) (2017): 4238-4245.

[31] Deng, J., et al. Nanosensor Composed of Nitrogen-Doped Carbon Dots and Gold Nanoparticles for Highly Selective Detection of Cysteine with Multiple Signals. Analytical Chemistry 87(4) (2015): 2195-2203.

[32] Dong, Y., Wu, H., Shang, P., Zeng, X., and Chi, Y. Immobilizing water-soluble graphene quantum dots with gold nanoparticles for a low potential electrochemiluminescence immunosensor. Nanoscale 7(39) (2015): 16366-16371.

[33] Lewis, G., J Ditucci, M., and Phillips, S. Quantifying Analytes in Paper-Based Microfluidic Devices Without Using External Electronic Readers. Vol. 51, 2012.

[34] Townsend, D.M., Tew, K.D., and Tapiero, H. The importance of glutathione in human disease. Biomedicine & Pharmacotherapy 57(3) (2003): 145-155.

[35] Michelet, F., Gueguen, R., Leroy, P., Wellman, M., Nicolas, A., and Siest, G. Blood and plasma glutathione measured in healthy subjects by HPLC: relation to sex, aging, biological variables, and life habits. Clinical Chemistry 41(10) (1995): 1509-1517.

[36] Iversen, R., Andersen, P.A., Jensen, K.S., Winther, J.R., and Sigurskjold, B.W. Thiol−Disulfide Exchange between Glutaredoxin and Glutathione. Biochemistry 49(4) (2010): 810-820.

[37] Banerjee, S., Kar, S., Perez, J.M., and Santra, S. Quantum Dot-Based OFF/ON Probe for Detection of Glutathione. The Journal of Physical Chemistry C 113(22) (2009): 9659-9663.

[38] Chen, G., Wang, J., Wu, C., Li, C.-z., Jiang, H., and Wang, X. Photoelectrocatalytic Oxidation of Glutathione Based on Porous TiO2–Pt Nanowhiskers. Langmuir 28(33) (2012): 12393-12399.

[39] M. Kirihara, Y.A., S. Ogawa, T. Noguchi, A. Hatano, Y. Hirai. A Mild and Environmentally Benign Oxidation of Thiols to Disulfides. Synthesis (2007): 3286-3289.

[40] Kong, F., Liu, R., Chu, R., Wang, X., Xu, K., and Tang, B. A highly sensitive near-infrared fluorescent probe for cysteine and homocysteine in living cells. Chemical Communications 49(80) (2013): 9176-9178.

[41] Elghanian, R., Storhoff, J.J., Mucic, R.C., Letsinger, R.L., and Mirkin, C.A. Selective Colorimetric Detection of Polynucleotides Based on the Distance-Dependent Optical Properties of Gold Nanoparticles. Science 277(5329) (1997): 1078-1081.

[42] Giles, N.M., Giles, G.I., and Jacob, C. Multiple roles of cysteine in biocatalysis. Biochemical and Biophysical Research Communications 300(1) (2003): 1-4.

[43] Reddie, K.G. and Carroll, K.S. Expanding the functional diversity of proteins through cysteine oxidation. Current Opinion in Chemical Biology 12(6) (2008): 746-754.

[44] Shahrokhian, S. Lead Phthalocyanine as a Selective Carrier for Preparation of a Cysteine-Selective Electrode. Analytical Chemistry 73(24) (2001): 5972-5978.

[45] Fini, M., Torricelli, P., Giavaresi, G., Carpi, A., Nicolini, A., and Giardino, R. Effect of L-lysine and L-arginine on primary osteoblast cultures from normal and osteopenic rats. Biomedicine & Pharmacotherapy 55(4) (2001): 213-220.

[46] Breau, R.H., et al. The Effects of Lysine Analogs During Pelvic Surgery: A Systematic Review and Meta-Analysis. Transfusion Medicine Reviews 28(3) (2014): 145-155.

[47] Yang, X., Guo, Y., and Strongin, R.M. Conjugate Addition/Cyclization Sequence Enables Selective and Simultaneous Fluorescence Detection of Cysteine and Homocysteine. Angewandte Chemie International Edition 50(45) (2011): 10690-10693.

[48] Akyilmaz, E., Erdoğan, A., Öztürk, R., and Yaşa, İ. Sensitive determination of l-lysine with a new amperometric microbial biosensor based on Saccharomyces cerevisiae yeast cells. Biosensors and Bioelectronics 22(6) (2007): 1055-1060.

[49] Pérez-Ruiz, T., Martínez-Lozano, C., Tomás, V., and Martín, J. Flow injection chemiluminescent method for the successive determination of l-cysteine and l-cystine using photogenerated tris(2,2′-bipyridyl) ruthenium (III). Talanta 58(5) (2002): 987-994.

[50] Huang, S., et al. A simple and sensitive method for l-cysteine detection based on the fluorescence intensity increment of quantum dots. Analytica Chimica Acta 645(1) (2009): 73-78.

[51] Douša, M., Břicháč, J., Gibala, P., and Lehnert, P. Rapid hydrophilic interaction chromatography determination of lysine in pharmaceutical preparations with fluorescence detection after postcolumn derivatization with o-phtaldialdehyde. Journal of Pharmaceutical and Biomedical Analysis 54(5) (2011): 972-978.

[52] Głowacki, R. and Bald, E. Fully automated method for simultaneous determination of total cysteine, cysteinylglycine, glutathione and homocysteine in plasma by HPLC with UV absorbance detection. Journal of Chromatography B 877(28) (2009): 3400-3404.

[53] Ferin, R., Pavão, M.L., and Baptista, J. Methodology for a rapid and simultaneous determination of total cysteine, homocysteine, cysteinylglycine and glutathione in plasma by isocratic RP-HPLC. Journal of Chromatography B 911 (2012): 15-20.

[54] Shahrokhian, S. and Karimi, M. Voltammetric studies of a cobalt(II)-4-methylsalophen modified carbon-paste electrode and its application for the simultaneous determination of cysteine and ascorbic acid. Electrochimica Acta 50(1) (2004): 77-84.

[55] Sun, H., Wu, L., Gao, N., Ren, J., and Qu, X. Improvement of Photoluminescence of Graphene Quantum Dots with a Biocompatible Photochemical Reduction Pathway and Its Bioimaging Application. ACS Applied Materials & Interfaces 5(3) (2013): 1174-1179.

[56] Qian, Z.S., Shan, X.Y., Chai, L.J., Ma, J.J., Chen, J.R., and Feng, H. DNA nanosensor based on biocompatible graphene quantum dots and carbon nanotubes. Biosensors and Bioelectronics 60 (2014): 64-70.

[57] Wang, W., et al. Detection of Homocysteine and Cysteine. Journal of the American Chemical Society 127(45) (2005): 15949-15958.

[58] Zhang, D. Highly selective colorimetric detection of cysteine and homocysteine in water through a direct displacement approach. Vol. 12, 2009.

[59] Ipe, D.S. and Ulett, G.C. Evaluation of the in vitro growth of urinary tract infection-causing gram-negative and gram-positive bacteria in a proposed synthetic human urine (SHU) medium. Journal of Microbiological Methods 127 (2016): 164-171.

[60] Lee, S.K., Choi, M.G., Choi, J., and Chang, S.-K. Fluorescence signaling of Zn2+ levels in synthetic urine by dipicolylamine-armed hydroxynaphthalimide. Sensors and Actuators B: Chemical 207 (2015): 303-307.

[61] Ninnemann, A.L., Lechner, W.V., Borges, A., and Lejuez, C.W. Synthetic cannabinoids to avoid urine drug screens: Implications for contingency management and other treatments for drug dependence. Addictive behaviors 63 (2016): 72-73.

[62] Gao, L., Wang, Y., Lu, M., Fa, M., Yang, D., and Yao, X. Simple method for O-GlcNAc sensitive detection based on graphene quantum dots. RSC Advances 7(50) (2017): 31204-31211.

[63] Wang, Y., Zhao, Y., Zhang, F., Chen, L., Yang, Y., and Liu, X. Fluorescent polyvinyl alcohol films based on nitrogen and sulfur co-doped carbon dots towards white light-emitting devices. New Journal of Chemistry 40(10) (2016): 8710-8716.

[64] Liu, J.-J., Chen, Z.-T., Tang, D.-S., Wang, Y.-B., Kang, L.-T., and Yao, J.-N. Graphene quantum dots-based fluorescent probe for turn-on sensing of ascorbic acid. Sensors and Actuators B: Chemical 212 (2015): 214-219.

[65] Dong, Y., et al. Blue luminescent graphene quantum dots and graphene oxide prepared by tuning the carbonization degree of citric acid. Carbon 50(12) (2012): 4738-4743.

APPENDIX

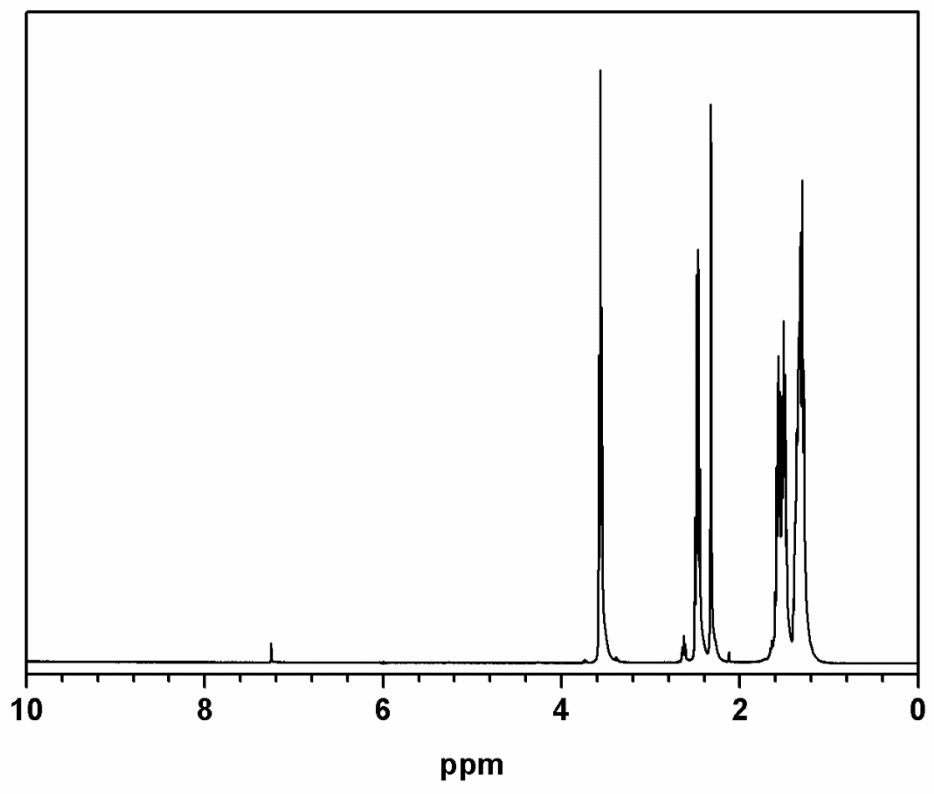

Figure A.1. The ^{1}H-NMR spectrum of 6-mercaptohexanol

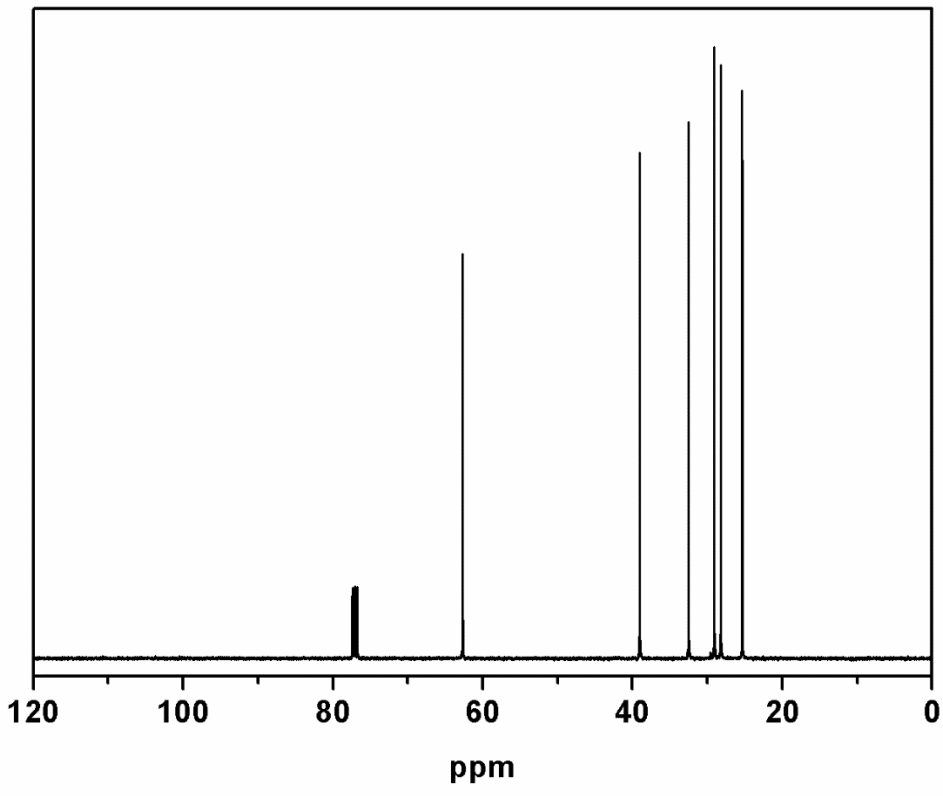

Figure A.2. The ^{13}C-NMR spectrum of bis(6-hydroxyhexyl)disulfide, **S2**

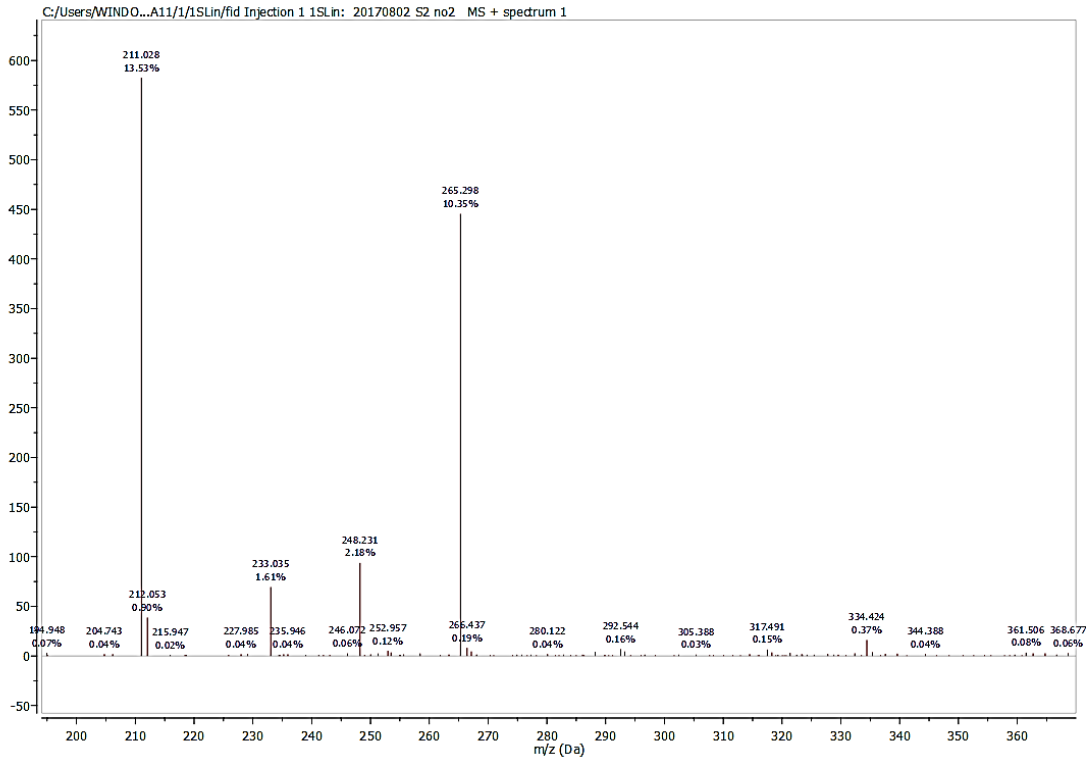

Figure A.3. The mass spectrum of bis(6-hydroxyhexyl)disulfide, **S2**

VITA

General Information

Miss Chiraporn Chaicham was born on June 2, 1986 in Chaiyaphum, Thailand. She graduated with a high school diploma from Phukhieo School, Phukhieo Chaiyaphum in 2005. She received her Bachelor's degree of Science in Chemistry from Khonkean University in 2008. Thereafter, she has been a graduate student at the Department of Chemistry, Chulalongkorn University. Since 2008 become a member of the Supramolecular Chemistry Research Unit under supervision of Assistant Professor Dr. Boosayarat Tomapatanaget and finished her Master's degree of Science in the academic year 2011. She continued to study in Ph. D at the Department of Chemistry, Chulalongkorn University under supervision of Assistant Professor Dr. Boosayarat Tomapatanaget. Since 2017, she has been a graduate student at the Department of Chemistry, Chulalongkorn University.

Fellowships & Scholarships

- Human Resource Development in Science Project (Science Achievement Scholarship of Thailand, SAST) to support covering full tuition and stipend in academic program at Khonkean University in 2005-2008 and Chulalongkorn University in 2008-2017.

- The 90th Anniversary of Chulalongkorn University to support scholarships and research throughout academic program in 2017.